

Faculty of Science and Technology  
Department of Geology

# **Geology and Origin of the Cu-sulphide Ores in the Tynset-Alvdal Region, southern Scandinavian Caledonides**

**Maren Galguften Lunsæter**

*GEO-3900 Master's Thesis in Geology*

*May 2016*





## **Acknowledgements**

Puh! There is the finish-line. So many people have helped me to cross it and I want to start with my supervisors: Krister Sundblad, without you this would be impossible. Thank you for everything you have done, for your enthusiasm, your care, your help and your great belief in me. Sabina Strmic Palinkas: Thank you for all the hours, days and afternoons you have spent teaching me in ore-microscopy and with geochemical analysis, and that you have been so optimistic and helpful, even though I was probably not in your plans this year!

A special thanks goes to David D. Gee, such an interesting and inspiring person. Thanks to Hanne-Kristin Paulsen for proof-reading, new ideas and constructive criticism. Thanks to Marcello Imaña for constructive criticism and discussion. And thanks to Steffen Bergh for your open-door policy. I also want to thank the ladies at the lab: you are some fantastic, cheerful and helpful persons! Thanks to Norges Geologiske Undersøkelse for the financial support.

I was told that the time at the university is the best time of my life. I can now truly agree with that. I have got to know the best friends of my life and experienced a lot. Thanks Karianne and Silje (Trekløveret) for tolerating “søringen” throughout 5 years. That also apply to Frank. Thanks to all the others that have made my time super here! A small thanks to Thomas, I really appreciate your sense of humour and smile.

Finally, I want to thank my family for their support and belief in me.

*Maren Galguften Lunsæter*

Tromsø, May 2016



## **Abstract**

The Trondsvangen-Baugberget Cu-bearing ore deposits are located in the Tynset-Alvdal region, Hedmark county, central Norway. The earliest documented work in these mines are from the late 17<sup>th</sup> century, with extensive mining between 1880 and 1911. The ore deposits are located within volcanic and metasedimentary sequences of the Lower Seve Nappes of the Middle Allochthon, Scandinavian Caledonides. The ore-bearing rocks are tectonostratigraphically located above the Tännäs Augen Gneiss, lowermost Middle Allochthon, and beneath the ultramafic pods that form an extension of the Vågåmo Ophiolite, in the lowest parts of the Köli Nappes.

Based on the petrographical and field observations the host rocks are greenschist and mica schist, with the greenschist located on top. However, the stratigraphic polarity was never determined and the entire sequence may be inverted. The geochemical investigation revealed that the greenschist originated as ocean-floor basalts with a tholeiitic signature associated with a mid-ocean ridge, and the mica schist as a greywacke deposited in a continent-margin environment sea. The altered equivalents show both a depletion and enrichment in the mobile elements, indicating hydrothermal alteration.

The greenschist-hosted ores represent a chalcopyrite-sphalerite-bearing pyrite-rich massive ore type, while the mica schist-hosted ores represent a chalcopyrite-sphalerite-galena pyrrhotite-rich irregular and semi-massive ore type. The stratigraphy is proposed to be inverted, with the mica schist formed on top of the greenschist, which yields similarities with the Cyprus VMS type for the greenschist-hosted ores and with the Escanaba and/or subsea-floor replacement VMS types for the mica schist-hosted ores, where the latter may be the most similar. The entire environment show similarities with the present Red Sea in terms of tectonic setting, magmatism and sedimentation.

The host rocks are believed to have formed during the early rifting and opening up of the Iapetus Ocean during the Ediacaran in the late Precambrian. The ore-bearing sequences at Tronsvangen-Baugberget may thus be the oldest and lowermost Cu-bearing VMS ore deposits within the Scandinavian Caledonides.



# Table of Contents

<b>1. Introduction</b> .....	<b>1</b>
1.1 Context of the study .....	1
1.2 Purpose of the study .....	1
1.3 Geography .....	2
1.4 Previous work .....	2
1.5 Geological background and mining history .....	3
1.5.1 The Scandinavian Caledonides .....	3
1.5.2 The geology of the Alvdal-Røros region .....	6
1.5.3 The sulphide ores in the Tynset-Alvdal region .....	9
1.5.4 Mining history .....	12
1.6 VMS-type deposits .....	13
1.6.1 Introduction .....	13
1.6.2 The formation of volcanogenic massive sulphide deposits .....	13
1.6.3 Classification of VMS deposits .....	14
1.6.4 VMS ore deposits within the Scandinavian Caledonides .....	18
<b>2. Methods</b> .....	<b>19</b>
2.1 Archive and literature studies .....	19
2.2 Field work and sample collection .....	19
2.3 Preparation for microscope samples .....	19
2.4 Microscopy work .....	19
2.5 Preparation for geochemical analysis .....	20
<b>3. Observations and results</b> .....	<b>21</b>
3.1 Revised geological maps .....	21
3.2 Field observations of rocks and ore deposits .....	23
3.2.1 Volcanic rocks .....	23
3.2.2 Metasedimentary rocks .....	23
3.2.3 Volcanic-hosted ores .....	23
3.2.4 Metasedimentary-hosted ores .....	24
3.3 Petrographic description of rocks .....	24
3.3.1 Volcanic rock .....	24
3.3.2 Metasedimentary rock .....	26
3.4 Petrographic description of ore mineralization .....	28
3.4.1 Volcanic rock-hosted ores .....	28
3.4.2 Metasedimentary rock-hosted ores .....	30
3.5 Geochemistry .....	33
3.5.1 Volcanic rock .....	33

3.5.2 Altered volcanic rock .....	40
3.5.3 Metasedimentary rock .....	41
3.5.4 Altered metasedimentary rock .....	43
3.5.5 Geochemical comparison of volcanic vs metasedimentary rocks.....	44
3.5.6 The ore deposits .....	45
<b>4. Discussion .....</b>	<b>49</b>
4.1 Geological setting of the volcanic and meta-sedimentary units and interpretation of the geological environment .....	49
4.1.1 Tectonostratigraphic position .....	49
4.1.2 The origin of the host rocks and the geological environment .....	49
4.1.3 Geochemistry and tectonic setting of the host rocks.....	50
4.2 Geological environment and ore-forming processes of the ores .....	51
4.2.1 Greenschist-hosted ores.....	51
4.2.2 Mica schist-hosted ores .....	52
4.2.3 Deformation of the ore minerals and their textures.....	52
4.3 Regional geological context .....	54
<b>5. Conclusion .....</b>	<b>57</b>
<b>References .....</b>	<b>59</b>
<b>Appendices .....</b>	<b>65</b>
A. Abbreviated mineral names (from Kretz, 1983). .....	65
B. Overview of samples .....	67
C. Scanned thin sections.....	71
D. Geochemical data .....	77
D.1 Certificate of analysis, Actlabs.....	77
D.2 Major element diagram (%) of host rocks.....	78
D.3 Rare-earth element diagram (ppm) (only for greenschist samples) .....	79
D.4 Trace element diagram (ppm) (only for greenschist samples).....	79
D.5 Metal contents in ore samples .....	80
E. Ore element correlation.....	81
E.1 Correlation plots .....	81
E.2 Ore element correlation tables .....	85
F. SEM/EDS analysis .....	87
F.1 Bi-Te bearing phases in galena, ML1526 .....	87
F.2 Altered chalcopyrite, ML1503 .....	88
F.3 Altered pyrrotite, ML1544 .....	89



# **1. Introduction**

## **1.1 Context of the study**

In Norway, the first copper production was established in the 1630's, first at Kvikne Verk in Hedmark, followed by Røros Kobberverk in 1636 and Løkken Verk in 1652, both in Sør-Trøndelag. The Tynset-Alvdal sulphide-ore deposits, Hedmark county, which this thesis will discuss, were small but played a significant role in the copper production during the 18th and 19th centuries. They are not as well known as the adjacent and more classical ore districts of Røros and Folldal, and have therefore not experienced the same interest in historical and geological literature.

The Tynset-Alvdal ore deposits have previously not been appropriately investigated in a geological perspective, but this thesis will summarize all available knowledge of the ores (and their mining history) and document their geological, petrological and geochemical characteristics, their relations to the host rocks, as well as their general geological setting in a tectonostratigraphic perspective. They are believed to be volcanogenic-massive sulphide (VMS) deposits.

## **1.2 Purpose of the study**

The purpose of this study is to document the geological features and the tectonostratigraphic position of the Cu-VMS ore deposits in the Tynset-Alvdal region.

In addition, the goal of this thesis is to document the mineralogy, petrology and geochemical characteristics of ore mineralization and the surrounding host rocks to determine the origin and the ore-forming process. No previous literature has determined the origin nor the ore-forming process. In addition, these ore deposits will be put in a regional context and compared to other similar ore deposits and geological environments.

Field work, literature study, petrographic description of rocks and minerals and geochemical analysis will be used to solve the problems.

### 1.3 Geography

The study area is located in Alvdal and Tynset municipalities, Hedmark county, in the central-eastern part of Norway. The investigated mines are located in two areas: the most extensive area (Tronsvangen, Grøtådalen and Vesletronden) is situated along the southern foot hills of the mountain Tron, while the other area is situated at Baugsberget (Figure 1).

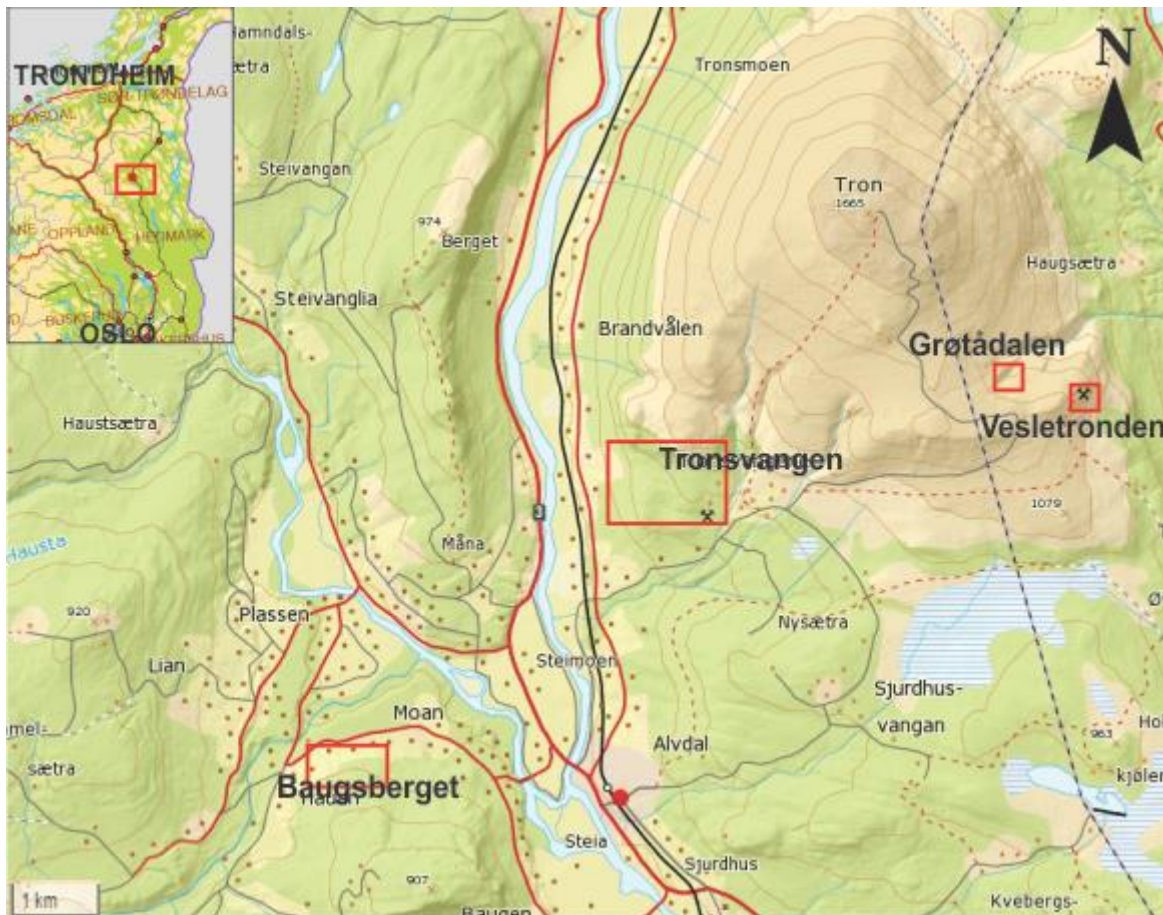


Figure 1: Location of Baugsberget, Tronsvangen, Grøtådalen and Vesletronden in relation to the municipality Alvdal. Modified from [www.ut.no/kart](http://www.ut.no/kart).

### 1.4 Previous work

Several scientists and explorers have worked in this area with different purposes and time aspects. The first written reports date back to the period when the mines were in operation (1880's-1907), and when the geologists Holmsen, Thesen, Rasmussen and Mortenson (Holmsen et al., 1907) were hired by the mining companies to secure a HMS-safe and sustainable operation. Each of them wrote about the working conditions, description of each mine, the future aspects and geology of the area and the ore deposits.

The most impressive work was done by Aalen in 1908, who made a detailed map of the Tronsvangen mining area. Other reports by Thorkildsen (1913), Riiber (1923) and Geis (1958)

describes the geology, mineralization, history and ore zones of the copper mines and deposits. Airborne magnetic and electromagnetic measurements were done in 1967 and other geophysical measurements (IP) in 1968 by NGU. The results are described in the reports of Aalstad (1967) and Eidsvig (1968). In 1974, Dreyer published his Ph.D. thesis of the Tronfjell-massiv and its surroundings. He established the geological setting for the various mineralizations in a regional perspective, including the lithologies of this thesis. The most recent report was done by Bjerkgård (1998), who summarized the mining history and previous work and briefly documented the ores and their host rocks.

## **1.5 Geological background and mining history**

### ***1.5.1 The Scandinavian Caledonides***

The Scandinavian Caledonides are located in Norway and Sweden, extending from southernmost Norway, through the central parts on both sides of the Norwegian-Swedish border and into Finnmark county, with a total length of around 1800 km and a width varying from 375 km to 750 km (Figure 2). This mountain belt is a typical example of a major continent-continent collision orogenic belt, formed by the collision of Baltica/Fennoscandia (North-Europe and Scandinavia) and Laurentia (North-America and Greenland) in the Silurian, following a long-time break up in Neoproterozoic and closure of the Iapetus Ocean (Gee & Sturt, 1985; Roberts, 2003; Corfu *et al.*, 2014a).

The formation of the Caledonides occurred during several events and is best illustrated with a Wilson cycle: starting with rifting of the supercontinent Rodinia and opening up of the Iapetus Ocean (late Precambrian-early Cambrian), subduction and formation of volcanic arc complexes, closing of the ocean when Laurentia drifted towards Baltica/Fennoscandia and finally collided during the Silurian-Early Devonian time (Roberts, 2003; Ramberg *et al.*, 2007).

The Scandinavian Caledonides are composed of Autochthonous/Paraautochthonous units at the base, overlaid by several allochthonous thrust units, including the Lower, Middle, Upper and Uppermost Allochthons (Figure 2) (Gee & Sturt, 1985). In the present nappe pile, these elements are all stacked upon each other, making up a series of allochthonous thrust sheets, on top of the autochthonous units in the east. The more or less endemic basement, with undeformed sedimentary cover rocks, is situated at the base, referred to as the Autochthon and Paraautochthonous units (Bergström & Gee, 1985). The Lower and Middle Allochthons are composed entirely of successions derived from the continental shelf and rise related to the passive margin of Baltica (Roberts & Gee, 1985). Most of the material have been torn apart

from the Precambrian basement as slices composed entirely of low-grade Neoproterozoic to Cambrian sedimentary cover sequences (Gee *et al.*, 1985a; Corfu *et al.*, 2014a; Corfu *et al.*, 2014b). The Upper Allochthon has a dominant oceanic signature with various ophiolite sequences and island-arc complexes, arc-related sedimentary and volcanic sequences derived from the Iapetus Ocean. The Uppermost Allochthon is composed of a more continental crust character with granitoids and gneissic basement rocks, and may descend from Laurentia (Gee & Zachrisson, 1979; Gee *et al.*, 2008). Generally, the lowest allochthons were shortly transported, while the structurally higher units were transported over a longer distance.

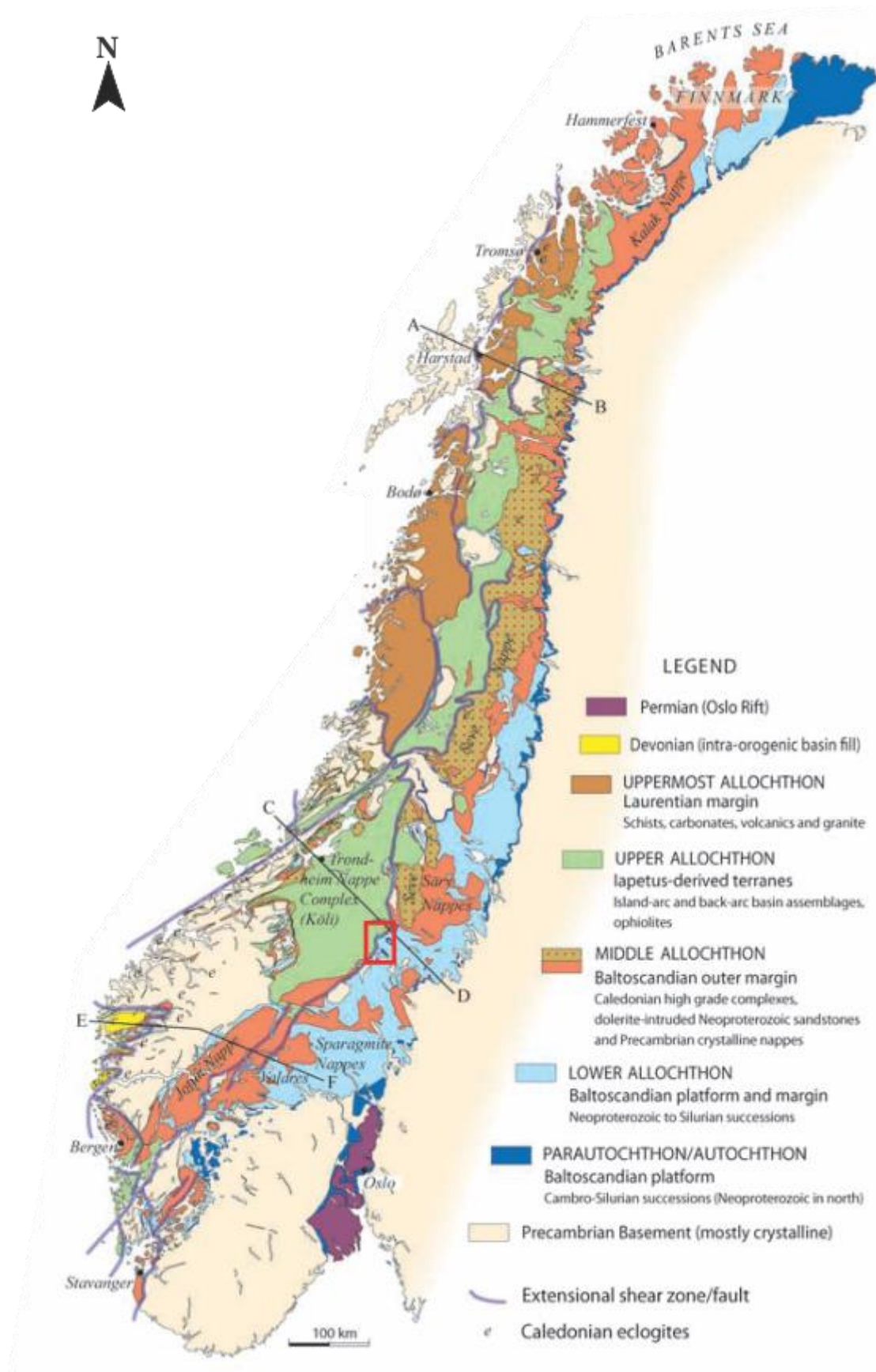


Figure 2: Geological map of the Scandinavian Caledonides where the red square shows the study area (Gee et al., 2008).

### ***1.5.2 The geology of the Alvdal-Røros region***

The Alvdal-Røros region is located in the eastern part of central Norway, 300 km north of Oslo and 70 km west of the Swedish border (see Figure 1). In a tectonostratigraphic perspective, this area is located within the Middle and Upper Allochthon (Gee *et al.*, 1985b) (Figure 4). In earlier literature on the central part of the Caledonides (Gee & Sturt, 1985), the Upper Allochthon was subdivided into the Köli and Seve Nappes. Later literature, Gee, *et al.* (2008) have redefined the Seve Nappe to be part of the Middle Allochthon due to the similarities in lithology (compared to other units in this allochthon) and a decrease in the metamorphic grade downwards into and through the Middle Allochthon. This paper will use the latest definition that the Seve Nappe is part of the Middle Allochthon.

The lowest part of the Upper Allochthon or the Köli Nappe Complex, has a great variation in lithologies, composition, deformation characters and metamorphic grades/alteration, making it the most heterogeneous and complex unit in the Scandinavian Caledonides (Stephens *et al.*, 1985). Volcanosedimentary and igneous rocks derived from the Iapetus Ocean, including ophiolites and island arc complexes, dominate this unit, with an estimated age of the sediments to the Early Paleozoic (Gee *et al.*, 2010). The metamorphic grade ranges from greenschist to granulite and eclogite facies.

The Middle Allochthon is composed of a basal basement-derived thrust sheet (the Tännäs Augen Gness Nappe; (Röshoff, 1978)). The Särvi Nappe is situated above the Augen gneiss nappe, consisting mainly of unfossiliferous high-strain, planar foliated Neoproterozoic metasandstone, tillite, greywacke and a dolerite dyke-swarm (Gee & Zachrisson, 1979). The metamorphic grade ranges from greenschist to epidote-amphibolite facies. The dolerite dyke-swarm that intruded the Särvi Nappe, shows a tholeiitic composition, related to the early stages of opening-up of the Iapetus Ocean and has an early Ediacaran age (580-610 Ma) (Gee *et al.*, 1985a; Kumpulainen *et al.*, 2016; Gee *et al.*, in prep.). On top of these units, having a higher metamorphic grade (mostly amphibolite and locally eclogite or greenschist facies; (Gee *et al.*, 2010), the Seve Nappe Complex makes up the uppermost unit of the Middle Allochthon. The Seve Nappe Complex is composed of psammitic and pelitic schists, gneisses, metasedimentary rocks and meta-volcanics/amphibolites with interbedded limestone, quartzite and ultramafic rocks (Du Rietz, 1935; Dyrekus *et al.*, 1980; Corfu *et al.*, 2014a). The sediments of this part of the Middle Allochthon were deposited on the western part of the Baltic basement and were later transported tectonically eastwards during the Scandian orogeny (Gee, 1975), probably representing the transition between the passive continental margin and the oceanic crust of the

Iapetus Ocean. The Seve Nappe complex has probably undergone a lingering history of sedimentation, magmatism and deformation during the whole Neoproterozoic (Corfu *et al.*, 2014a).

A post-metamorphic thrust separates the Seve Nappes from the overlying Köli Nappes (Gee *et al.*, 1985a). This thrust boundary can also be distinguished by a gradual increase in the metamorphic grade when moving down section in the units. A dismembered ophiolite can locally be recognized along the border between the Seve and Köli Nappes (e.g. Vågåmo in Gudbrandsdalen (Nilsson *et al.*, 1997) and Handöl in Jämtland (Bergman, 1993). Incomplete ophiolite fragments have also been recognized elsewhere along the Seve-Köli border, e.g. at Harsjøen east of Røros (Sundblad *et al.*, 2010) and at Raudfjellet further to the north in Trøndelag (Nilsson & Roberts, 2014). Furthermore, numerous solitary ultramafite pods, consisting of serpentine- and talc-altered dunites, harzburgite and lherzolite, can be followed for 150 km along the Seve-Köli border from Gudbrandsdalen to Røros (Nilsson *et al.*, 1997) (Figure 3).

Table 1 summarizes the lithology and stratigraphy within the Upper and Middle Allochthons of the Alvdal-Røros district.

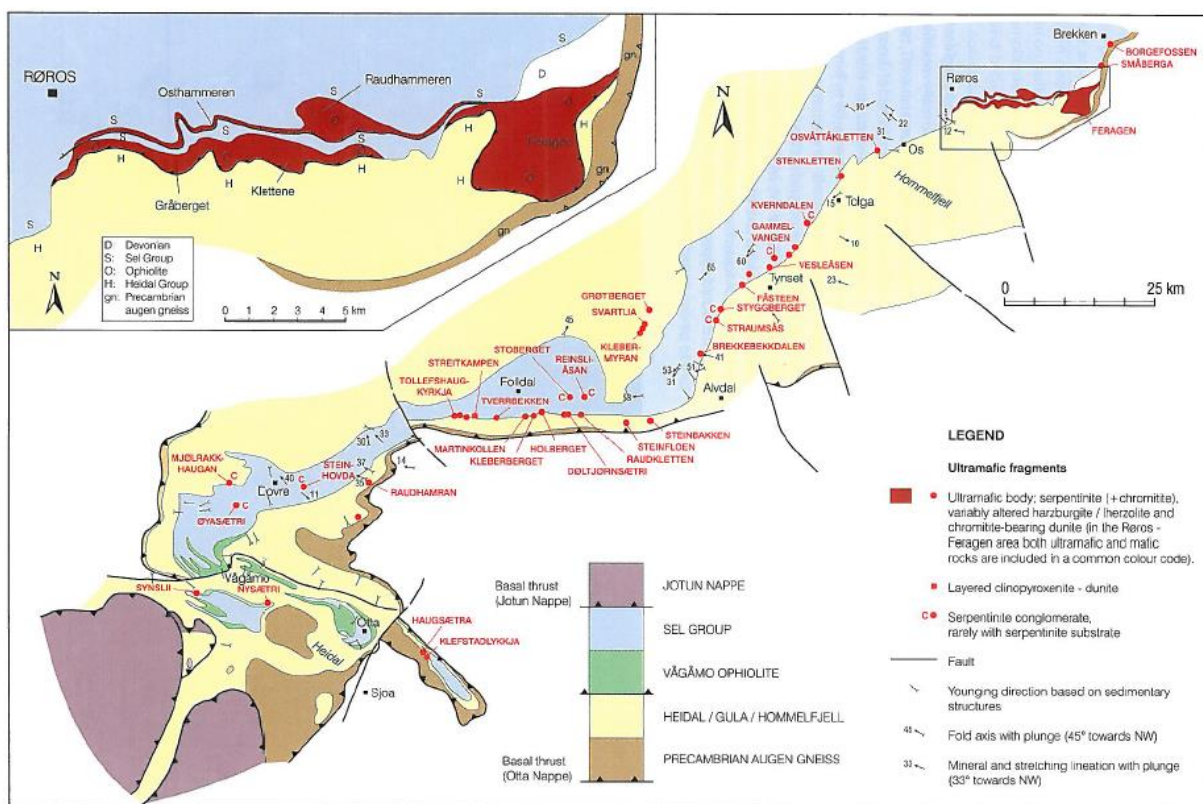




Figure 3: Geological map of the Røros-Gudbrandsdalen area, showing the location of ultramafic fragments (Nilsson *et al.*, 1997). The Tynset-Alvdal region is located (east) under the ultramafic fragments, within the Heidal/Gula/Hummelfjell group, in the central part of the picture.

Table 1: Overview of the units in the Upper and Middle Allochthons.

	Unit	Lithology	Metamorphic grade	Mineralisation
<b>Upper Allochthon</b>	<b>Tronden Complex</b>	Gabbro (olivine-bearing, noritic), dunites, metagabbro		
	<b>Köli Nappe Complex</b>	Volcanosedimentary and igneous rocks, ophiolite  Post-metamorphic thrust	Greenschist, granulite and eclogite	 <b>VMS</b>
<b>Middle Allochthon</b>	<b>Ultramafic fragments</b>	Serpentine- and talc-altered dunites, harzburgite, lherzolite		
	<b>Seve Nappe Complex</b>	Amphibolite, gneiss metasediments, migmatite, schist	Amphibolite (locally eclogite and greenschist)	Greenschist  <b>VMS</b> Mica schist
	<b>Särv Nappe</b>	Precambrian crystalline rocks, metasandstone, schist, marble, dolerite	Greenschist to epidote-amphibolite	
	<b>Tännäs Nappe</b>	Augen gneiss  Thrust sheet		



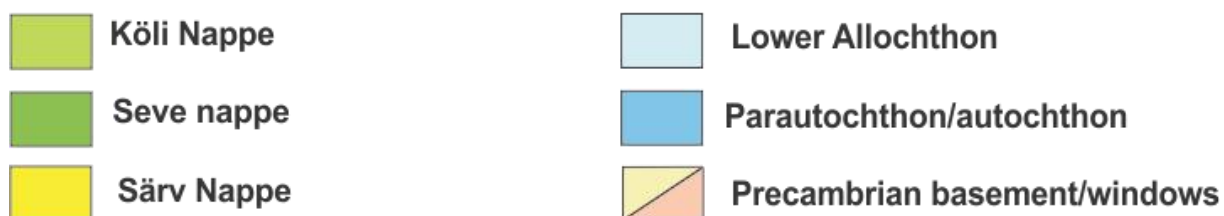
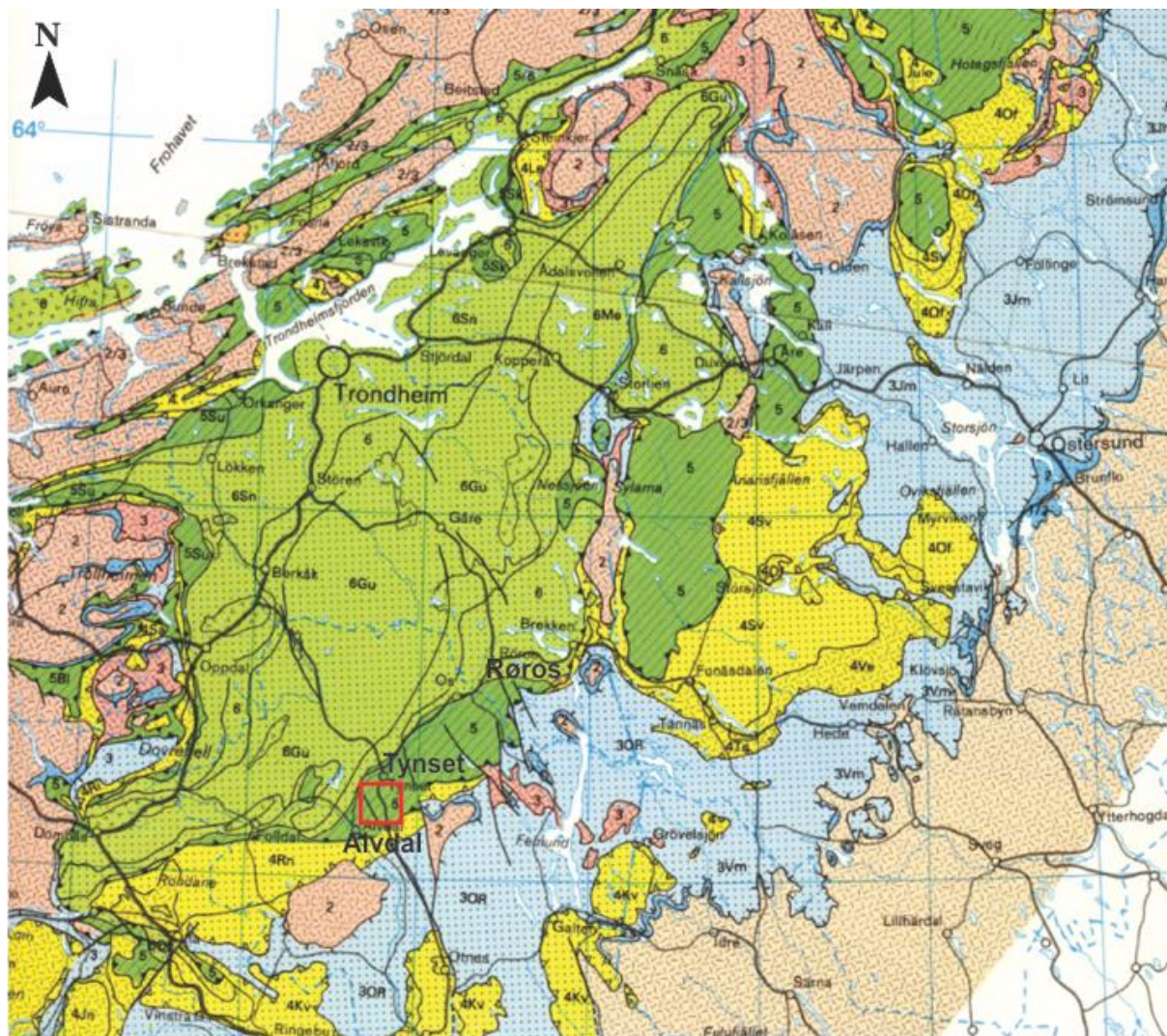


Figure 4: Geological setting of the major tectonic units in the central part of the Scandinavian Caledonides. The red square shows the study area (detail of a map published by (Gee et al., 1985b)).

### 1.5.3 The sulphide ores in the Tynset-Alvdal region

The study area is located within the Hummelfjell Group of the Seve Nappe (Ramsay & Siedlecka, 2001). The red square on the map in Figure 4 shows the study area and Figure 5 is a zoomed view, showing the locations of the mines. The Hummelfjell group is mainly composed of altered volcanic and sedimentary rocks, that have been affected by two tectonometamorphic events; the second related to the Scandian orogeny (Wellings & Sturt, 1998).

In the map in Figure 5, the Tännäs Augen gneiss is located to the southeast of the mountain Tron. The solitary ultramafites, that mark the boundary between the Seve and Köli Nappe Complex, trend NE-SW in the north-western part of the map. The sulphide ores investigated in this thesis, are located within lithologies that are situated between the ultramafites and the augen gneiss, stating a tectonostratigraphic position in the Middle Allochthon, most probably the Seve Nappe Complex.

The mountain Tron (or the Tronden Complex) is a layered mafic intrusion consisting of dunites and olivine-bearing to noritic gabbros and forms part of the Upper Allochthon (Wellings & Sturt, 1998). This mountain forms a synform, surrounded at the rims by a tectonic border to metamorphosed supracrustal rocks of the underlying Hummelfjell Group and is divided into three units: a central zone of olivingabbro, troctolite and pyroxenite; a transition zone of fine-grained olivingabbro, gabbro-norite; and a rand-zone of metagabbro and norite (Dreyer, 1974). Age determinations of the complex has not been done, but Wellings and Sturt (1998) assumed a pre-Scandian Orogenic age.

The ores are located within two different lithological units in the Hummelfjell group: greenschist/greenstone and chloritic to sericitic mica schist (Holmsen *et al.*, 1907; Bjerkgård, 1998). The greenschist, that locally is silicified, has an east-west trending foliation (with some variations SE-NW) with a dip to the north (and NE) (Bjerkgård, 1998). Ore minerals are mostly pyrite, pyrrhotite and chalcopyrite with some sphalerite and magnetite. The ore zone occurs as bands with semi-massive, fine-grained minerals (pyrite grains can be up to 2-3 mm wide) and is seen as a continuous zone in the mines (Geis, 1958). The ore minerals are often associated with quartz and chlorite, where the quartz appears as rounded clasts and chlorite as sheets. The altered rock is mainly expressed as a fine-grained chlorite-amphibolite schist and the parent rock is basalt (Bjerkgård, 1998).

The mica schist ranges from sericite to a chlorite-muscovite rich quartzo-feldspatic meta-sediment with an east-west trending foliation and a dip to the north (Holmsen *et al.*, 1907; Riiber, 1923). The sediment-hosted ores are dominated by chalcopyrite and pyrrhotite. Pyrite is common in the ore zone, and sphalerite is only seen in the southernmost part of the Tronsvangen area and in the Baugsberget mines. H-P Geis stated in 1958 that the ore zone has a great width, but the mineralization is mostly composed of irregular lenses of chalcopyrite and is therefore estimated as a non-profit mining area. The ore minerals are often associated with quartz, which is irregular and lens-shaped but follows the foliation of the mica schist. The

altered rock is a semipelitic to psammitic chlorite-muscovite schist and the parent rock is greywacke (Bjerkgård, 1998).

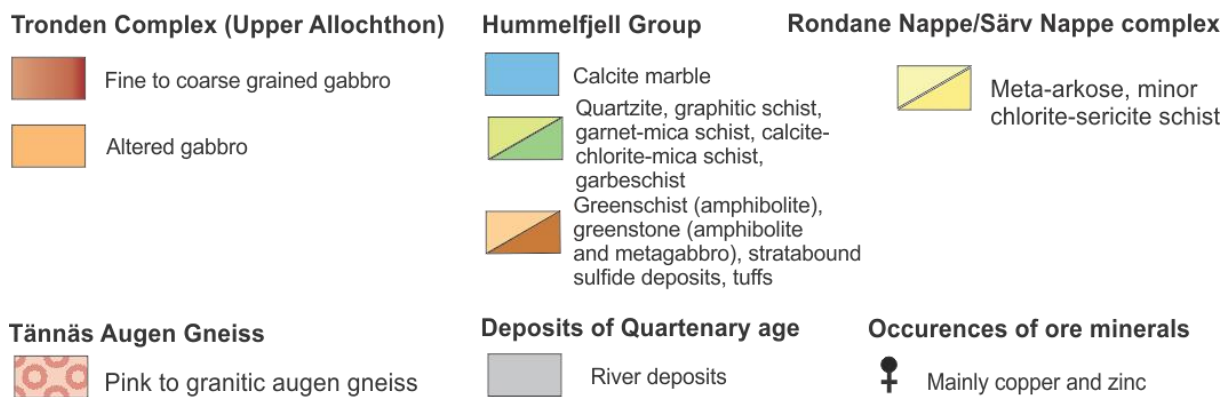
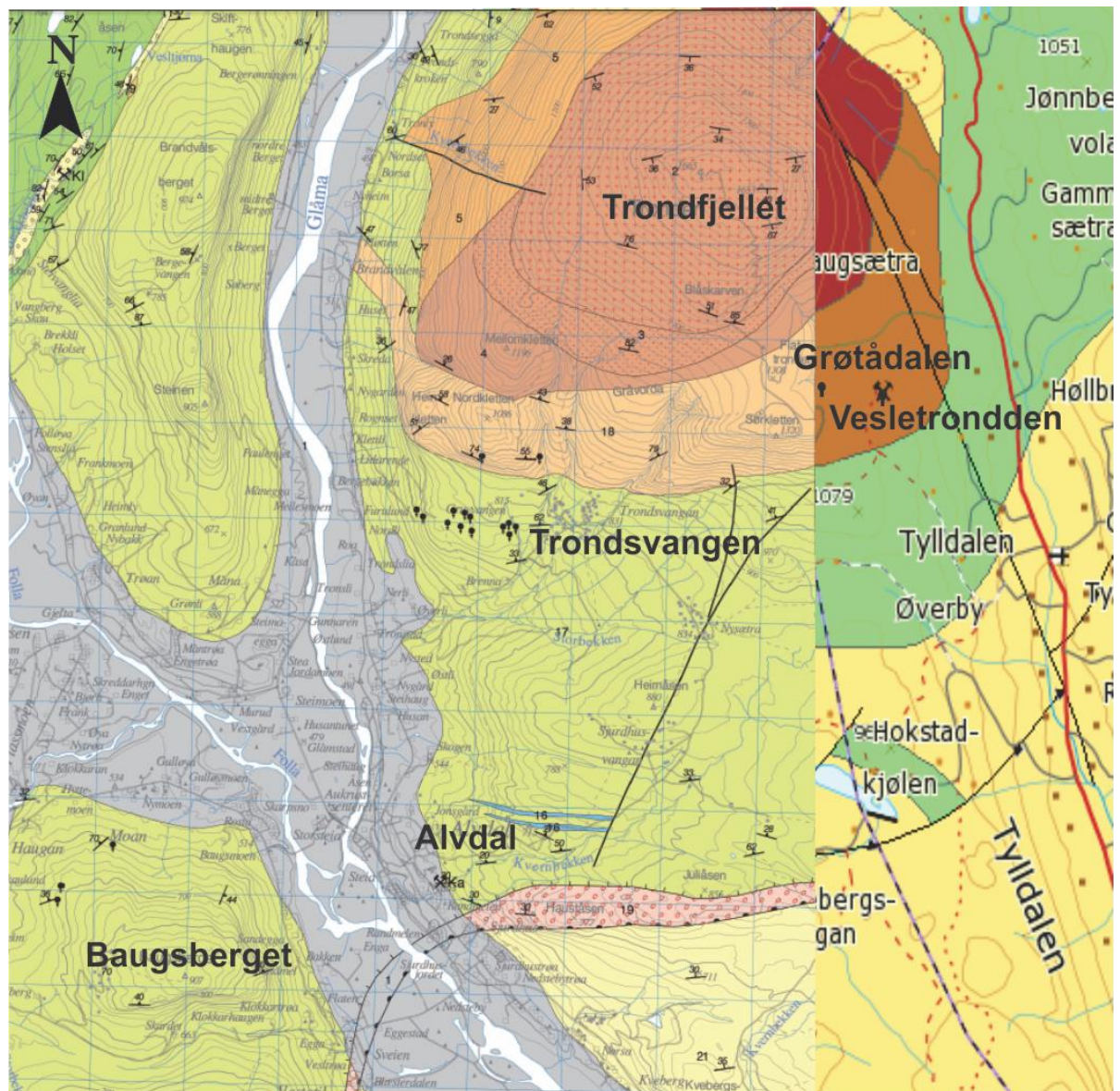


Figure 5: Bedrock map of the Tynset-Alvdal region with location of ancient mines. All the mines are located south of Trondfjellét and at Baugsberget. Modified from Nilsen and Wolff (1989)(right-hand part) and Ramsay and Siedlecka (2001)(left-hand and central parts).

#### ***1.5.4 Mining history***

During the early 17<sup>th</sup> century, King Christian IV initiated a national search throughout Norway to find metals, minerals and ores (Braseth, 1995). The first copper ores were discovered at Kvikne, Hedmark, around 1630 and at Røros, Sør-Trøndelag, in 1644 (Steimoeggen, 1966). The subsequent results of mining these resources were important for social and economic development and improvement of peoples living condition in the valleys of central-Norway. The demand of workers increased rapidly, followed by an increase in the population with associated building of new farms – a progress that was unthinkable without the mines. Local farmers and hunters were the ones to prospect and mine the metals, as well as establishing several local companies.

The first copper ore discovered in the Tynset-Alvdal region was at Baugsberget in 1658, and was mined by Lille-Elvedals Verk (Braseth, 1995). The mine was shut down in 1685 due to too low copper grades and limited amounts of ore, but was re-opened in 1739. A smelter (Lovise hytte) was established a kilometre from the Baugsberget mine in 1748, and in 1752 another mine (Nye Baugsberget) was opened. In 1762, 17 people and a supervisor worked in the mines (Braseth, 1995).

The golden years for mining in Alvdal was around 1760, when the copper price was high, with several mines and smelters in operation, all owned by Fredriks Gave Verk. After 1770, when less ore was excavated due to less ore available, the mining company had to find new targets. Gamle Tronsli mine was discovered in 1770 and was operated, together with the Tjæremyr mines, until the 1780s. There is little documentation about the amount of copper that was excavated, but in an overview from 1787 (Braseth, 1995) a total number of 1058 barrels of copper were reported taken from Gamle and Nye Baugsberget and Gamle Tronsli. The mining stopped when the smelter Lovise Hytte burnt down in 1818.

In the 1840s, the Nye Tron mine (located in Grøtådalen) was operated by the company Trondfjeld Interessentskab (Streitlien, 1978). In spite of sparse documentation, the remnants of the operations (dumps and holes) indicate quite a work done in the steep hillside.

The largest mine area is called Tronsli-feltet, located east of Tronsvangen, consisting of seven different mines and several exploration targets over a distance of 1 km. Gamle Tronsli and Tjæremyrgruvene were first mined in the 1770s, before a new company (Tronsli Grubesamlag) restarted mining in the 1880s (Steimoeggen, 1966). St. Knuts gruve is the only mine that has been documented in detail throughout the production years. In the 1880s and -90s over 700 tons

of copper-ore, with grades ranging from 6-14 %, was sold and around 1 500 tons of ore with uncertain quality was stocked (Holmsen *et al.*, 1907; Riiber, 1923). In 1887 the mine was operated by Christiania Minekompagni until it was shut down in the early 1890s due to low copper prices, primitive conditions for mineral separation and lack of exploration results. In 1907 a new company (A/S St. Knuts Gruber) claimed the area and started exploration work, both with negative and positive results. An adit at Sättå was initiated from the west, to investigate the mineralization zone from Sättå in the west to St. Knut in the east – a length of 1 km. Only 80 meters were finished when the money was consumed and the mines were shut down in 1911 (Steimoeggen, 1966). An overview of the location of the mines are shown in Figure 8 and 9.

## **1.6 VMS-type deposits**

### ***1.6.1 Introduction***

Volcanogenic massive sulphide (VMS) is a descriptive term used for several types of ore deposits, which are syngenetic accumulations of massive sulphides in submarine volcanic-hosted, volcanic-associated and volcano-sedimentary-hosted successions (Solomon, 1976; Franklin *et al.*, 1981; Large, 1992; Galley *et al.*, 2007). These types represent a major source for Cu and Zn, but some sub-types have also Pb, Ag and Au as economic important metals (Robb, 2005). They are also significant sources for Co, Sn, Se, Mn, Cd, In, Bi, Te, Ga and Ge, whereas some deposits also contain As, Sb and Hg (Galley *et al.*, 2007). The term “exhalation” is used here as fluid emanations from the sea floor (Franklin *et al.*, 1981; Doyle & Allen, 2003).

### ***1.6.2 The formation of volcanogenic massive sulphide deposits***

VMS deposits are formed by a hydrothermal ore-forming process, the same process that we can observe in “black smokers”. The precipitation of sulphides happens when exhaling hot hydrothermal fluids mix with seawater, resulting in accumulation of metal-rich sulphides at or near the sea floor in volcanically active marine environments (Large, 1992; Ohmoto, 1996; Franklin *et al.*, 2005). VMS deposits are found in a variety of tectonic settings (Robb, 2005) and are often referred to as volcanogenic, volcano-associated and/or volcano-clastic hosted massive sulphides.

In most VMS deposits, two components are essential related to the location of the ore zones (Figure 6): 1) a typical mound-shape to tabular, stratabound and stratiform massive sulphide ore body, and 2) in form of stockwork ore zone, consisting of veins and disseminated sulphides, often referred to as the stringer zone (Ohmoto, 1996; Doyle & Allen, 2003). Generally, the

massive ore body contains 90% or more of the heavy metals, the remaining <10% is found in the stockwork. The stockwork represents the hydrothermal fluids channel way and the massive ore is the accumulation area, either on the seafloor and/or within unconsolidated sediments.

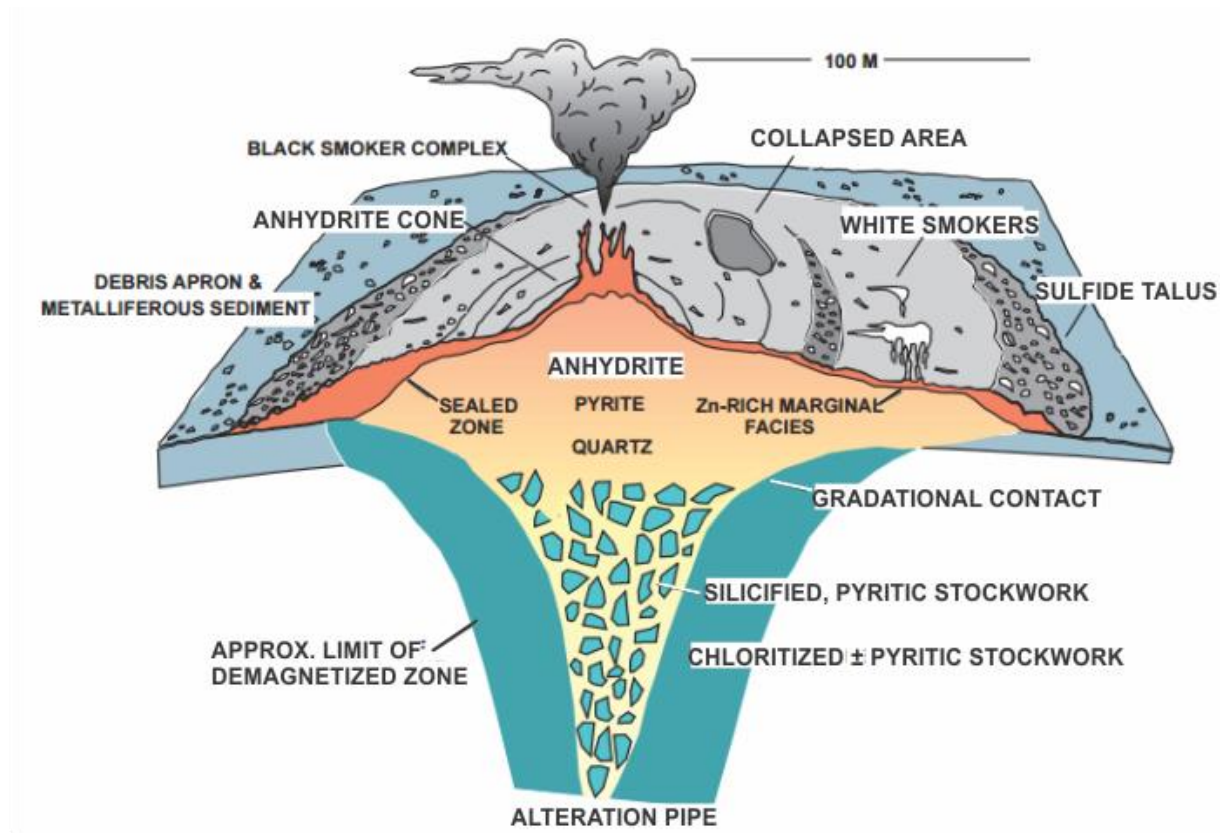


Figure 6: Schematic cross section through a typical VMS deposit and black smoker, with a semi-massive to massive sulphide ore body underlain by a stockwork vein system and an associated alteration zone. From Galley et al. (2007).

### 1.6.3 Classification of VMS deposits

A classification of VMS deposits can be based on the tectonic regime and/or lithology. The following is a generalized explanation of classical examples of different VMS deposit types, and some more recently discovered types.

**The Kuroko type** is a Cu-Zn-Pb variant related to island arc volcanism, consisting mainly of chalcopyrite, sphalerite and galena (Figure 7B) (Ohmoto, 1996). A broader term in Japan is used for all VMS deposits of Miocene age, but this type is found in older island arc systems in other part of the world. This type is formed by subduction of the oceanic crust, creating magma of intermediate to acidic composition. Zonation is typical in the Kuroko ores, where the typical Kuroko-ore (meaning black ore in Japanese) is massive banded sphalerite-galena-chalcopyrite-baryte ore located at the rims of the hydrothermal vent. The Cu-rich Oko and Keiko ore zones occur beneath the Kuroko ore.

**The Cyprus type** is a Cu-Zn variant formed along mid-ocean ridges as “black smokers” associated with ophiolites (Figure 7A) (Franklin *et al.*, 1981; Robb, 2005; Galley *et al.*, 2007). This type is represented by a lens of massive sulphide ore, consisting mainly of pyrite, chalcopyrite and sphalerite, located at the ocean floor and overlying the stockwork zone of disseminated sulphides. This type was first discovered in the Troodos ophiolite complex at Cyprus.

**The Escanaba type** is a VMS deposit hosted by turbiditic and hemipelagic sedimentary rocks and have been discovered by research in the Galapagos Rise, offshore South-America (1977), in the Escanaba trough, offshore Northern California (1979) and in the Guaymas basin, offshore north-western Mexico (Morton *et al.*, 1994). These studies showed that hydrothermal venting occurred at oceanic spreading centres, overlain by several kilometres thick turbidite layers, and that the deposition of sulphides took place on top of the sediment pile. Evidence of synsedimentary igneous activity was proven by the occurrence of gabbroic dykes within the turbidites, which is part of the oceanic rift. VMS deposition and related stringer zones occur in the uppermost part of the sediments. A sediment-starved mid-ocean ridge reflect the interaction between salt water and basalt, resulting in similar deposition and composition of the VMS deposits. The above-mentioned examples are all sediment-dominated mid-ocean ridges, where the composition of the hydrothermal fluids and the process are controlled by the sediments, resulting in different hydrothermal deposits and content of ore minerals.

**The Besshi Cu-rich VMS ore** has its name from one of the most classical ore districts in Japan and is located in sediment-dominated terranes with some mafic igneous rocks. It shows similarities to the Cyprus type regarding the ore-forming environment, but the entire system is deformed, metamorphosed and disrupted from its original position. The Besshi ore type has, therefore, been questioned whether it is a suitable example for a type deposit or not (Ohmoto, 1996; Sundblad *et al.*, 2006).

**The subsea-floor replacement VMS deposit type** is not as familiar as the other types of VMS deposits, but recent research indicates that this process is an important component and mechanism that contributes to the formation of large tonnage and/or high-grade VMS deposits (Doyle & Allen, 2003; Piercey, 2015). Subsea-floor replacement VMS deposits is characterized by the formation of sulphides and the replacement (infiltration and precipitation) in unconsolidated volcanic, volcano-sedimentary and sedimentary material in open spaces (fractures, voids) within the layers. Doyle & Rodney (2003) have formulated five criteria for distinguishing subsea-floor replacement in massive sulphide deposits:

1. Intervals of mineralization within rapidly emplaced volcanic or sedimentary facies.
2. Pieces of the host rock within the mineral deposit.
3. Occurrences of replacement fronts between the mineral deposit and the host rock.
4. Discordance between the mineral deposit and bedding.
5. A strong hydrothermal alteration that is evident also in the hanging wall without any decrease in the intensity.

Criteria 1-3 are diagnostic of replacement, while 4-5 may suggest so but are not alone diagnostic. A typical texture in the ores are the growth of framboidal pyrite as well as reduced sulphur in the host rock (Piercey, 2015). Three different types of massive sulphide deposits that are dominated by subsea-floor replacement have been identified by Doyle & Allen (2003): Subsea-floor replacement deposits in volcanoclastic rocks, within lavas and intrusions, and within limestone (Figure 7F-L).



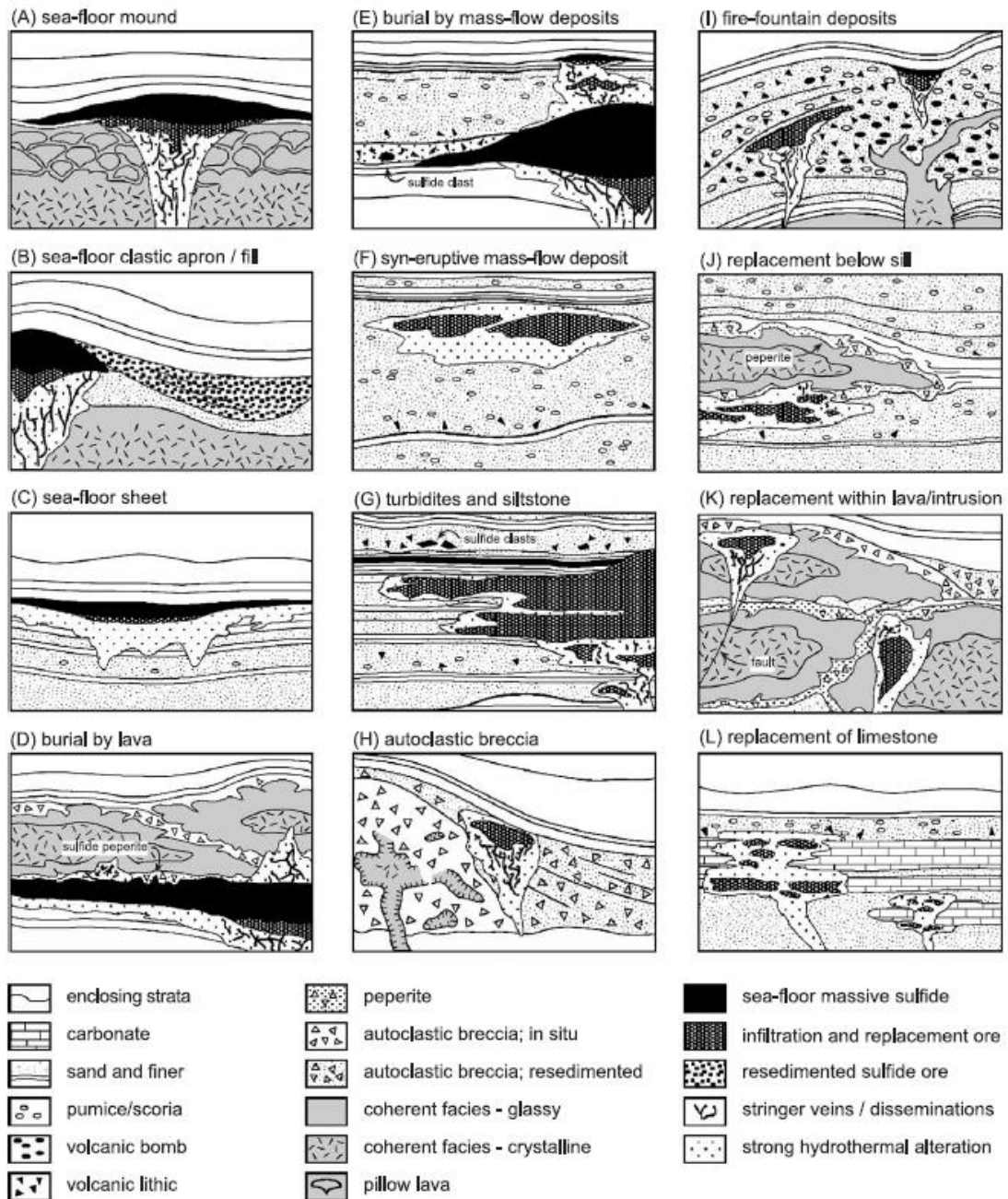


Figure 7: Schematic overview of the different types of VMS deposits presented by Doyle & Allen (2003) showing the relationship between lithology, alteration and massive sulphides. A-C show seafloor deposits (A is the Cyprus type, B is the Kuroko type, C is a variation of the Escanaba type), D-E show sea-floor deposits modified after burial by lava or volcaniclastic deposits, F-L represent subsea-floor replacement (F-J represent subsea-floor replacement deposits in volcaniclastic rocks, K represents within lavas and intrusions, and L represents deposition within limestone).

#### ***1.6.4 Sulphide ore deposits within the Scandinavian Caledonides***

Sulphide ore deposits within the Scandinavian Caledonides are found in the Autochthon, the Middle, Upper and Uppermost Allochthon. The VMS ores in the Köli Nappes were formed at the same time as the surrounding rocks, thus constituting several examples of syngenetic ore deposition. The ores related to ophiolite sequences (e.g. Løkken and Visnes) are typical examples of the "Cyprus type" (Grenne, 1989) while the ores related to the island arcs (e.g. Stekenjokk) are typical examples of the "Kuroko type" (Zachrisson, 1984). The turbidite-hosted VMS ores in the Røros district (Norway) as well as at Ankarvattnet and Ruonasvagne (Sweden) have been proposed to be related to an "Escanaba model" (Sundblad, 1981; Sundblad, 1991; Sundblad *et al.*, 2006; Sundblad *et al.*, 2010). Although few studies of the genesis of the sulphide ores (e.g. Bleikvassli) and oxide ores (e.g. Dunderlandsdalen) in the Rödingsfjället Nappe Complex have been done, these ores are also considered as syngenetic (Cook *et al.*, 1998; Lindberg, 2015). In contrast, the Pb-Zn mineralization in sandstone along the Caledonian Front (e.g. Laisvall and Vassbo) are typical examples of epigenetic processes, where fluids created the mineralizations during the late Silurian to early Devonian in conjunction with the final phase of the Caledonian orogeny. The fluids migrated eastwards from the inner parts of the Caledonides (and the Precambrian basement) and precipitated galena, sphalerite, calcite and fluorite in high-porosity rocks (as sandstones) (Grip, 1954; Rickard *et al.*, 1979; Kendrick *et al.*, 2005).

## **2. Methods**

### **2.1 Archive and literature studies**

Prior to the field work, research about the mines was necessary for getting appropriate knowledge on their history and location. Information about the mining history was received from historical books available at the local libraries at Tynset and Alvdal, and documents in the archives of NGU. The documents span from old mining reports and maps (e.g. Aalen, 1907) to recent reports by Terje Bjerkegård (1998) and geological map made by Ramsay and Siedlecka (2001). Several local residents, among them Berit Kjølhøg (Haugan) and Roar Hokstad (Tyllaldalen), were also interviewed to obtain valuable unwritten knowledge.

### **2.2 Field work and sample collection**

The fieldwork was done during 5 weeks in June, August, September and October 2015 with GPS, compass, hammer and measure tape as the most important tools. The first and most critical task was to locate all the mines and dumps, which was followed by mapping and characterizing geological elements as rock/ore types, alteration zonation and structures, as well as measuring and mapping mine pits, dumps, prospecting wells and ditches. Another important task was to collect samples of ore, altered rock and host rock for petrographical and geochemical investigations (all in all 74 samples). Ore samples were collected based on the amount and quality of ore, altered rocks were taken close to the ore mineralization, and samples of the host rock were taken a distance of at least 100 m from the mines to avoid contamination from the ore forming processes. An overview of the samples are presented in the appendices.

### **2.3 Preparation for microscope samples**

Thirty-seven of the 74 samples were selected for making thin sections, where the selected ones have to be a representative amount of the ore sample or host/altered rock. The samples were cut into cubes (~1.5x2x3 cm), prepared and polished in the laboratory at the Department of Geology, UiT (an overview of all the thin sections are listed in the appendices).

### **2.4 Microscopy work**

Microscopy of the thin sections were done using the petrographical microscope Leica DM4500P. Both transmitted and reflected light was used together with plane- and cross-polarized light to determine the minerals. All thin sections contain silicates and several also contain opaque minerals (sulphides and oxides). A camera mounted on the microscope was used to take pictures of the thin sections. The software CorelDraw was used to process the pictures.

SEM (Scanning Electron Microscopy) and EDS (Energy Dispersive X-ray Spectroscopy) were used to obtain the chemical composition of the mineral grains to assist the determination of unidentified minerals seen in the Leica microscope.

A list of abbreviated mineral names used from (Kretz, 1983) is enclosed in the appendices.

## **2.5 Preparation for geochemical analysis**

A representative amount of 34 selected rock samples were cut in cubes of  $\sim 5\text{cm}^3$  and sent to Activation laboratories Ltd. in Ontario (Canada) for whole rock geochemistry. All the samples were prepared by ActLabs (crushing and milling). Then the samples were analysed using Major Elements Fusion package and the mineralized samples were analysed using assay packages.

The methods used were Code RX-1, 4LITHO Major Elements Fusion ICP(WRA)/Trace Elements Fusion, ICP/MS(WRA4B2), code UT-3 INAA (INAAGEO)/Total digestion ICP (Total) Total Digestion ICP/MS.

All of the analytical work, methods, detection limits and standardized values are described in the certificated analytical report A15-10688 produced by Actlabs Ltd. A complete overview of the analytical data is presented in the appendices.

The analytical data were processed in Excel and GCDkit in order to construct various element diagrams and petrology plots.

### 3. Observations and results

#### 3.1 Revised geological maps

The field area has few outcrops besides the nearest surroundings to the mines, and the mapping was challenging. However, some lithological and structural measurements were done in restricted areas, revealing two distinct lithologies (mica schist and greenschist) with a metamorphic fabric in an overall east-west trending foliation with a moderately inclined dip to the north. The maps in figure 8 show the three studied areas, while the map in figure 9 is a zoomed overview of the Tronsvangen area, all marked by red squares in figure 1. The sample locations are indicated by yellow (ore) and red (bedrock) circles.

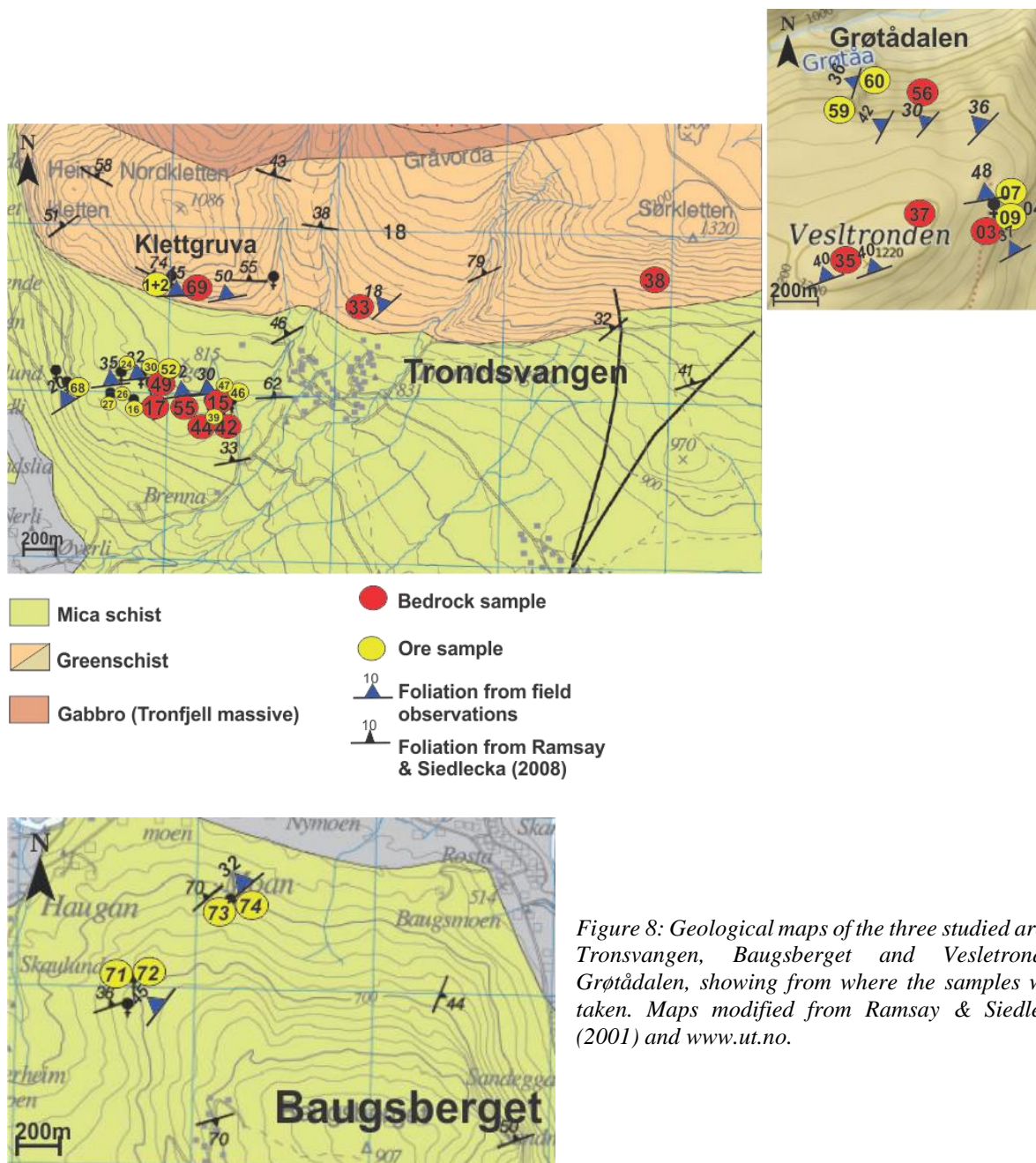


Figure 8: Geological maps of the three studied areas: Tronsvangen, Baugsberget and Vesletronden-Grøtdalen, showing from where the samples were taken. Maps modified from Ramsay & Siedlecka (2001) and www.ut.no.

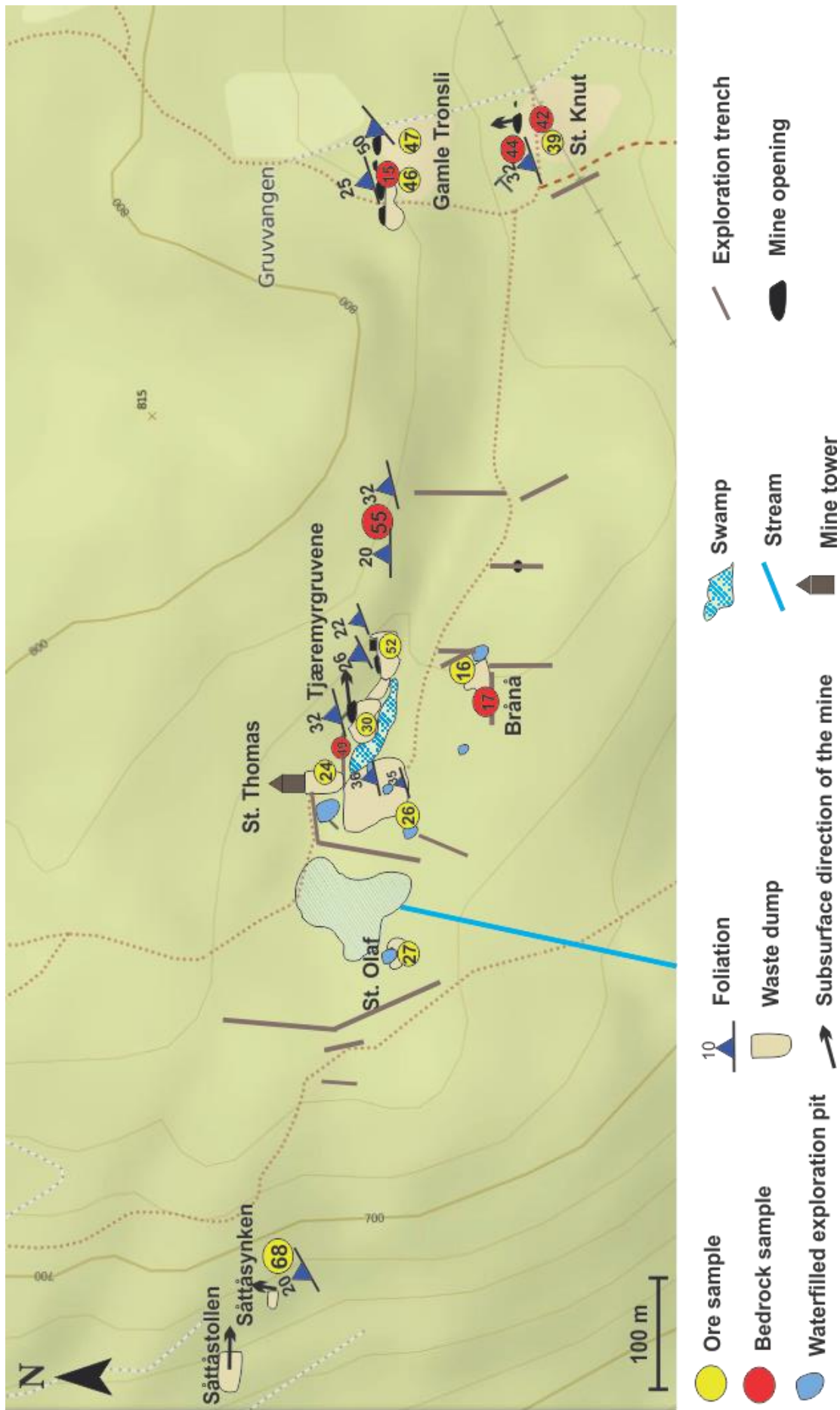


Figure 9: Overview map of the Tronsvangen area, showing structural measurements, from where the samples were taken and the location of the mines and waste dumps.

## **3.2 Field observations of rocks and ore deposits**

### **3.2.1 Volcanic rocks**

The upper lithology, extending in an east-west trending direction from Tronsvangen to the foot of the mountain Tron, is a greenschist/greenstone rock (Figure 8). The rock is massive, homogenous, has a greenish color, looks like a metamorphosed igneous rock with uniform grain size ranging from fine to very-fine grained. The only structural element observed is a foliation with approximately 10-20 cm wide beds. The rock is generally hard with poor cleavage. Calcite veins occur as infill in cracks. The minerals that were determined in hand specimen are chlorite (green), amphibole (black), quartz/feldspar (light) and calcite, (with a ratio of 1:1:1 between the chlorite, quartz/feldspar and amphibole).

### **3.2.2 Metasedimentary rocks**

A different lithology, a mica schist, occurs south of the greenschist, from the Tronsvangen area towards the south to Alvdal and west to Baugsberget. The rock is heterogeneous and sandy-arkosic in some outcrops and more mica-rich in others, medium to fine grained and green to greyish. It has a strong NE-SW trending foliation with a dip to the northwest. This rock is locally easy to break between the fingers with a flour-like consistency, while in other localities it needed a hammer to be broken. Some small-scale folding is observed, but this could not be followed into big-scale folds. It consists of quartz, mica (sericite), chlorite and feldspar. Quartz appears both as grains in the matrix of the rock and in lenses following the foliation, length ranging from 5 to 20 cm.

### **3.2.3 Ores hosted in volcanic rocks**

Observations done in the field revealed that only Klettgruva and Grøtådalen have open mine entrances. The mines were never explored or examined inside, due to the risk of possible rock falls. Therefore, the ore zone was observed at the entrance and by studying the material located at the dumps. The ore mineralization is massive and straight with a clear rusty zone on both sides. The ore zone follows the foliation of the layers, with a dip towards the north (west). Minerals observed are pyrite and chalcopyrite, and sometimes a darker mineral is also observed, probably sphalerite. The host rock is interpreted to be a dark green-grey greenschist, the altered rock ranges between a quartz-sericite schist and a dark grey amphibolitic schist. The dump wastes are examined in every locality, showing massive mineralization of pyrite and chalcopyrite. All ore samples are taken from the dumps.

### **3.2.4 Ores hosted in metasedimentary rocks**

The mines situated within the mica schist still have open entrances, except Sättåstollen. None of them were explored or examined inside, due to the risk of rock fall. The ore zone was observed at the entrance and by looking as far as possible within the mines. The field observations revealed that the ore mineralization is irregular with lenses and bands of semi-massive to massive mineralization, which show local small-scale folding. The observed ore minerals are pyrite, chalcopyrite, sphalerite and pyrrhotite. Malachite is often seen at the mine entrances, not far away from the mineralized zone. The direction of the ore mineralization is constant in every mine: north-west/south-east. A clear rusty zone is seen around the ore zone. The host rock is a chloritic mica schist and the altered rock is a sandy equivalent of the host rock.

## **3.3 Petrographic description of rocks**

### **3.3.1 Volcanic rocks**

This rock type is characterized by the large amount of chlorite, presence of amphibole and plagioclase, and the relatively low content of quartz (only observed in the fine-grained matrix together with plagioclase) (Figure 10). This represents a typical mineral assemblage for basalts which has undergone greenschist facies metamorphism (Le Maitre *et al.*, 1989). Accessory minerals are calcite (as vein material) and epidote (included in the chlorite).

Chlorite grains are green (pale to dark) in PPL and shows anomalous interference colors (turquoise, yellow, blue, red, pink) in CPL (Figure 10). It has flake-like anhedral grains with a preferred orientation, with grain size ranges from 20  $\mu\text{m}$  to above 2mm.

The feldspar is typical pale/colorless which shows fractures and cloudy texture in PPL, and shows Carlsbad twinning in CPL. The grains are anhedral to subhedral, ranging from very-fine grained (when appearing as matrix) to 0.1 mm. This feldspar is concluded to be the plagioclase anorthite. Quartz is only seen in the matrix.

Amphibole is not seen in every sample, but shows a typical 60-120 degree cleavage and high interference colors (yellow and pink) in CPL (Figure 10F). The grain size varies between 60 and 500  $\mu\text{m}$ . In one sample (*what sample*) the amphibole is altering towards chlorite.

Quartz and mica, often foliated and sometimes folded, are the dominating minerals in ore samples (Figure 10D). The quartz grains are anhedral, aligned in layers and show subgrains and undulatory extinction.



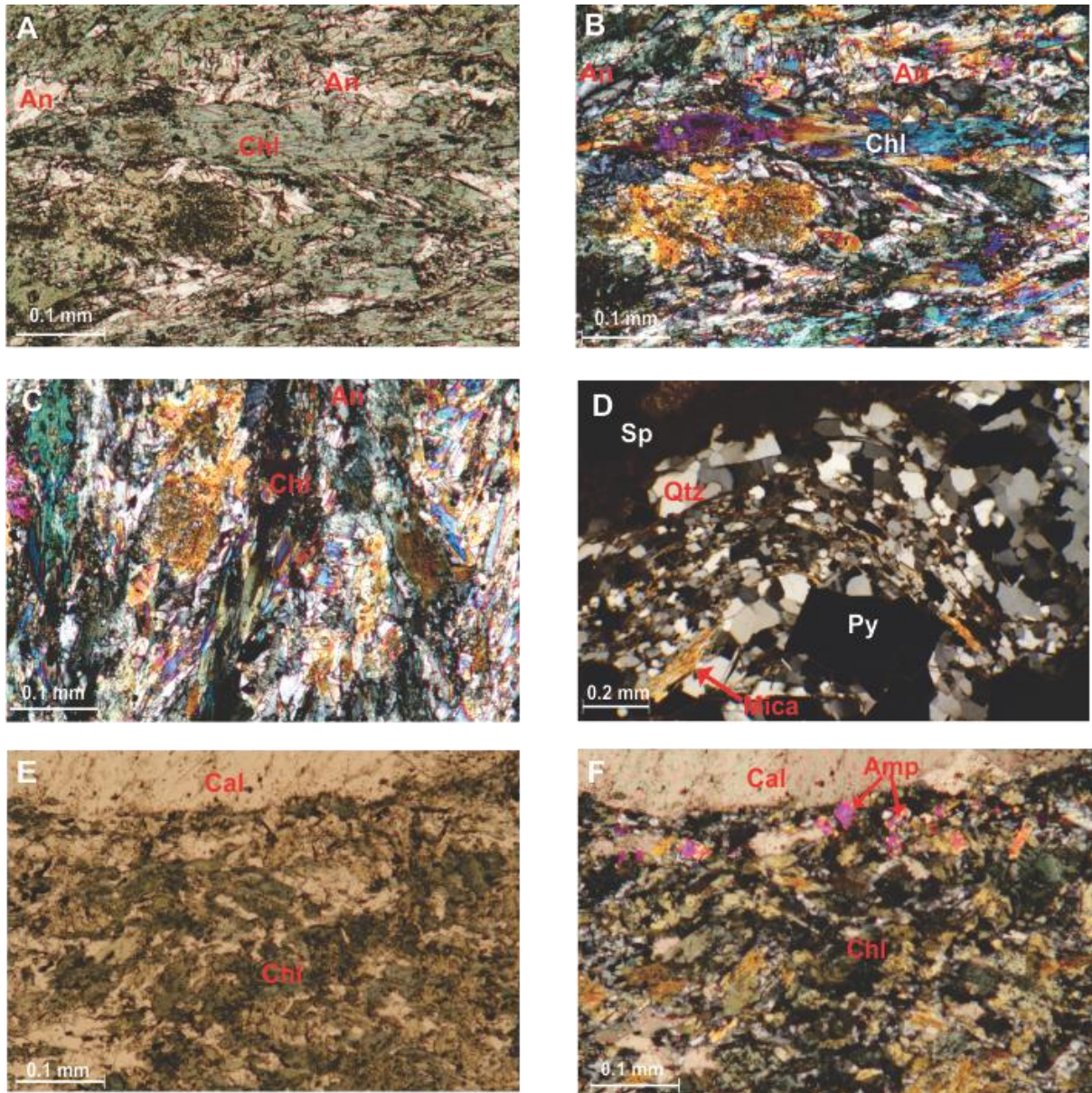


Figure 10: A: Chlorite and plagioclase dominate the sample, observed in PPL. B: The same view in CPL. C: Picture B turned 90 degrees, where the anomalous colors of chlorite and extinction are seen. D: Greenschist-hosted ore sample, showing foliation and folding of quartz and mica between sphalerite and pyrite. E: Typical greenschist, note the big calcite grain at the top. F: Picture E in CPL, where amphibole grains are clear. Chlorite do not show anomalous colors. Pictures A-C are from ML1535, picture D is from ML1503, E and F are from ML1556.

### ***3.2.2 Metasedimentary rocks***

The metasedimentary rock is characterized by foliated quartz and white mica as the dominating minerals, with the presence of plagioclase. Accessory minerals are calcite and chlorite. This rock type is determined to be a mica schist based on the mineral assemblage and structure (Travis, 1970).

Quartz grains are anhedral, often aligned in layers oriented with the foliation, irregular grain boundaries, show subgrains (core-mantle structure) and undulatory extinction with grain sizes ranging from 0.1 to 0.4 mm. Quartz also appears as very fine-grained in thin layers between coarser grained layers, often associated with chlorite (Figures 11 D, E). The deformation is called dislocation creep by subgrain rotation, indicating a medium temperature and water content deformation/recrystallization (Passchier & Trouw, 2005).

The white mica has typically elongated flake grains with perfect cleavage, white or colorless in PPL and show variable interference colors in CPL (pink, yellow, blue, green and orange). They have a preferred orientation, with grain size very constant around 0.2 mm, but appears also as fine-grained masses (~0.05 mm) (Figures 11 G, H).

Plagioclase occurs as rounded to subangular clasts with grain sizes ranging from 0.15 to 0.6 mm, oriented randomly without subgrains. Smaller quartz grains are found at the front and tail (aligned with the foliation) of some clasts (Figures 11 A-C).

Calcite is observed as both veins and single crystals within the matrix, with a grain size between 0.1 to 0.5 mm (Figures 11 G, H).

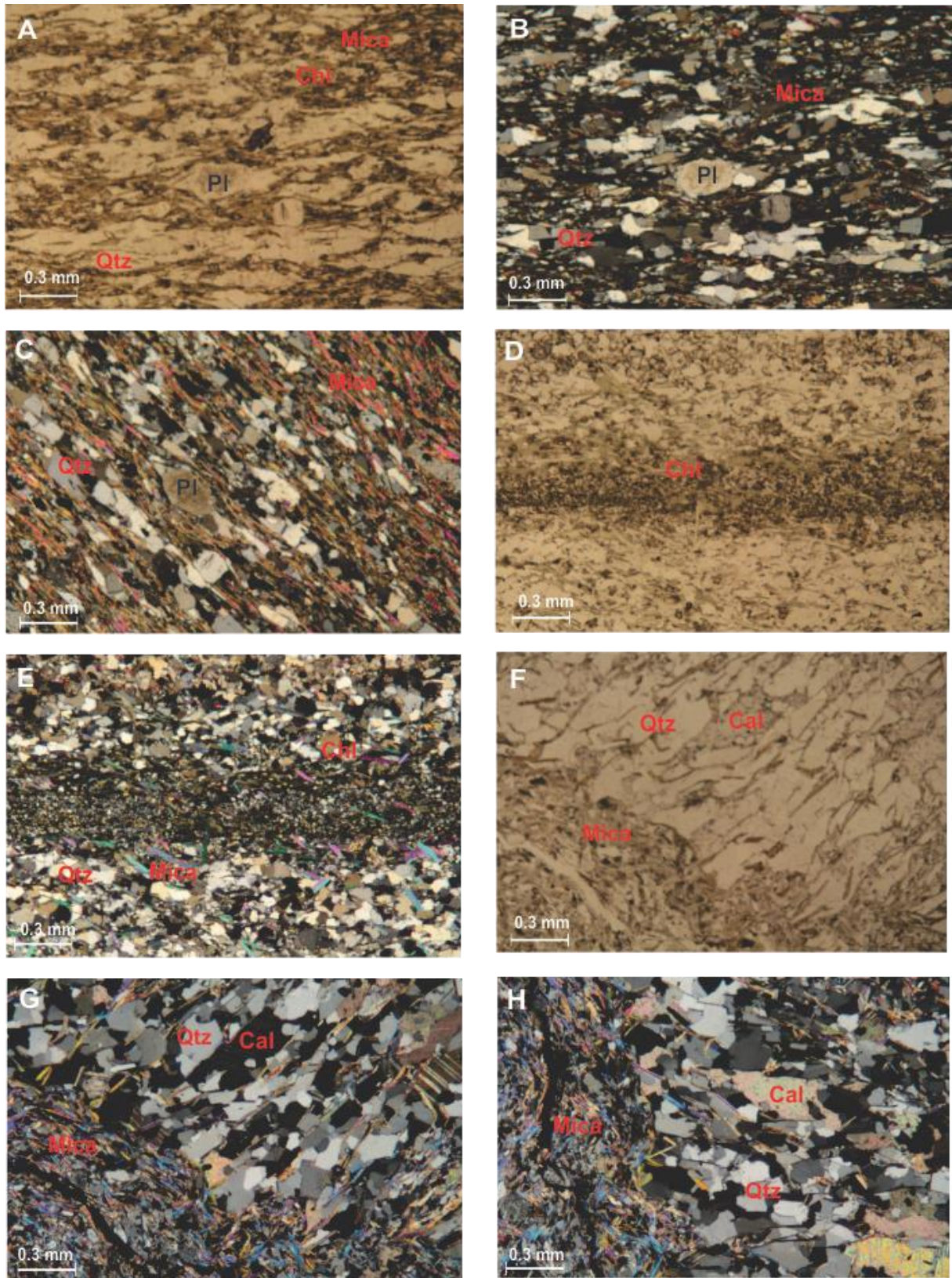


Figure 11: Picture A-C show a typical mica schist, with layered mica and quartz, and randomly distributed clasts of plagioclase. B and C are in CPL (pictures are from sample ML1549). D-E: Layers of different grain sizes of quartz associated with chlorite (sample ML1555). F-H: Quartz with subgrains, calcite and mica cut perpendicular by a mass of mostly mica (sample ML1554).

### **3.4 Petrographic description of ore mineralization**

#### **3.4.1 Ores hosted by volcanic rocks**

Thin section studies show that the greenschist-hosted ores are dominated by pyrite, with variable contents of chalcopyrite and sphalerite, and with little or no pyrrhotite. The matrix is always dominated by quartz, with variable contents of chlorite and mica.

Pyrite appears in many varieties: as perfect cubes to round grains, sizes ranging from 0.05 to 2 mm. The pyrite may exhibit pores and inclusions, and can be homogenous and without fractures to heavily fractured and brecciated. Pyrite grains are found both as single grains and as aggregates where they are intergrown with each other; they are impinging on another (Figures 12 A-D). Rounded and fractured grains are interpreted to be caused by "Durchbewegung" (Vokes, 1969).

Sphalerite and chalcopyrite occur almost always together and appear as massive mineralization along rims or in cracks of fractured pyrite (Figures 12 B, G-H). Chalcopyrite-disease, i.e. the frequent occurrence of small chalcopyrite blebs in sphalerite (Barton & Bethke, 1987), is also observed. A dark rim around chalcopyrite is observed and investigated in the SEM/EDS, concluding to be a weathering towards sulphates (appendix F). Sphalerite also occurs as massive veins, in pyrite grains and cracks in the host rock itself (Figures 12 C, H).

Only one greenschist-hosted ore deposit, Grøtådalen, (samples ML1559+60) has pyrrhotite, which occurs both as massive aggregates and as disseminated single grains. The single grains show two distinct textures (Figures 12 E, F): one is fibrous/flame-like and the other is irregular elongated and/or subhedral with bays and spits. Both types show light-brown grains that are found on a brighter yellow base/matrix. Fractures are also seen. The fibrous grains (Figure 12 F) have irregular, subangular and subspherical shapes when they are in contact with other pyrrhotite grains, and show more irregularities when they are in contact with other opaque ore minerals (pyrite, chalcopyrite). The grain sizes range from 0.15 to 1.25 mm. The fibrous texture within the grains do not have a fixed orientation. The fibers have not been successfully determined microscopically, but are interpreted to be an alteration/weathering towards iron oxide-hydroxides based on SEM and EDS analysis (appendix F). The sizes of the irregular elongated/subhedral grains (Figure 12 E) range from 0.2 to 1 mm. This texture is called a "Zwischenproduct" by Ramdohr (1980), or a decay texture, which means that pyrrhotite is altered to a pyrite-like substance.

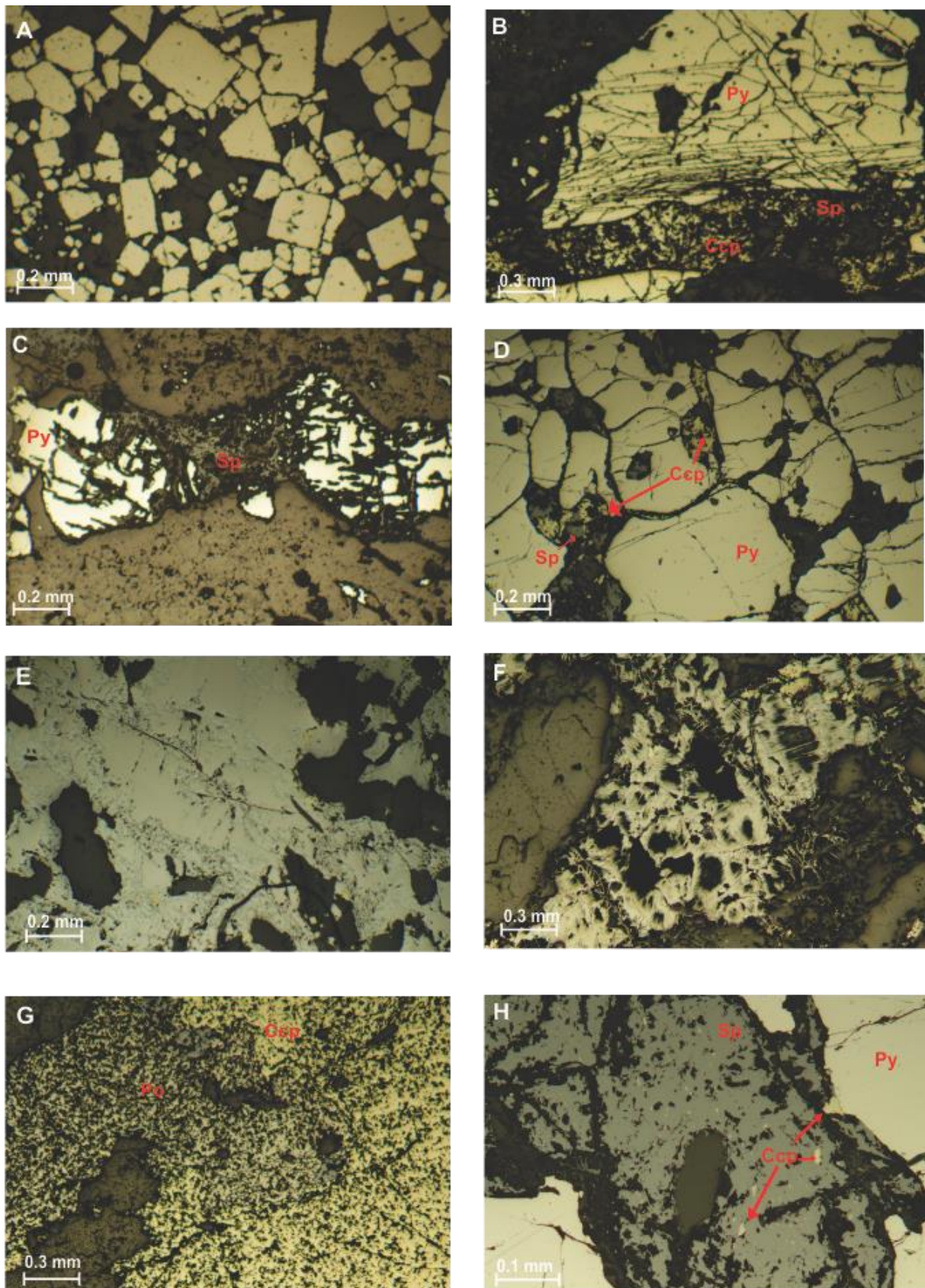


Figure 12: Ore mineralization in greenschist: A) Typical cubic and angular shapes of pyrite grains in different sizes. B) Fractured and cataclastic pyrite grains. Chalcopyrite and sphalerite are localized between the two pyrite grains. C) Pyrite grains fractured and filled with sphalerite. D) Rounded and fractured pyrite grains. Note that chalcopyrite and sphalerite have filled in cracks between the pyrite grains. E) Pyrrhotite showing a decay texture.

*F) Weathered, fibrous pyrrhotite grains. G) A distinct boundary between massive pyrrhotite and chalcopyrite. H) Chalcopyrite-disease in sphalerite. Pictures are taken from samples ML1501, -02, -04, -07, -5 and -60.*

### **3.4.2 Ores hosted by metasedimentary rocks**

The ores hosted by the mica schist are dominated by pyrrhotite, with little or no pyrite, and variable contents of chalcopyrite, sphalerite and galena. Some samples are very rich in chalcopyrite, while others are rich in sphalerite. The matrix is mainly composed of chlorite and mica, with variable contents of quartz, often seen as lenses or clasts.

Pyrrhotite is the dominating ore mineral in the mica schist-hosted ores, and forms massive aggregates and single grains (Figures 13 C, E-H). The single grains show two distinct textures: one is fibrous/flame-like and the other is irregular elongated and/or subhedral with bays and spits. Both types show light-brown grains that are found on a brighter yellow base/matrix. The fibrous grains range from 0.07 to 0.30 mm have not been successfully determined, but are interpreted to be a weathering towards iron oxide-hydroxide, based on SEM and EDS analysis (appendix F). The other texture, which is the most abundant, is a result of the decay texture, alteration of pyrrhotite to pyrite. The grain size ranges from 0.10 0.35 mm.

Pyrite is the most common sulphide mineral in all samples and occurs in a wide variety (Figures 13 A-C, E). The grains are cubic, angular and rounded with sizes ranging from 0.02 to 1 mm. The grains are moderately fractured and impinge on each other, showing evidence of annealing. The space between the grains is often filled with chalcopyrite. Several samples show spheroidal or colloidal botryoidal pyrite grains in a pyrrhotite matrix (Figure 13 C). They occur as small concentric grains with sizes ranging from 0.05 mm to 0.3 mm and show a clear zoning of growth circles.

Chalcopyrite and sphalerite occur often together in massive aggregates, often with common chalcopyrite-disease textures (Figure 13 D). Sphalerite occurs also as scattered small blebs within chalcopyrite (Figure 13 G). A darker orange/brownish rim is seen around chalcopyrite in some samples, often in contact with calcite, which has been investigated in SEM and concluded to be a weathering.

Galena has been recognized sparsely in three mines in the central part of the Tronsvangen area (St. Thomas, St. Olaf and Tjæremyr), with grain sizes ranging from 10 µm to 0.15 mm. The galena grains are localized along rims of chalcopyrite and sphalerite (grain boundaries), within the other ore mineral grains and in holes within the silicate minerals. Use of SEM and EDS revealed that the galena grains contain small inclusions (10µm) of bismuth and tellurium bearing phases (appendix F).

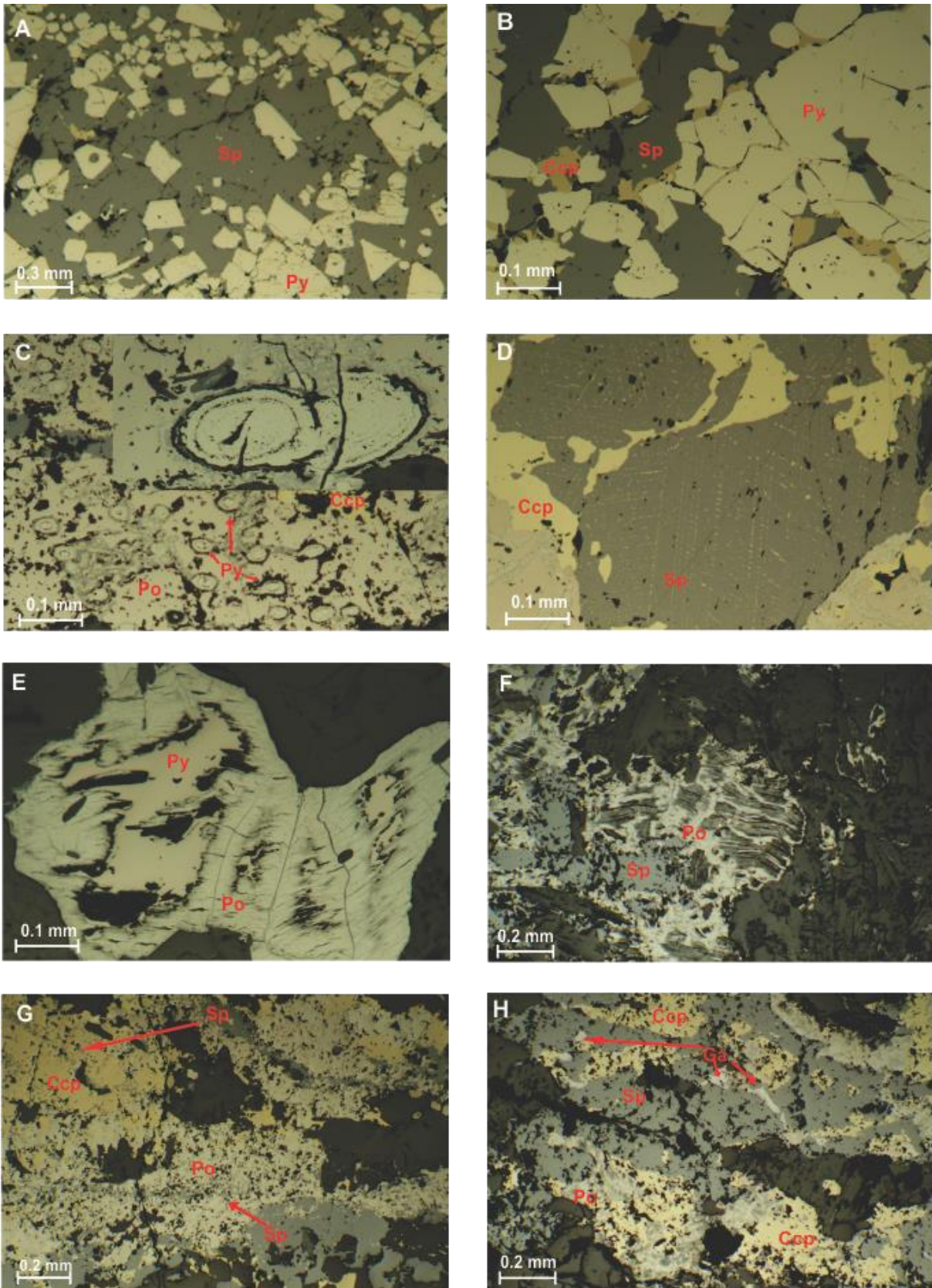


Figure 13: Typical ore mineralization in mica schist: A) Variable sizes and shapes of pyrite grains in a sphalerite matrix. B) Rounded and annealed pyrite grains in a sphalerite matrix. Note the chalcopyrite infill in cracks and between pyrite grains. C) Different sizes of botryoidal or colloform texture in pyrite in a pyrrhotite matrix. D) Chalcopyrite-disease in sphalerite. E) Decay texture of pyrrhotite to pyrite. F) Fibrous and altered pyrrhotite.

G+H) Typical assemblage of ore minerals in mica schist: sphalerite, chalcopyrite, pyrrhotite and galena. Note the blebs within chalcopyrite in G. Pictures are taken from samples ML1517, -26, -27, -52, -68 and -71.

Table 2: Summary and overview of the mineral content, texture and location of the ores.

	Sample	Locality	Py	Po	Ccp	Sp	Ga	Texture
GREENSCHIST-HOSTED ORES	ML1501	Klettgruva	X			X		Fractured pyrite
	ML1502	Klettgruva	X		X	X		Rounded and fractured pyrite, chalcopyrite-disease
	ML1503	Vesletronden	X		X	X		Fractured and rounded pyrite, chalcopyrite-disease
	ML1504	Vesletronden	X		X	X		Fractured and rounded pyrite.
	ML1507	Vesletronden	X		X	X		Heavily fractured and rounded pyrite
	ML1509	Vesletronden	X		X	X		Heavily fractured and rounded pyrite
	ML1559	Grøtådalen		X	X	X		
	ML1560	Grøtådalen		X	X	X		Decay and fibrous pyrrhotite
MICA SCHIST-HOSTED ORES	ML1516	Brånå		X	X	X		
	ML1517	Brånå	X	X	X	X		Botryoidal pyrite, chalcopyrite-disease
	ML1524	St. Thomas		X	(X)	X	X	
	ML1526	St. Thomas	X	X	X	X	X	Decay and fibrous pyrrhotite.
	ML1527	St. Olaf	X	X	X	X	X	Decay of pyrrhotite, alteration of chalcopyrite.
	ML1530	Nedre Tjæremyr	X	X	X	X		Botryoidal pyrite, decay of pyrrhotite.
	ML1539	St. Knut		X	X	X		Chalcopyrite-disease, decay of pyrrhotite.
	ML1546	Gamle Tronsli		X	X	X		Decay of pyrrhotite
	ML1547	Gamle Tronsli	(X)	X	X	X		
	ML1552	Øvre Tjæremyr	X	X	X	X		Botryoidal pyrite, decay of pyrrhotite
	ML1568	Såttå	X	X	X	X		Chalcopyrite-disease, decay of pyrrhotite
	ML1571	Store Baugsberget	X		X	X		Fractured and rounded pyrite, annealing of pyrite, chalcopyrite-disease.
	ML1572	Store Baugsberget	X	X	X	X		Decay of pyrrhotite
	ML1573	Lille Baugsberget	X	X	X	X		Fractured and rounded pyrite, fibrous pyrrhotite, chalcopyrite-disease.
	ML1574	Lille Baugsberget	X	X	X	X		Rounded and fractured pyrite,



## 3.5 Geochemistry

### 3.5.1 Volcanic rock

The geochemical data were acquired from Actlabs as described in chapter 2.5. The main purpose of the geochemical investigation is to characterize the geochemical composition of the unaltered meta-volcanic and meta-sedimentary rocks and with help of discrimination diagrams determine the protoliths of these rocks. A further purpose is to describe and interpret the geochemical balance between these rocks and the ore-forming fluids, when the ores were formed. A third purpose is to provide multi-element information on the metal and sulphur contents of the ores.

The protolith classifications were based on whole rock chemistry, since these metamorphic rocks do not have any primary minerals preserved. Under greenschist facies conditions,  $\text{TiO}_2$ ,  $\text{Al}_2\text{O}_3$  and  $\text{Cr}_2\text{O}_3$  are the only major elements that are immobile, while the others ( $\text{Na}_2\text{O}$ ,  $\text{CaO}$ ,  $\text{MgO}$ ,  $\text{FeO}$  and  $\text{K}_2\text{O}$ ) are mobile with  $\text{SiO}_2$  behaving as both immobile and mobile dependent on the physical properties (Pearce, 1975). Based on the metamorphic grade observed in the rock, Harker diagrams and total alkali vs silica (TAS) cannot be used (Floyd & Winchester, 1978). However, several diagrams based on major element oxides are used in petrology to describe the nature of volcanic rocks and such diagrams are therefore used in this thesis. Other elements that are mobile during alteration are Ba and Sr, and are unsuitable as primary diagnostic elements to determine the rock type. Cr and Ni on the other hand, are immobile.

Several diagrams and plots from a range of authors (Pearce & Cann, 1973; Pearce *et al.*, 1975; Pearce, 1976; Le Maitre *et al.*, 1989) were used to determine and classify the rock type. The samples ML1533, ML1535, ML1538 and ML1569 represent the greenschist. The first diagram, the total alkali vs. silica (TAS) diagram of Le Maitre *et al.* (1989) (Figure 14), is useful for the classification of volcanic rocks and for distinguishing between alkalic and tholeiitic parental magma, where  $\text{SiO}_2$  contents are plotted against the sum of  $\text{Na}_2\text{O}$  and  $\text{K}_2\text{O}$  (in weight percent).

Analyzed samples (black squares in Figure 14) plot within the spectrum of basalt. The subdivision of the diagram into alkaline or subalkaline/tholeiite, shows that the samples are within the subalkaline/tholeiite serie.

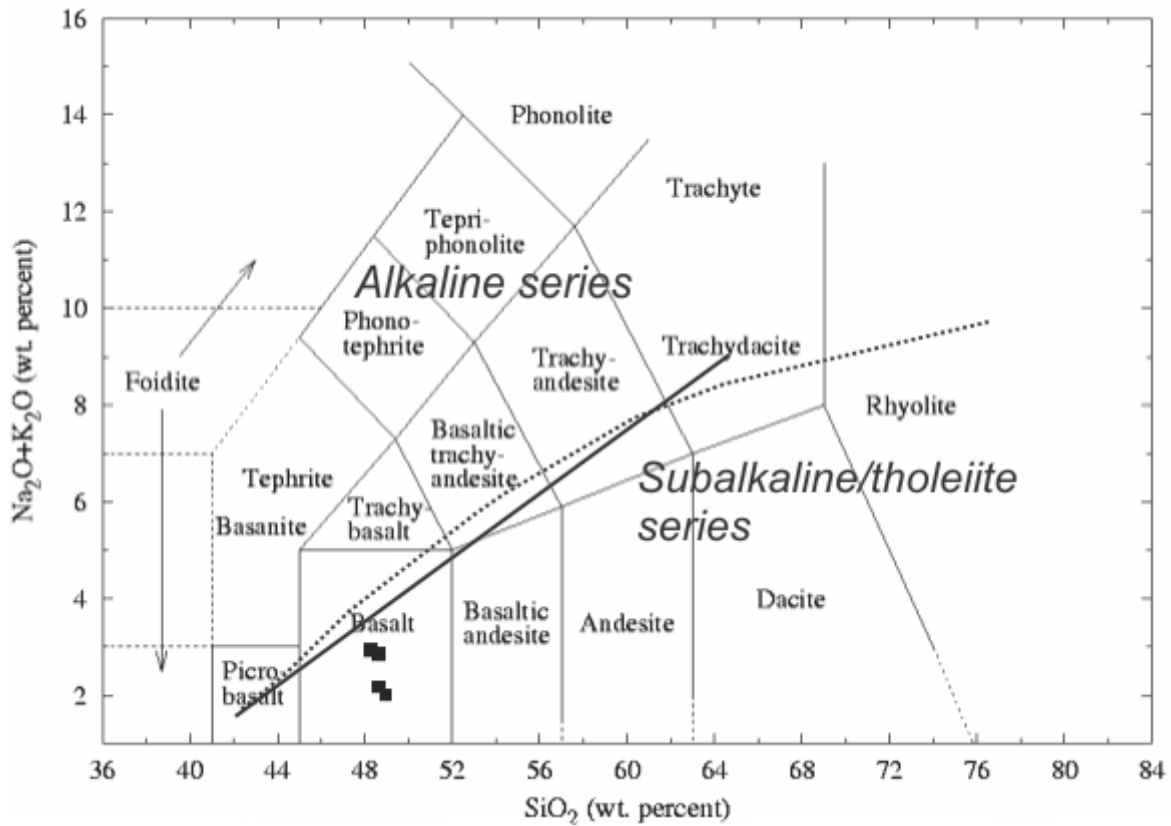


Figure 14: Total alkali-silica (TAS) diagram showing what type of igneous mafic rock type the greenschist originates from (Le Maitre et al., 1989). The boundaries subdivide the volcanic rocks into alkaline and subalkaline/tholeiite series: the Solid straight line is from MacDonald (1968), dashed curved line is from Irvine and Baragar (1971)

The major element discriminant diagram of Pearce (1976) tells what magma type the rock descends from (Figure 15). It separates ocean-floor basalts (OFB), volcanic arc basalts (calc-alkaline basalt (CAB) + low-K tholeiite (LKT) + shoshonite (SHO)) and within-plate basalts (ocean island basalt (OIB) + continental basalt (CON)). The functions for determining the axes (F1 and F2), are:

$$F_1 = + 0.0088SiO_2 - 0.0774TiO_2 + 0.0102Al_2O_3 + 0.0066FeO - \\ 0.0017MgO - 0.0143CaO - 0.0155Na_2O - 0.0007K_2O$$

$$F_2 = - 0.0130SiO_2 - 0.0185TiO_2 - 0.0129Al_2O_3 - 0.0134FeO - 0.0300MgO \\ - 0.0204CaO - 0.0481Na_2O + 0.0715K_2O$$

The first function (F1), related to the ratio between  $TiO_2$  and  $SiO_2$ , works best for separating high  $TiO_2$ /low  $SiO_2$  within plate basalts from low  $TiO_2$ /high  $SiO_2$  volcanic arc basalts. The second function (F2), is related to the ratio between  $K_2O$  and  $MgO$ , and works best for separating the low  $K_2O$ /high  $MgO$  ocean-floor basalts from the high  $K_2O$ /low  $MgO$  volcanic arc basalts.

All samples in Figure 15 plot well within the area of ocean floor basalts.

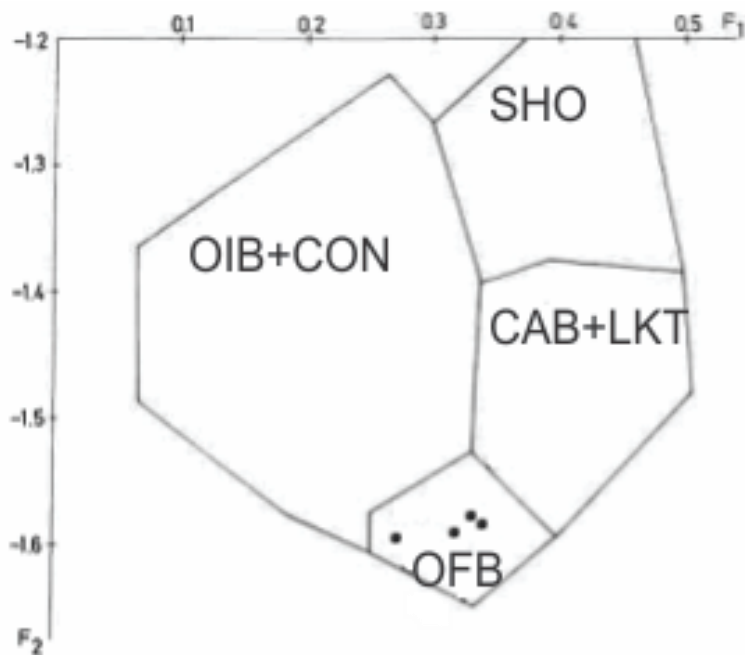


Figure 15: Major element discriminant diagram from Pearce 1976. This diagram states what type of magma the rocks descends from: within plate boundary (OIB+CON), ocean-floor basalts (OFB), and volcanic-arc basalts (CAB+LKT+SHO).

The ternary plot of Pearce & Cann (1973) has the same purpose as the discriminant diagram: to determine the origin of the magma and in what geotectonic setting it erupted. It discriminates between within-plate basalts (ocean island and continental basalts), ocean-floor basalts (OFB), low-K tholeiites (LKT) and calc-alkaline basalts (CAB) (Figure 16). In this plot, the elements Ti, Zr and Y are used since they are immobile and are not sensitive to secondary processes (Cann, 1970). Another discriminant diagram (Pearce & Cann, 1973) in which the ppm concentration of Ti is plotted versus Zr, determines if the rock originated as an ocean floor basalt, calc-alkaline basalt or low-K basalt (Figure 17).

All samples plot within the field for ocean floor basalts in both of the mentioned diagrams from Pearce and Cann (1973) (Figure 16+17).

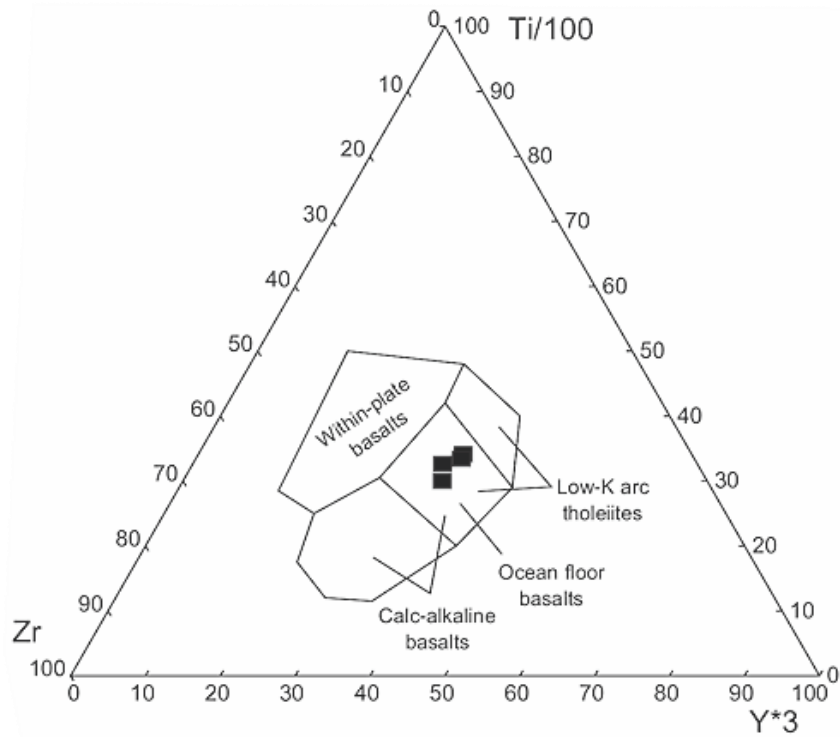


Figure 16: Ternary plot of Ti, Zr and Y of Pearce & Cann (1973). This plot determines what type of magmatic rock the rock originates from and is divided into within-plate basalts, calc-alkaline basalts, ocean floor basalts and low-K arc tholeiites.

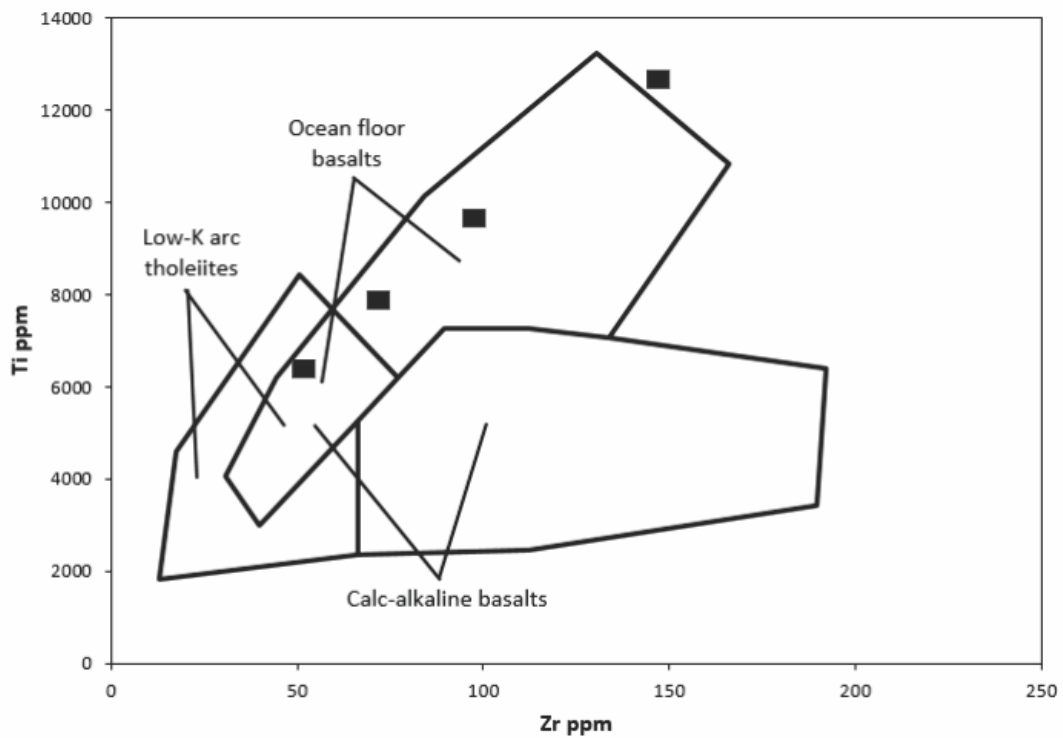


Figure 17: Discriminant diagram of Pearce & Cann (1973), using Zr vs Ti (ppm). This diagram distinguishes rocks with an origin as ocean-floor basalts, low-K tholeiites or calc-alkaline basalts from each other.

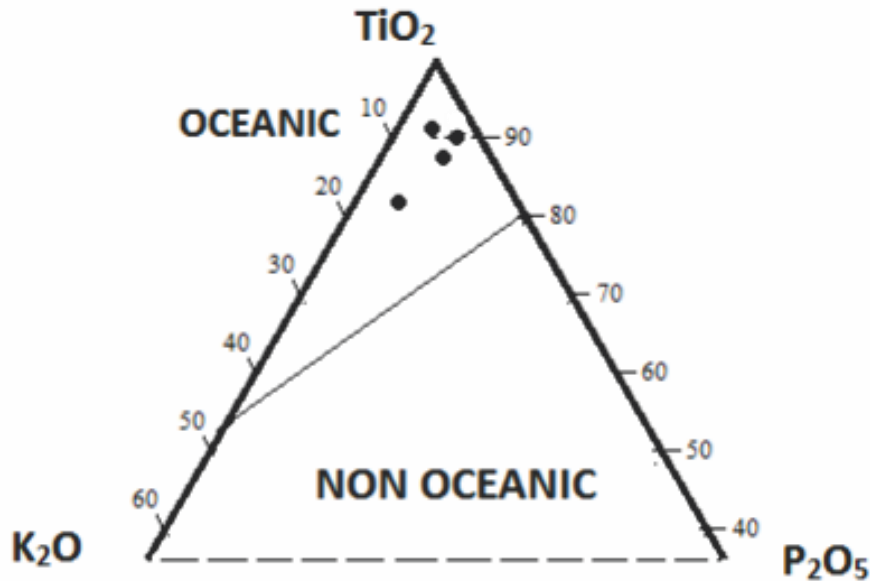


Figure 18: Ternary plot where  $TiO_2$ ,  $K_2O$  and  $P_2O_5$  are the components, revealing if the rock is originated from an oceanic or non-oceanic environment from (Pearce *et al.*, 1975).

The ternary plot of Pearce *et al.* (1975) uses  $TiO_2$ ,  $K_2O$  and  $P_2O_5$  to indicate what type of environment the rock originates from: an oceanic vs non-oceanic. Figure 18 shows that all samples plot within the oceanic field, implying that the investigated meta-basalts erupted in an oceanic environment.

The rare earth elements (REE) constitute the series of metals with atomic numbers between 57 and 71; La to Lu. They have all a 3+ charge except Eu, which can be +2 and Cs, which can be +4. With increasing atomic number, their ionic size decreases and the compatibility increases, e.g. La is the most incompatible element while Lu is the most compatible element. Because the REE's are immobile they can be used to discriminate between different petrological processes (Rollinson, 1993). REE concentrations are normalized to a reference standard, often chondritic meteorites, since chondrites are assumed to represent the bulk composition of the Earth.

REE plots are presented as concentration vs. atomic number, where the concentrations are normalized to the chondritic reference, and are expressed with a logarithmic base. The shape of

the REE patterns, may reveal the petrological process. In figure 19, the normalized chondrite values are from Nakamura (1974).

The shape of the plotted samples indicate a MORB affinity (White, 2013) with a small depletion of Eu (Figure 20). Data for the altered greenschist are plotted in figure 20 and show both a depletion of all the REE (except La) and a general similar trend as the unaltered greenschist.

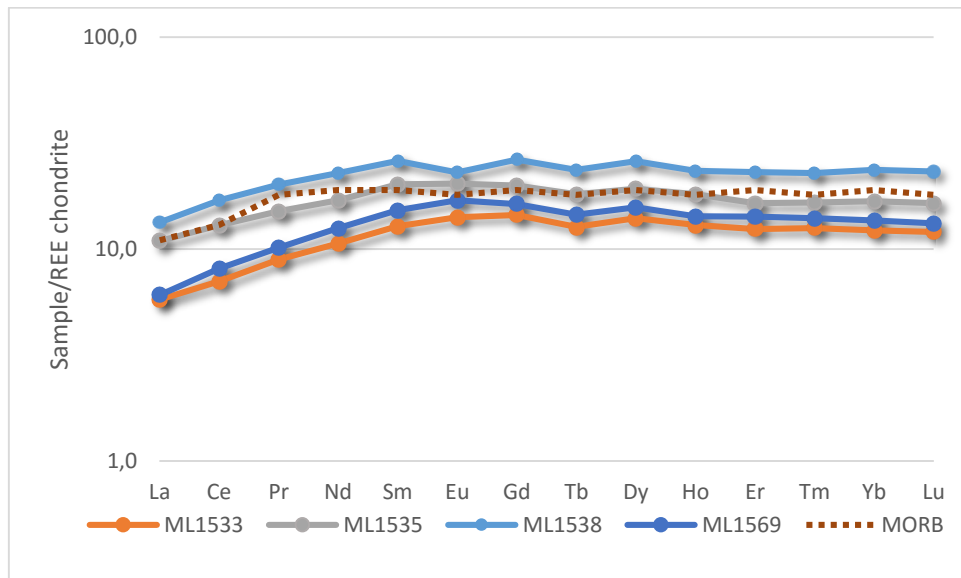


Figure 19: Rare earth element diagram showing a similar trend as a MORB (dashed line). Normalization values are from Nakamura (1974).

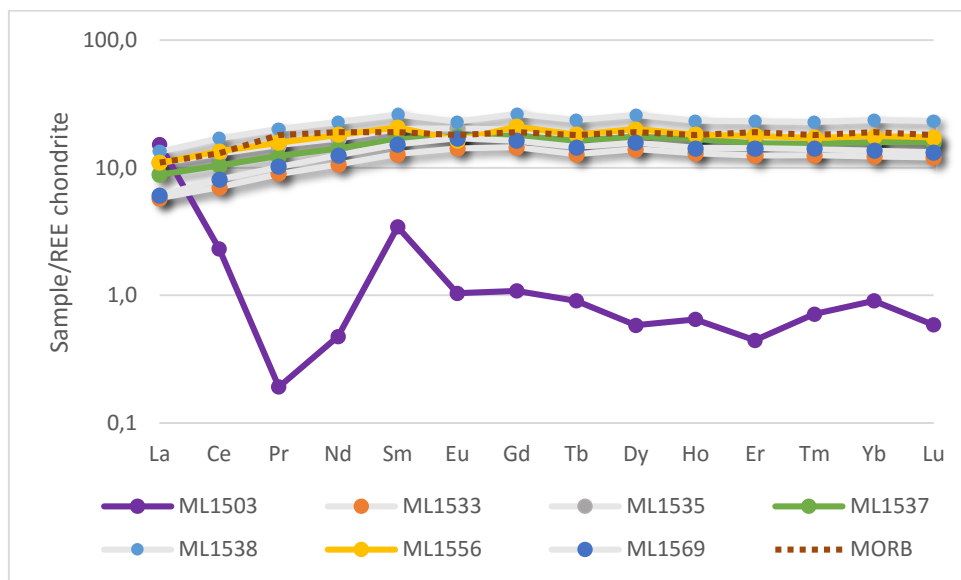


Figure 20: Rare earth element diagram, where the proper greenschist is shown as shaded grey, and the altered greenschist has colors. All the REE are depleted in the altered sample ML1503 compared to the unaltered greenschist, except La, and the other altered greenschist samples ML1537 and 56 show the same trend as the unaltered greenschist.

Normalized multi-element diagrams use incompatible elements to depict basalt chemistry and are extensions of the chondrite-normalized REE diagrams (Rollinson, 1993). Both primitive mantle values and chondritic meteorites are used for normalization. In this diagram, the elements are arranged from the left to right in order of increasing compatibility. Element concentrations are plotted in a logarithmic scale. The elements can also be divided into mobile elements (Rb, Ba, K, Sr, Ta, Nb, U (only in oxidized environments)) and immobile elements (Hf, Zr, Ti, Y) based on their behavior during post-magmatic processes. The concentrations of the mobile elements can be controlled by fluids and the content changes during hydrothermal alteration, while the immobile elements are mostly resistant to these processes and reflect the chemistry of the source rock and the crystal/melt process. The mobile elements can also indicate crustal contamination in magmas.

Normalization values from McDonough *et al.* (1991) are chosen to represent the primordial mantle (Figure 21). The general trend of all plots are similar to that of a MORB (Rollinson, 1993), but with some differences: Th is depleted in sample ML1533 and ML1559; Nb and P show negative anomalies; Ta shows positive anomaly; and Y is slightly depleted. Rb values have not been used since they are below the detection limit (except for sample ML1533). Depletion of Nb normally indicates a subduction-related magmatism or a continental crust affinity (Kelemen *et al.*, 1993; Baier *et al.*, 2008).

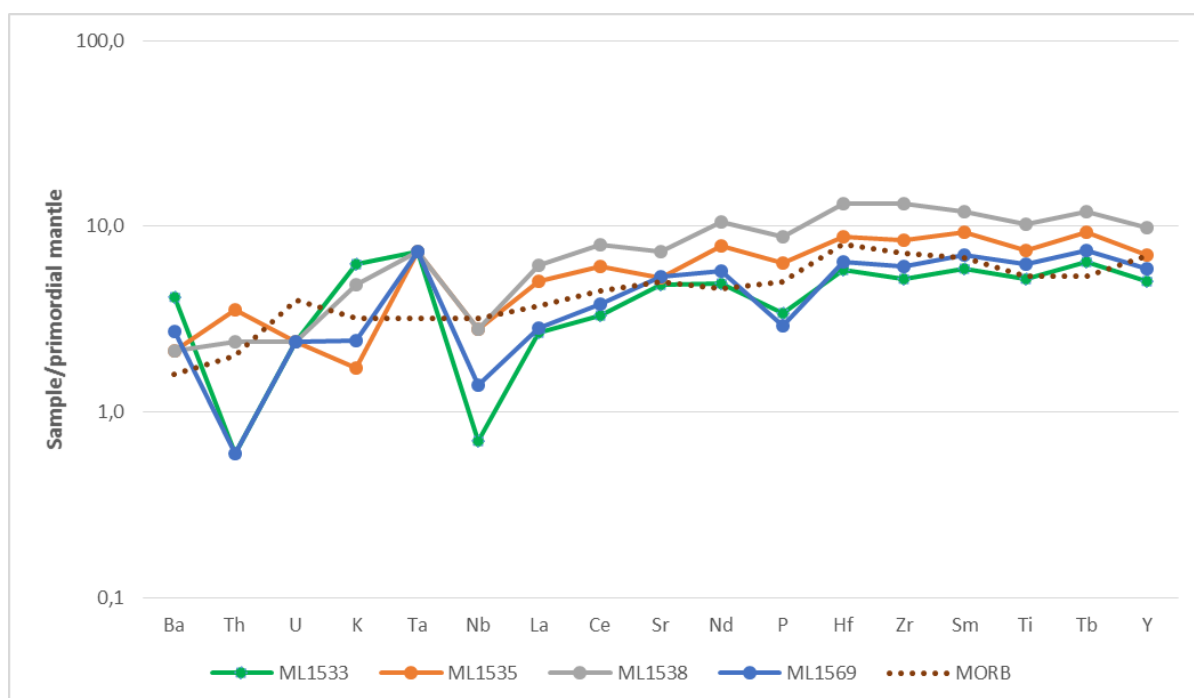


Figure 21: Multi-element diagram where the normalization values are from a primordial mantle, from (McDonough *et al.*, 1991). The general trend is similar to that of a MORB (dashed line)(Rollinson, 1993), but with negative anomalies of Th, Nb and P.

### 3.5.2 Altered volcanic rock

The geochemical data for the altered greenschist, samples ML1503, ML1537 and ML1556, have been compared with the data for the unaltered greenschist. A few trends are clear when considering the depletion or enriched levels of major elements, as shown in figure 22. Ca is depleted, while Na is both enriched and depleted. The bars also indicate different levels of alteration: ML1503 is the most altered sample, and ML1556 the least. ML1503 may have undergone a different alteration since the silica and sodium content have decreased while the iron content has increased compared to the other two altered samples.

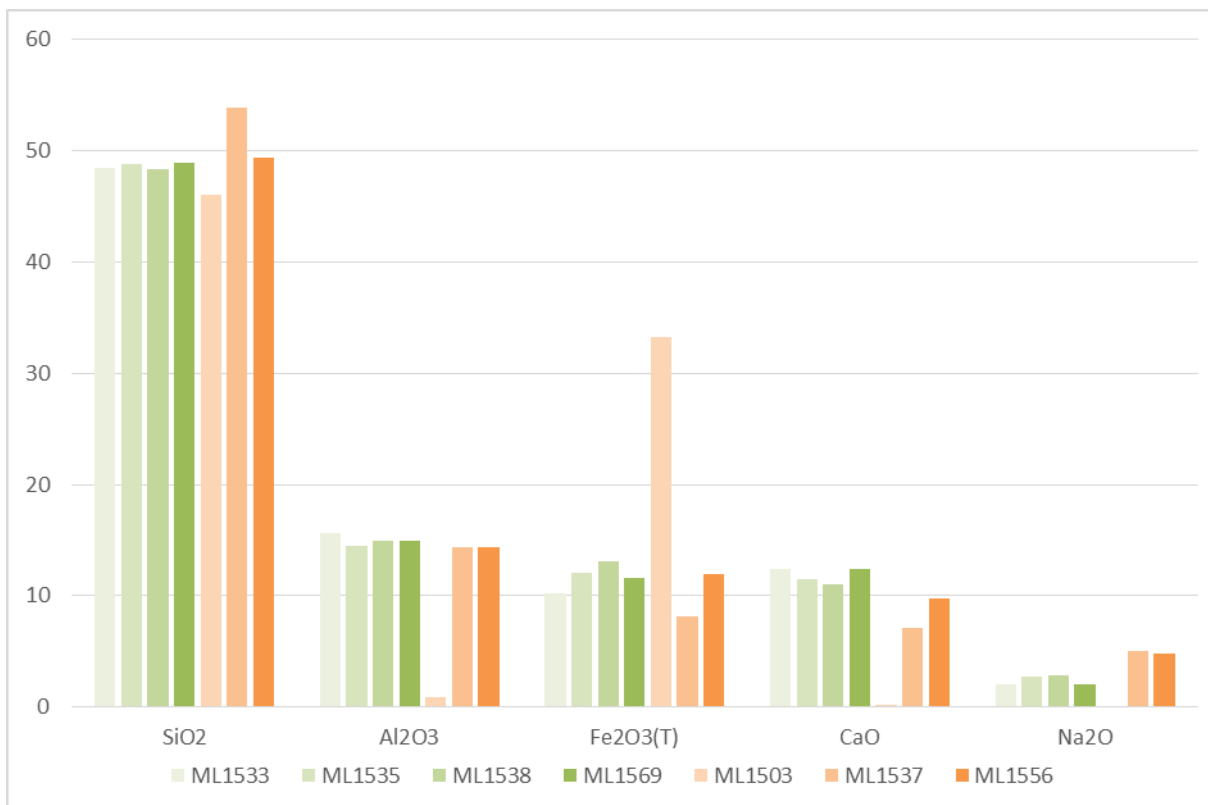


Figure 22: Graphical view of selected geochemical data for greenschist, from appendix D2. Green colors are the unaltered rock, orange colors are the altered rock.



### **3.5.3 Metasedimentary rock**

Interpretation models of geological environments based on geochemical data for sedimentary rocks are not as well developed as for igneous rocks (Rollinson, 1993). Sedimentary rock classification is often based on features that can be observed in hand specimen or in thin section, such as grain size, mineralogy and matrix. Geochemical classification of sandstones differentiates between mature and immature sediments, where the  $\text{SiO}_2$  content and the  $\text{SiO}_2/\text{Al}_2\text{O}_3$  ratio are the most common criteria used for sediment maturity (Potter, 1978). These criteria reflect the silica, clay and feldspar content in the sedimentary rocks. Another ratio that estimates the feldspar content is the alkali content ( $\text{Na}_2\text{O}+\text{K}_2\text{O}$ ), which also is a useful index for the chemical maturity.

Pettijohn *et al.* (1972) have made a classification diagram using the chemical maturity and the  $\text{Na}_2\text{O}/\text{K}_2\text{O}$  ratio for making a plot of  $\log(\text{Na}_2\text{O}/\text{K}_2\text{O})$  versus  $\log(\text{SiO}_2/\text{Al}_2\text{O}_3)$ . This diagram has to be used with care, since Na and K are mobile elements during metamorphism. All metasedimentary samples investigated in this thesis plot within the area of greywacke (Figure 23).

Another diagram proposed by Wimmenauer (1984) plots the  $\text{SiO}_2/\text{Al}_2\text{O}_3$  ratios vs.  $\text{K}_2\text{O}/\text{Na}_2\text{O}$  and separates arkoses from greywackes. In figure 24 all samples plot within the field of greywacke.

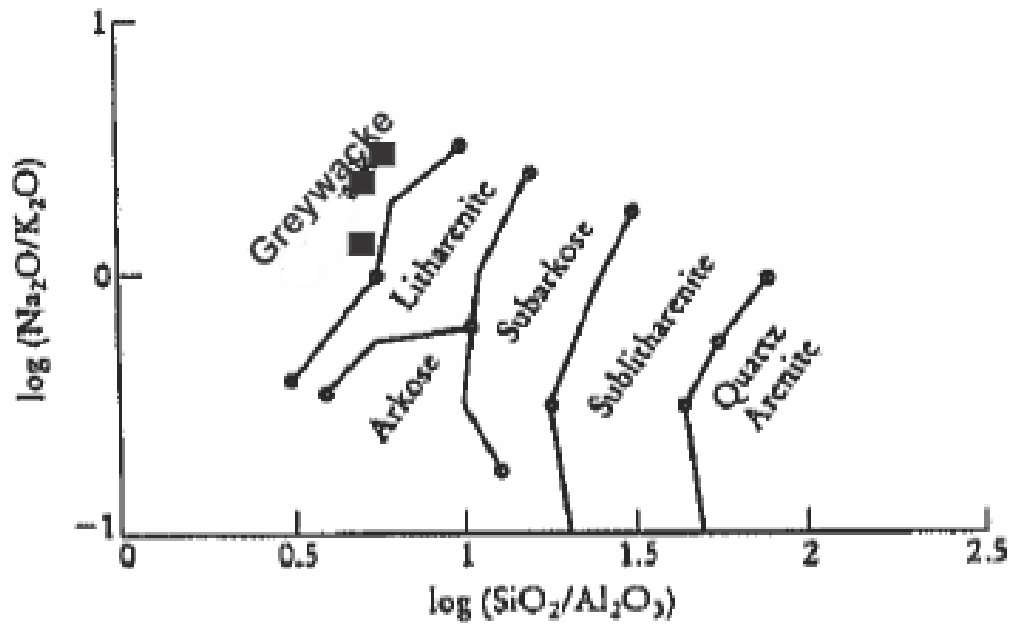


Figure 23: Investigated metasedimentary rocks (samples M1515, 49 and 55) in the classification diagram of (Pettijohn et al., 1972).

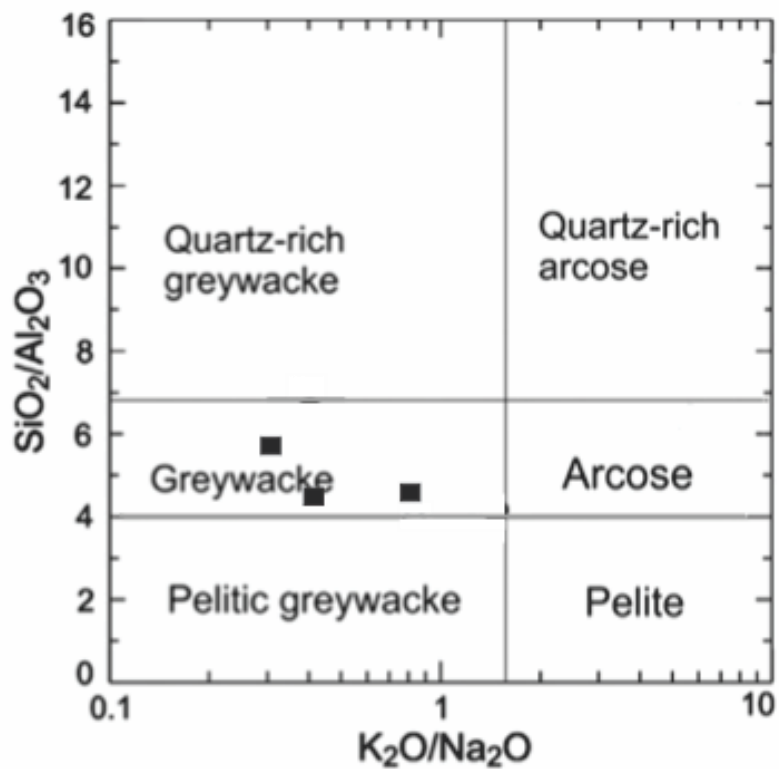


Figure 24: Investigated metasedimentary rocks (samples 1515, 49 and 55) in the classification diagram of Wimmenauer (1984).

### 3.5.4 Altered metasedimentary rock

The altered meta-sediments show similar trends as the altered greenschist: Ca and Na have been depleted (nearly gone), the same with Al and silica (Figure 25). The K content is stable or shows a small increase. There is also a big increase in the iron content.

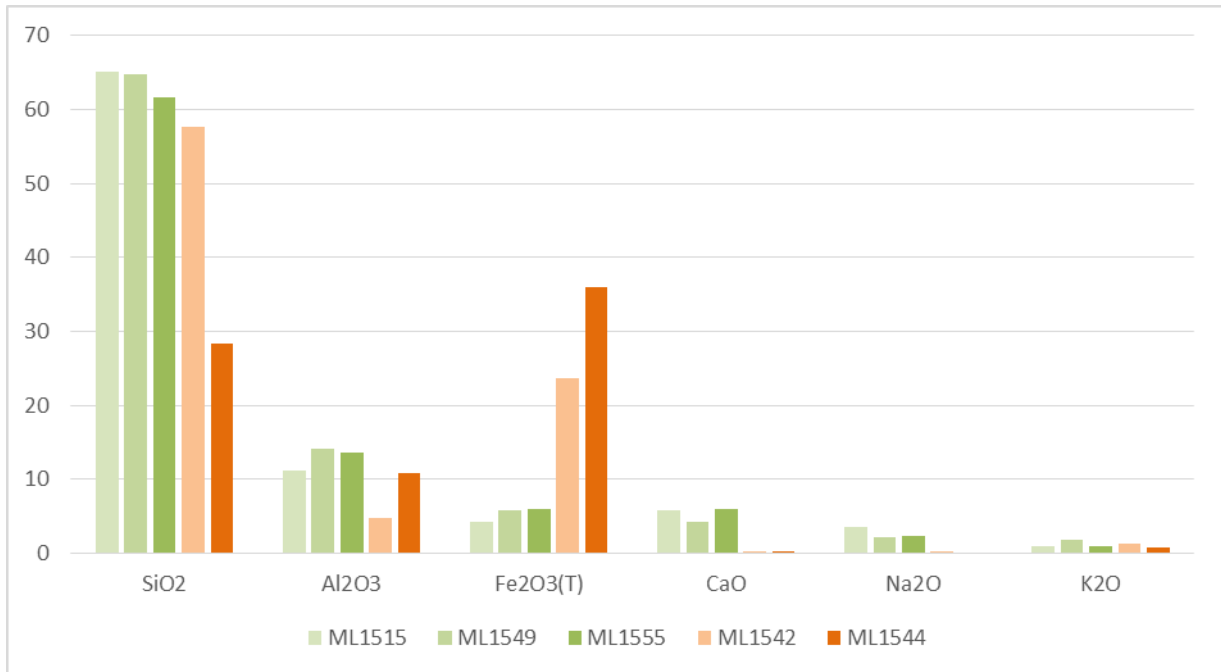


Figure 25: Graphical view of selected geochemical data for mica schist, from appendix D2. Green colors are the unaltered rock, orange colors are the altered rock.

### 3.5.5 Geochemical comparison of volcanic vs metasedimentary rocks

A multi-element diagram where both the mica schist and greenschist are plotted, using normalization values of chondrite (Wood *et al.*, 1979), will reveal if there are differences in what type of element the rocks may be enriched or depleted in. As figure 26 shows, the mica schist is enriched in incompatible elements compared to the greenschist.

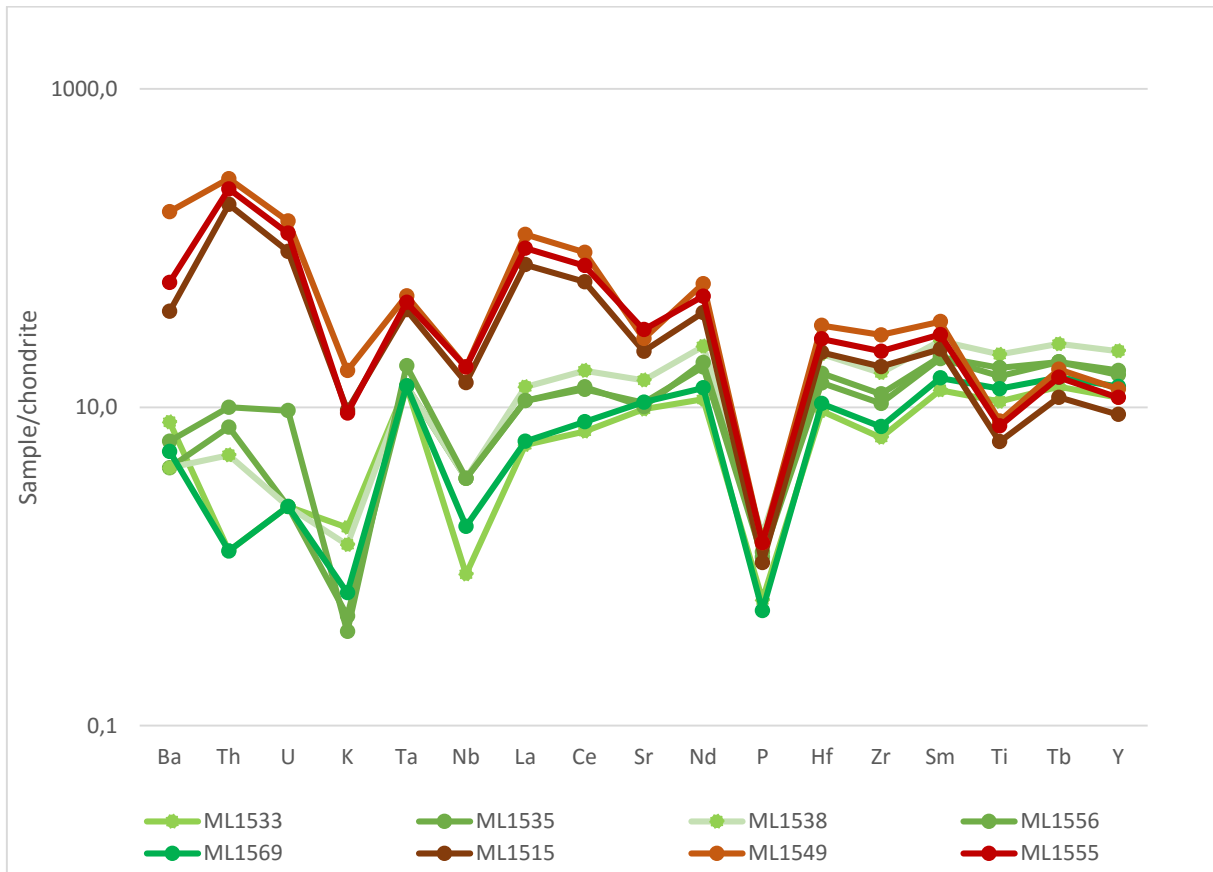


Figure 26: Multi-element diagram displaying data for both mica schist (red color) and greenschist (green color).

### 3.5.6 The ore deposits

As previously mentioned, the ores are located within two different lithologies. The greenschist hosted ores have a (Fe)Cu-Zn signature with no particular enrichment in trace elements (Table 3). Statistical analysis were done on ore samples, where Ag correlates positively with Cd, Zn and Pb, and Cu correlates negatively with Fe and S and positively with Mn (appendix E).

Table 3: Selected element contents of the greenschist-hosted ores. Red color indicates high level and orange medium level of the elements compared to other samples.

Sample	Cu (%)	Zn (%)	Fe (%)	S (%)	Pb (ppm)	As (ppm)	Hg (ppb)	In (ppm)	Cd (ppm)
ML1501	0.07	0.18	28.2	35.3	25.1	27.8	<10	<0.1	4.7
ML1502	1.16	1.89	38.1	45	471	43.7	10	1.5	54.3
ML1503	1.04	0.17	21.9	26.8	94.4	160	<10	0.4	5.6
ML1504	1.57	0.07	26.1	31.5	61	135	<10	0.7	2.7
ML1507	1.75	0.08	31.3	35.3	87.6	206	<10	0.7	3
ML1509	2.52	0.71	20.5	23	28.9	97	550	1.1	24
ML1559	4.6	0.13	11.4	7.69	1.8	8.9	<10	1	35.5
ML1560	5.32	0.06	18.8	14.8	2.3	9.9	<10	1.6	16.2

The sediment-hosted ores have a general Fe-Cu-Zn-Pb signature, with anomalies of different trace elements (Table 4). A division of the mines in the Tronsvangen area (ML1516-68) can be done based on the Zn and Pb contents: A Zn-Pb mineralization can be seen in the central part (Brånå (ML16-17), St. Olav (ML5127) and Tjæremyr (ML1530)), while the surrounding mines have higher Cu-contents.

The Baugsberget mines (ML1571-74) have the highest Zn-contents and the most significant anomalies of Hg, In, As and Cd.

Statistical analysis revealed that Au correlates positively with As, Ag with Cu, Zn with Cd, Hg and In, and Pb with Mo, Bi and Ca (appendix E). Generally the mica schist-hosted ores are more enriched in incompatible elements than the greenschist.

Table 4: Selected element contents of the sediment-hosted ores. Red color indicates high level and orange medium level of the elements compared to other samples.

Sample	Cu (%)	Zn (%)	Fe (%)	S (%)	Pb (ppm)	As (ppm)	Hg (ppb)	In (ppm)	Cd (ppm)
ML1516	0.3	2.19	16.4	9.92	51.4	5.4	<10	3.7	88.6
ML1517	4.21	5.58	34.6	28.7	170	8.5	70	9.1	206
ML1524	0.2	1.02	39.6	19.7	1640	5.8	<10	6.9	26.5
ML1526	0.34	0.06	33.1	14.6	19.1	4	<10	0.2	0.3
ML1527	1.28	2.05	38.9	27.8	2820	8.4	10	3.9	64.4
ML1530	1.60	3.91	28.7	19	2880	6.9	160	8	91.7
ML1539	8.21	0.96	19.9	13.7	9.4	6.4	<10	6	59.8
ML1546	1.71	0.03	26.7	17.1	48.1	7.2	<10	0.5	2.5
ML1547	23.9	0.23	24.3	29	782	7.7	60	2.2	25.3
ML1552	0.27	0.03	19.6	12.9	8.2	7.2	<10	0.2	0.1
ML1568	14.1	0.9	27.2	26.8	262	10.9	50	1.8	23.7
ML1571	0.96	22.4	27.1	44.9	153	1250	7380	40.1	704
ML1572	0.69	5.73	40.3	35.1	116	545	3390	16.7	226
ML1573	1.42	0.39	42.1	38.9	293	1740	350	5.4	8.3
ML1574	4.96	0.59	34.6	39.5	48.2	2750	870	4.4	17.2

Correlation diagrams of metals and trace elements are useful to distinguish between ore types. The diagrams in appendix E show that some elements have a positive correlation in the greenschist-hosted ores (like Ag vs Cd, Figure 27), but a negative correlation in the mica schist-hosted ores, and vice versa. None of the diagrams have the same correlation in ores hosted by greenschist and mica schist respectively.

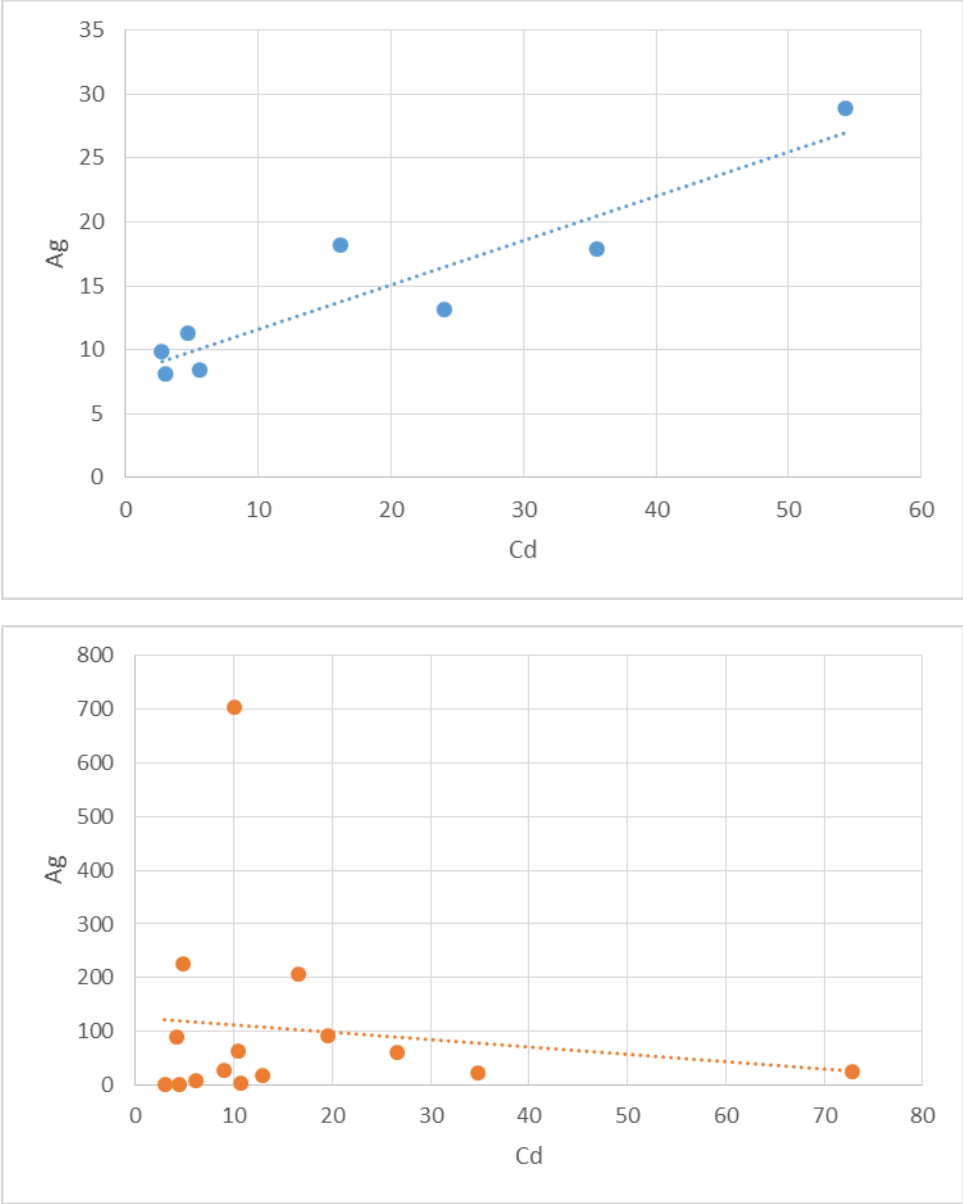


Figure 27: Correlation diagram of Ag vs Cd in greenschist-hosted ores (top diagram, blue color) and in mica schist-hosted ores (bottom diagram, orange color).





## **4. Discussion**

### **4.1 Geological setting of the volcanic and meta-sedimentary units and interpretation of the geological environment**

#### ***4.1.1 Tectonostratigraphic position***

The ore-bearing supracrustal units in the Tynset-Alvdal region are located above the Augen gneiss, a zone extending from the south of Baugsberget to the type area for the Tännäs Augen gneiss, which is situated at the base of the Särvi Nappe (Figs. 3, 5). This implies that the supracrustal units in the Tynset-Alvdal region must be part of the Middle Allochthon (or higher tectonic units). The Tynset-Alvdal sequence is also located beneath the Tronden Complex, which forms part of the Upper Allochthon and rests tectonically as a klippe on top of the greenschist (Wellings & Sturt, 1998). Furthermore, the Tynset-Alvdal sequence is located beneath the ultramafic rocks situated to the north-west (Ramsay & Siedlecka, 2001) (Figure 3), which can be traced to the Vågåmo ophiolite in Gudbrandsdalen and to other ophiolitoid complexes that recently have been recognized south of Røros (Sundblad *et al.*, 2010) and north in Nord-Trøndelag (Nilsson & Roberts, 2014). Since these ultramafic units form the border between the Seve Nappe Complex (Middle Allochthon) and the Köli Nappe Complex (Upper Allochthon), it can be concluded that the Tynset-Alvdal sequences must be part of the Middle Allochthon. The presence of volcanic rocks in the sequences exclude a Särvi affinity, and it is more likely that the sequences are part of the Seve Nappe. As a conclusion, the Tynset-Alvdal sequence is interpreted to be part of the Seve Nappe within the Middle Allochthon of the Scandinavian Caledonides.

#### ***4.1.2 The origin of the host rocks and the geological environment***

Based on field observations, the rock types in the investigated area are interpreted to be low-grade metamorphosed volcanic and sedimentary rocks, more specific greenschist and mica schist. The mineral assemblages of the host rock (chlorite, plagioclase, amphibole and quartz in the greenschist; white mica, quartz, chlorite and plagioclase in the mica schist), the foliation, presence of quartz lenses aligned with the foliation and local small scale folding support this interpretation. The two rock types have different physical features: the mica schist shows sedimentary features, has a sandy texture, generally low hardness and is light grey in color, while the greenschist shows magmatic features, is massive and harder, and has dominantly a dark green color. The contact is hard to distinguish because of the heavy vegetation, but one location shows a repeated sequence of mica schist and greenschist, that indicates coeval deposition of the rocks or imbrication during the orogeny. Even though the metamorphic grade

is low and the deformation mild, it was strong enough to wipe out the sedimentological features and the possibility to determine way up directions in the stratigraphy. It can be concluded from the field study, that 1) the greenschist originated in a magmatic environment, probably marine, and the mica schist in a continent-margin marine environment, and 2) that they both are metamorphosed during the Caledonian Orogen. The stratigraphic polarity has not determined: the present tectonostratigraphy (with greenschist on top of mica schist) can be inverted.

#### **4.1.3 Geochemistry and tectonic setting of the host rocks**

The geochemical investigation shows that the greenschist originated as ocean floor basalts in a marine environment and has a chemical signature similar to tholeiitic basalts from the mid-ocean ridge (Figs. 15-19, 21). The mica schist originated as a greywacke, deposited in a marine environment close to a continent (Figs. 23, 24). Figure 26 shows that the mica schist is more enriched in the more incompatible elements than the greenschist, indicating that the mica schist has a more continental crust origin (Hofmann, 1988). Since these two units appear together, the environment of deposition and magmatic eruption indicates a marine igneous rift environment in a coast near position, similar to the present Red Sea (Bosworth *et al.*, 2012).

Even though all the diagrams and plots show that the greenschist originated as ocean-floor basalts, the depleted level of Nb in the multi-element diagram (Figure 21) rather indicates a subduction-related magmatism or a continental crust affinity (Kelemen *et al.*, 1993; Baier *et al.*, 2008). Since all the other elements in the same diagram show a MORB-trend, the Nb anomaly's origin remains a mystery. Another notable feature is that Nb and Ta generally behave similar (Baier *et al.*, 2008), but in Figure 21, Nb shows a negative anomaly and Ta a positive anomaly. Briquet *et al.* (1984) have suggested that since Ti shows no anomaly, Nb and Ta will show anomalies, which is typical for tholeiitic basalts. Another possibility for enriched Ta and depleted Nb, is that this trend is common for medium-Ti (MORB/island-arc tholeiitic intermediate) basalts, resulting in no strange anomalies (Saccani, 2015).

Geochemically, the altered rocks differ from the unaltered ones, especially in the levels of K, Na and Ca. These elements are mobile during alteration and indicates a hydrothermal alteration process for the rocks. A definite geochemical interpretation of the altered rocks is difficult, due to the uncertainty of where the dump samples originally were located in relation to each ore type. The total alkali vs silica (TAS) diagram is used in this thesis, even though the alkali minerals and SiO<sub>2</sub> may be mobile under metamorphism, because it is assumed that the grade of metamorphism is low and have not affected these elements significantly.

Petrographic analysis of the two rock types revealed that the quartz has undergone deformation (Figs. 10D, 11), while the plagioclase has not, indicating a low-grade metamorphic event (Passchier & Trouw, 2005). Nevertheless, the geochemical data suggest that variations are due to hydrothermal influence rather than the metamorphic event, because of the removal of the mobile elements.

The studied greenschist shows similarities with the greenschist of Ramundberget, Sweden 150 km NE of the Tynset-Alvdal region (Hill, 1980) in terms of tectonostratigraphic position, geotectonic environment and geochemistry. The Ramundberget sequence is also an example of a mid-ocean ridge origin, formed during an early rifting phase, and shows similarities with the present Red Sea. It is thus likely that these two areas (Tronsvangen-Baugberget and Ramundberget) may be connected and/or related with each other.

## **4.2 Geological environment and ore-forming processes of the ores**

### **4.2.1 Greenschist-hosted ores**

The greenschist-hosted ores are a chalcopyrite-sphalerite-bearing pyrite-rich massive ore type, located in the lower part of the greenschist sequence. The adjacent volcanic sequence is clearly hydrothermally altered (disturbed K-Ca-Na balance), indicated by geochemical data (Figure 22) and field observations. Based on the massive sulphide mineralization and appearance within the host rock, these ores are similar to a VMS type of ore deposit (Robb, 2005). If these ores are a VMS type, the best fit is to have them in the upper part of the volcanic pile, which indicate an inverted stratigraphy vs. the present one. Inverted supracrustal sequences with VMS ores have been reported from several areas in the Köli Nappes: by Halls *et al.* (1977) in the Gjersvik Nappe, by Sundblad (1980) in Ankarvattnet and by Stephens (1982) in the Stikke Nappe.

The greenschist-hosted ores show similarities to the Cyprus type of VMS deposits (Franklin *et al.*, 1981; Galley *et al.*, 2007), because of the mid-ocean ridge related magmatism, the ore mineral assemblage (mostly pyrite, chalcopyrite and sphalerite) and the lithology (greenschist that may be related to an ophiolite). However, these ore deposits are not a perfect example of the Cyprus type, since the host rock is a greenschist (meta-basalts) and due to the lack of sheeted dykes, gabbro and ultramafics that all are components in an ophiolite. It is possible that the studied metabasalts may have a relation to the ophiolite, and if so (meaning an inverted stratigraphy in the Tronsvangen area) the segments from the ophiolite must have been sliced off by the Tron Complex shear zone.

Local geochemical zonation patterns are found within the Tronsvanger mines. The central area (with St. Thomas, St. Olaf, Tjæremyrgruvene and Brånå) is enriched in Pb and Zn whereas the outboard area has higher Cu grades (Table 3), indicating a segregation of the hydrothermal fluids that have occurred during the ore-forming process.

#### **4.2.2 Mica schist-hosted ores**

The ores hosted by the mica schist are of a chalcopyrite-sphalerite-galena bearing pyrrhotite-rich type that is irregularly distributed at various levels in the sedimentary sequence. The adjacent metasedimentary sequence is clearly hydrothermally altered, indicated by geochemical data (Figure 25) and field observations. Several elements like Hg, In, Zn and As, are enriched in this type compared to the greenschist-hosted ores (Table 4). Locally high levels of Cd, Hg and In are found particularly in the Baugsberget ores. These elements correlate well with Zn (appendix E), suggesting that they occur within the sphalerite lattice.

A precise evaluation of the mica-schist hosted ores is difficult. If the stratigraphy is inverted, as suggested for the greenschist-hosted ores, then the Tronsvanger ores will be located stratigraphically above the greenschist ores and in a geological setting that reminds on the Escanaba and/or subsea-floor replacement models (Morton *et al.*, 1994; Doyle & Allen, 2003; Piercey, 2015).

The correlation plots and diagram (appendix E) show positive and negative correlations between different elements in the greenschist-hosted ores, compared to the mica schist-hosted ores and vice versa, concluding that the ore are not of the same type.

#### **4.2.3 Deformation of the ore minerals and their textures**

Fracturing or brecciation of ore mineral grains is an evidence for brittle deformation of hard minerals, such as pyrite (Figure 12B) (Craig & Vaughan, 1994). When pyrite grains impinge upon each other, local brecciation occurs, but if the pyrite grains are mixed with chalcopyrite or pyrrhotite, the pyrite usually suffers little deformation because the strain is taken up by the softer sulphides. An exception from this is when the pyrite cubes have been rounded by being “rolled” in the matrix, often pyrrhotite and chalcopyrite, during deformation. The term “Durchbewegung” by Vokes (1969) is a deformation style where minor brecciation to complex cataclasis with increasing degree of fragmentation and disorientation have occurred. It is common that softer ore minerals have been injected into fractures and cleavages in brittle ore minerals, like pyrrhotite and chalcopyrite. Pyrite grains tend to recrystallize and anneal under

greenschist metamorphic grades and above, and generally the grain size increases with increasing metamorphic grade (Craig & Vokes, 1993).

Botryoidal pyrite (Figure 13C) is a secondary generation reflecting fast precipitation of pyrite. Ramdohr (1980) named this texture Melnikovite-pyrite or colloform pyrite, which has crystallized from a FeS<sub>2</sub> gel. This type is very common in sedimentary and hydrothermal deposits formed at low temperatures. Other settings that favor fast precipitation of botryoidal pyrite is the sulfur fugacity, and an alkaline solution (Tarr, 1927).

The decay or “Zwischenproduct” texture in pyrrhotite (Figs. 12E, 13E) is a transformation of pyrrhotite to pyrite directly, or via an intermediate product marcasite, reflecting the increase in the sulfur fugacity and the change in the Fe:S ratio (Ramdohr, 1980; Qian *et al.*, 2011). Pyrite is formed by direct replacement of pyrrhotite and by overgrowth from solution; the mechanism is called dissolution-reprecipitation or metasomatism. The fibrous grains (Figs. 12F, 13F) are an alteration or partial weathering of pyrrhotite to iron oxide/hydroxides (probably goethite), which have been investigated in SEM and EDS. This hydrous iron oxide forms in the sedimentary cycle, mostly as a weathering product of iron-bearing sulphides or minerals (Ramdohr, 1980). This weathering has happened later than the ore forming process in an oxidizing environment, most probably long after the metamorphic event.

The chalcopyrite-disease in sphalerite is characterized by randomly dispersed or crystallographically oriented rows of blebs and rods of chalcopyrite within sphalerite, also called sphalerite-chalcopyrite intergrowth (Figs, 12H, 13D) (Barton & Bethke, 1987). This texture was interpreted as a result of exsolution by e.g. Ramdohr (1980), since the crystal structure of chalcopyrite and sphalerite is very similar. Ramdohr (1980) also stated that a low iron content favors chalcopyrite in sphalerite, while high iron contents favors solution of chalcopyrite, but this process occurs in high temperature environments only (Craig & Vaughan, 1994). However, there is not only one process that has led to the formation of chalcopyrite-disease: Barton and Bethke (1987) concluded that the chalcopyrite in sphalerite either forms by epitaxial growth during sphalerite formation or by replacement as copper-rich fluids react with the Fe-bearing sphalerite after formation. It is also accompanied by a marked decrease in the iron content of the immediately adjacent host sphalerite (Barton, 1991), or it may remain unchanged or increase (Bortnikov *et al.*, 1991). Hutchinson and Scott (1981) proposed that the chalcopyrite-disease may be a product of a premetamorphic sphalerite-chalcopyrite intergrowth, or as exsolution from sphalerite. The formation of chalcopyrite-disease is a

common phenomenon in VMS deposits, indicating that the Cu-mineralization occurred later than the Zn-mineralization (Ohmoto, 1996).

The darker rim observed around chalcopyrite (appendix F) is caused by weathering in oxidizing environment towards sulphates based on SEM/EDS analysis. This weathering has occurred after the deposition of chalcopyrite, reflecting an increase in oxygen fugacity and a low water activity. In the field, malachite was often observed in the mine walls located close to the ore zone, also indicating weathering.

Galena is a very soft mineral, easily filling cracks and holes (Figs. 13G, H), but is very resistant to weathering and alteration. Based on observations in the microscope, it is concluded that galena, chalcopyrite and sphalerite precipitated together.

Based on observations made in the microscope, the low-grade metamorphism has overprinted and deformed the primary structures. Textures, like decay and fibrous pyrrhotite, botryoidal pyrite and chalcopyrite-disease, are more developed and common in the mica schist-hosted ores, while fractured and rounded pyrite are more common in the greenschist-hosted ores. This could be due to the difference in the rock strength during metamorphism and the mineralogical differences – that the ores are not the same type and have originated in different environments. This assumption is strengthened by the correlation plots (appendix E). The lack of limonite in the ores proves that the ores have not undergone heavily oxidation.

### **4.3 Regional geological context**

The rocks in the Tronsvängen-Baugberget sequence are of a low metamorphic grade, which is very different from the typical high grade Seve (e.g. Snåshögarna and Åre) where metamorphic diamonds have been reported (Majka *et al.*, 2014). Instead, the ore-bearing sequences in the Tronsvängen-Baugberget area remind more of the ore-bearing sequences in the Ramundberget-Vargtjärnsstöten areas, north of Funäsdalen, Sweden (Hill, 1980; Sundblad & Stephens, 1983) which form a lowermost part of the Seve Nappes, structurally above the Särvi Nappe, but structurally below the high-grade metamorphosed Seve units at Snåshögarna and Åre.

The recognition of syngenetic metalliferous deposition in a submarine environment in the lowermost tectonic units of the Seve Nappe, represents most likely the earliest phases of rifting during the opening up of the Iapetus Ocean (Figure 28). Such an event must be significantly older than any other VMS environment recognized in the Scandinavian Caledonides. Several ages have been estimated for the Särvi Nappe dolerites, related to the initial opening of the

Iapetus Ocean, ranging from 580-610 Ma, where the latest precise age estimation at 596 Ma was provided by Kumpulainen *et al.* (2016). The age of the (upper) Seve, where the dolerite dykes in the continent-oceanic transition zone (COT) complex is situated, was determined to 608 Ma by Svenningsen (2001). Under the COT complex (middle Seve) is a high-pressure metamorphic zone with an interpreted age of  $607\pm 2$  Ma (Root & Corfu, 2012). All these ages indicate an Ediacaran age of the Baltic igneous rift-related activity in the Särvi and Seve nappes. The Tronsvängen-Baugberget sequence, constituting the lowest parts of the Seve Nappe Complex, is probably of the same approximate age as the underlying Särvi units and the overlying Seve units, i.e. around 600 Ma. In contrast, all age estimates for supracrustal sequences with proper VMS ores in Løkken, Røros-Ankarvattnet and Stekenjokk (all located within the Köli Nappes), indicate much later events. The age of the Stekenjokk volcanics was determined to 490 Ma (Claesson *et al.*, 1987), which fits with the age for the lowermost Ordovician graphitic Dictyonema shales, found at the Stekenjokk level and at the base for the sedimentary sequences of the Røros and Ankarvattnet VMS systems ((Sundblad, 1980; Gee, 1981; Sundblad & Gee, 1984; Sundblad *et al.*, 2010). The age of the Løkken ophiolite was established to Early Ordovician (Grenne, 1989; Grenne *et al.*, 1999) ( $487\pm 5$  Ma by Dunning & Grenne, unpublished data). Other VMS ores associated with continent rifting and opening up of the Iapetus Ocean are Kvikne and Tverrfjellet, Hedmark, Leksdal, Sør-Trøndelag and Joma, Nord-Trøndelag. They are all located within the Köli Nappes, having ages ranging from early Cambrian to early Ordovician (Grenne *et al.*, 1999).

The ore forming process of the mica schist-hosted ores at Tronsvängen and Baugberget have similarities to the model formulated for the sulphide ores off-shore western North-America, where mid-ocean ridge related magma interferes with unconsolidated turbiditic sediments (Morton *et al.*, 1994), referred to as the Escanaba model. The similarity between the Tronsvängen-Baugberget and the Escanaba case is, however, far from perfect because the greenschist at Tronsvängen *extruded* on the sea floor (over or under the greywacke sediments) while the mafic magma in the Escanaba model *intrudes* into the wet sediments. The important thing in both these case is that the sulphide deposition within unconsolidated coast-near epiclastic sediments formed from the influence of heat generated by mid-ocean ridge igneous activity. The ore forming process of the mica schist-hosted ores can also be seen in the light of the concept “subsea-floor replacement in massive sulphide deposits” model (as described in chapter 1.6). The ores in the Tronsvängen-Baugberget area fulfil at least criteria 1, 2, (4) and 5 (see chapter 1.6.3) of the model proposed by Doyle & Allen (2003). Field observations, that

the ores are semi-massive, irregular and appears within the foliated bed of the synvolcanic sedimentary unit (mica schist), also strengthen the subsea-floor replacement model. The Zn-Cu Storliden deposit, Sweden, is hosted by volcanoclastic sedimentary rocks of Palaeoproterozoic age and is conceived to be a seafloor exhalation where the minor semi-massive Cu-ore has replaced the feeder zone (Imaña *et al.*, 2005; Imaña & Miettinen, 2016). The Zn-Cu Vihanti mines, Finland, is located in volcano-sedimentary rocks having an age of 1.93-1.92 Ga originated from island arc (Mäki *et al.*, 2015). This deposit is believed to have formed by combined processes involving exhalation and replacement. The ores in the Tronsvangen-Baugberget area show similar features with the Storliden and Vihanti deposits, like the host rock lithology, type of ore mineralization and occurrence of the ores within the host rocks.

The sequences seen in the Tronsvangen-Baugberget areas, their environment of deposition and magmatic eruption, and the style and formation of ores, have similarities to the present Red Sea (Robb, 2005; Bosworth *et al.*, 2012). Also, the greenschist in the Ramundberget area have also been compared with the Red Sea in style of deposition and generation of magma (Hill, 1980). Both these areas could thus be older equivalents of the present Red Sea.

## Ediacara

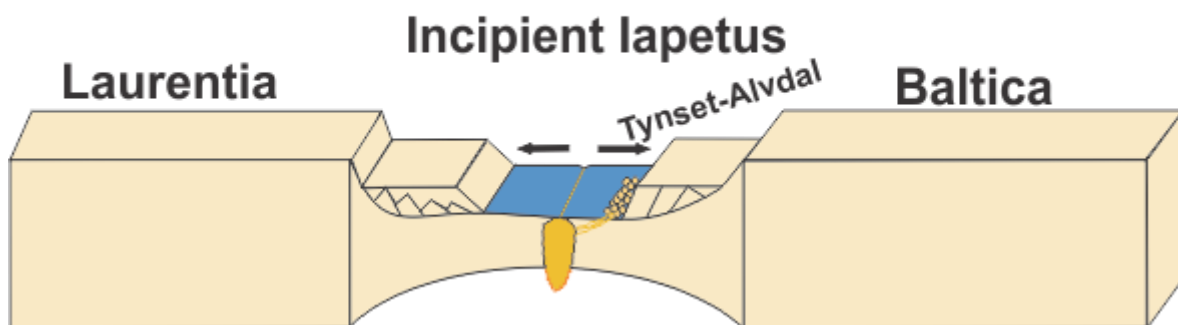


Figure 28: Suggested environment of the formation of the Tynset-Alvdal ore-bearing sequences in the Ediacara with rifting and early opening of the Iapetus Ocean.



## 5. Conclusion

The study of a set of ore-bearing rocks located in the Tynset-Alvdal region, Hedmark county, has resulted in the recognition of the lowermost (and oldest) Cu-bearing VMS ore deposits within the Scandinavian Caledonides.

The ore deposits are located in two different lithologies: greenschist and mica schist, in the lower part of the Seve Nappe, Middle Allochthon. The greenschist has originated as ocean-floor basalts with a tholeiitic signature from a mid-ocean ridge. The mica schist has originated as greywacke, deposited in a marine continental margin environment. They are both formed during the rifting and early opening up of the Iapetus Ocean during the late Precambrian to early Cambrian. Several age determinations of the igneous rocks in the Seve and Särsv nappes, yield Ediacaran ages (c. 600 Ma). The host rocks have most probably formed at the same time, due to their location and origin. Both host rocks have been affected by hydrothermal alteration (in connection with the ore-forming process), as seen in the geochemistry of the altered rocks in terms of mobile and immobile elements, and a metamorphic event in Late Silurian to Early Devonian (Caledonian Orogen), giving the rocks their present mineralogy and structure.

The greenschist-hosted ores are a chalcopyrite-sphalerite-bearing pyrite-rich massive ore type, and show similarities to the Cyprus VMS type. If so, then the ores are located within the upper part of the volcanic pile, indicating an inverted stratigraphy. The mica schist-hosted ores have a significant different mineralogical and geochemical signature: they are a chalcopyrite-sphalerite-galena bearing pyrrhotite-rich irregularly distributed ore type. This ore type has similarities with both the Escanaba and subsea-floor replacement VMS types, and with other deposits like the Vihanti mine, Finland, and the Storliden mine, Sweden.

The ore-bearing sequences at Tronsvangen-Baugberget (and Ramundberget) show similarities with the present Red Sea in concept of magmatism and sedimentation, and can therefore be late Precambrian examples of such a tectonic situation.



## References

- Aalen, O. E. (1908). St. Knut gruve. Oversiktskart St.Knut, Gml. Tronsli, St.Thomas og Tjæremyr., Norges Geologiske Undersøkelse; Bergarkivet., No. K 2578. 1:1 000.
- Aalstad, I. (1967). *Magnetisk og elektromagnetisk flymålinger Dovre-Alvdal*. NGU rapport nr. 687 Norges Geologiske Undersøkelse. pp. 7.
- Baier, J., Audetat, A., & Keppler, H. (2008). *The origin of the negative niobium tantalum anomaly in subduction zone magmas*. Earth and Planetary Science Letters, 267, pp 290-300.
- Barton, P. B. (1991). *Ore Textures - Problems and Opportunities*. Mineralogical Magazine, 55, pp 303-315.
- Barton, P. B., & Bethke, P. M. (1987). *Chalcopyrite Disease in Sphalerite - Pathology and Epidemiology*. American Mineralogist, 72, pp 451-467.
- Bergman, S. (1993). *Geology and Geochemistry of Mafic-Ultramafic Rocks (Köli) in the Handöl Area, Central Scandinavian Caledonides*. Norsk Geologisk Tidsskrift, 73, pp 21-42.
- Bergström, J., & Gee, D. G. (1985). The Cambrian in Scandinavia. In D. G. Gee & B. A. Sturt (Eds.), *The Caledonide Orogen - Scandinavia and related areas*. John Wiley & Sons Ltd. pp. 247-272.
- Bjerkgård, T. (1998). *Faktaark for Forekomstområde 438*. Norges Geologiske Undersøkelser. Malmdatabasen.
- Bortnikov, N. S., Genkin, A. D., Dobrovolskaya, M. G., Muravitskaya, G. N., & Filimonova, A. A. (1991). *The Nature of Chalcopyrite Inclusions in Sphalerite: Exsolution, Coprecipitation, or Disease?* Economic Geology, 86, pp 1070-1082.
- Bosworth, W., Huchon, P., & McClay, K. (2012). The Red Sea and Gulf of Aden basins A2 - Roberts, D.G. In D. G. Roberts & A. W. Bally (Eds.), *Regional Geology and Tectonics: Phanerozoic Passive Margins, Cratonic Basins and Global Tectonic Maps*. Boston. Elsevier. pp. 62-139.
- Braseth, L. (1995). *Drømmen om den store malmåra : Alvdals gruvehistorie*. Alvdal: Alvdal kommune.
- Briqueu, L., Bougault, H., & Joron, J. L. (1984). *Quantification of Nb, Ta, Ti and V anomalies in magmas associated with subduction zones: petrogenetic implications*. Earth and Planetary Science Letters, 68, pp 297-308.
- Cann, J. R. (1970). *Rb, Sr, Y, Zr, Nb in some ocean-floor basaltic rocks*. Earth Planet Science Letter, 10, pp 7-11.
- Claesson, S., Stephens, M. B., & Klingspor, I. (1987). *U-Pb zircon dating of felsic intrusions, Middle Köli Nappes, central Scandinavian Caledonides*. Norsk Geologisk Tidsskrift, 67, pp 89-97.
- Cook, N. J., Spry, P. G., & Vokes, F. M. (1998). *Mineralogy and textural relationships among sulphosalts and related minerals in the Bleikvassli Zn-Pb-(Cu) deposit, Nordland, Norway*. Mineralium Deposita, 34, pp 35-56.
- Corfu, F., Andersen, T. B., & Gasser, D. (2014a). The Scandinavian Caledonides: main features, conceptual advances and critical questions. In F. Corfu, D. Gasser, & D. M. Chew (Eds.), *New Perspectives on the Caledonides of Scandinavia and Related Areas*. London. Geological Society. Vol. 390, pp. 9-43.
- Corfu, F., Gasser, D., & Chew, D. M. (2014b). *New perspectives on the Caledonides of Scandinavia and Related Areas*. (Geological Society Special publications No. 390: Geological Society of London.

- Craig, J. R., & Vaughan, D. J. (1994). *Ore Microscopy & Ore Petrography* (2nd ed.). New York: John-Wiley & Sons Inc.
- Craig, J. R., & Vokes, F. M. (1993). *The metamorphism of pyrite and pyritic ores: an overview*. Mineralogical Magazine, 57, pp 3-18.
- Doyle, M. G., & Allen, R. L. (2003). *Subsea-floor replacement in volcanic-hosted massive sulfide deposits*. Ore Geology Reviews, 23, pp 183-222.
- Dreyer, G. (1974). *Kurzbericht über Geologie und Erzführung am Tronfjell-Massivs bei Alvdal/Hedmark*. Doctoral Dissertation, University of Mainz.
- Du Rietz, T. (1935). *Peridotites, serpentinites, and soapstones of northern Sweden*. Geol. Foren. Stockholm Förh., 57, pp 133-260.
- Dyrekius, D., Gee, D. G., Gorbatshev, R., Ramberg, H., & Zachrisson, E. (1980). *A profile through the central Scandinavian Caledonides*. Tectonophysics, 69, pp 247-284.
- Eidsvig, P. (1968). *Geofysiske målinger Stormyra, Hjerkin og St. Knuts grube, Tron*. NGU rapport nr. 847 Norges Geologiske Undersøkelse. pp. 33.
- Floyd, P. A., & Winchester, J. A. (1978). *Identification and Discrimination of Altered and Metamorphosed Volcanic Rocks Using Immobile Elements*. Chemical Geology, 21, pp 291-306.
- Franklin, J. M., Gibson, H. L., Galley, A. G., & Jonasson, I. R. (2005). *Volcanogenic massive sulphide deposits*. Economic Geology, 100th Anniversary Volume, pp 523-560.
- Franklin, J. M., Lydon, J. W., & Sangster, D. F. (1981). *Volcanic-associated massive sulfide deposits*. Economic Geology, 75th Anniversary Volume, pp 485-627.
- Galley, A. G., Hannington, M. D., & Jonasson, I. R. (2007). Volcanogenic massive sulphide deposits. In W. D. Goodfellow (Ed.), *Mineral Deposits of Canada: A Synthesis of Major Deposit-Types, District Metallogeny, the Evolution of Geological Provinces, and Exploration Methods*. Geological association of Canada, Mineral Deposits Division. Vol. Special Publication No. 5, pp. 141-161.
- Gee, D. G. (1975). *A tectonic model for the central part of the Scandinavian Caledonides*. American Journal of Science, 275-A, pp 468-515.
- Gee, D. G. (1981). *The Dictyonema-bearing phyllites at Nordaunevoll, eastern Trøndelag, Norway*. Norsk Geologisk Tidsskrift, 61, pp 93-95.
- Gee, D. G., Andréasson, P.-G., Li, Y., & Krill, A. (in prep.). *Baltoscandian margin, Sveconorwegian crust lost by subduction during Caledonian collisional orogeny*.
- Gee, D. G., Fossen, H., Henriksen, N., & Higgins, A. K. (2008). *From the early Paleozoic platforms of Baltica and Laurentia to the Caledonide orogen of Scandinavia and Greenland*. Episodes, 31, pp 44-51.
- Gee, D. G., Guezou, J.-C., Roberts, D., & Wolff, F. C. (1985a). The central-southern part of the Scandinavian Caledonides. In D. G. Gee & B. A. Sturt (Eds.), *The Caledonide Orogen – Scandinavia and related areas*. John Wiley & Sons Ltd. pp. 109-134.
- Gee, D. G., Juhlin, C., Pascal, C., & Robinson, P. (2010). *Collisional Orogeny in the Scandinavian Caledonides (COSC)*. Gff, 132, pp 29-44.
- Gee, D. G., Kumpulainen, R., Roberts, D., Stephens, M. B., Thon, A., & Zachrisson, E. (1985b). Scandinavian Caledonides - Tectonostratigraphic map. In D. G. Gee & B. A. Sturt (Eds.), *The Caledonide Orogen – Scandinavia and related areas*. John Wiley & Sons Ltd.
- Gee, D. G., & Sturt, B. A. (1985). *The Caledonide orogen: Scandinavia and related areas*. Chichester: Wiley.
- Gee, D. G., & Zachrisson, E. (1979). *The Caledonides in Sweden*. Svergies Geologiska Undersökning, C 769, pp 1-48.

- Geis, H. P. (1958). *Verkets skjerp ved Alvdal*. F. Verk. pp. 7.
- Grenne, T. (1989). *The Feeder Zone to the Løkken Ophiolite-Hosted Massive Sulfide Deposit and Related Mineralizations in the Central Norwegian Caledonides*. *Economic Geology*, 84, pp 2173-2195.
- Grenne, T., Ihlen, P. M., & Vokes, F. M. (1999). *Scandinavian Caledonide metallogeny in a plate tectonic perspective*. *Mineralium Deposita*, 34, pp 422-471.
- Grip, E. (1954). *Blymalmen vid Laisvall, dess geologi och en jämförelse med några utländska förekomster*. *Geologiska Föreningen i Stockholm Förhandlingar*, 76, pp 357-380.
- Hill, T. (1980). *Geochemistry of the greenschists in relation to the Cu-Fe deposit in the Ramundberget area, Central Swedish Caledonides*. *NGU Bulletin*, 360, pp 195-210.
- Hofmann, A. W. (1988). *Chemical differentiation of the Earth: the relationship between mantle, continental crust, and oceanic crust*. *Earth and Planetary Science Letters*, 90, pp 297-314.
- Holmsen, P., Thesen, G., Rasmussen, W., & Mortenson, P. (1907). *A/S St. Knuts gruber*. Bergarkivet; No. BA 2203 Norges Geologiske Undersøkelse. pp. 24.
- Hutchinson, M. N., & Scott, S. D. (1981). *Sphalerite Geobarometry in the Cu-Fe-Zn-S System*. *Economic Geology*, 76, pp 143-153.
- Imaña, M., Allen, R., & Barrett, T. (2005). *Volcanic stratigraphy, chemical stratigraphy and alteration system of the Storliden massive sulphide deposit, Skellefte district, northern Sweden*. Paper presented at the Mineral Deposit Research: Meeting the Global Challenge. Springer. pp 627-630.
- Imaña, M., & Miettinen, E. (2016). *Using altered enclaves in the identification of subseafloor replacement processes in the VMS systems*. Abstract volume, 32<sup>nd</sup> Nordic Geological Winter Meeting, Helsinki, Finland. *Bull. Geol. Soc. Finland. Special Volume*, pp p. 118.
- Irvine, T. N., & Baragar, W. R. A. (1971). *A guide to the chemical classification of the common volcanic rocks*. *Canadian Journal of Earth Sciences*, 8, pp 523-548.
- Kelemen, P. B., Shimizu, N., & Dunn, T. (1993). *Relative Depletion of Niobium in Some Arc Magmas and the Continental-Crust: Partitioning of K, Nb, La and Ce during Melt/Rock Reaction in the Upper-Mantle*. *Earth and Planetary Science Letters*, 120, pp 111-134.
- Kendrick, M. A., Burgess, R., Harrison, D., & Bjorlykke, A. (2005). *Noble gas and halogen evidence for the origin of Scandinavian sandstone-hosted Pb-Zn deposits*. *Geochimica Et Cosmochimica Acta*, 69, pp 109-129.
- Kretz, R. (1983). *Symbols for rock-forming minerals*. *American Mineralogist*, 68, pp 277-279.
- Kumpulainen, R. A., Hamilton, M. A., Söderlund, U., & Nystuen, J. P. (2016). *A new U-Pb baddeleyite age for the Ottfjället dolerite dyke swarm in the Scandinavian Caledonides - a minimum age for late Neoproterozoic glaciation in Baltica*. Abstract volume 32<sup>nd</sup> Nordic Geological Winter Meeting, Helsinki, Finland. *Bull. Geol. Soc. Finland. Special volume*, pp 171-172.
- Large, R. R. (1992). *Australian volcanic-hosted massive sulfide deposits: features, styles, and genetic models*. *Economic Geology*, 87, pp 471-510.
- Le Maitre, R. W., Bateman, P., Dudek, A., Keller, J., Lameyre Le Bas, M. J., Sabine, P. A., . . . Zanettin, B. (1989). *A classification of igneous rocks and glossary of terms: recommendations of the International Union of Geological Sciences, Subcommission on the Systematics of Igneous Rocks*. Oxford: Blackwell Scientific.
- Lindberg, M. (2015). *Strukturer og mineralomvandling i Stensundtjern malmfelt, og dannelse av jernmalmen i Dunderlandsformasjonen*. MSc Thesis, UiT - The Arctic University of Norway, Tromsø.

- MacDonald, G. A. (1968). Composition and origin of Hawaiian lavas. In R. R. Coats, R. L. Hay, & C. A. Anderson (Eds.), *Studies in volcanology: a memoir in honour of Howel Williams*. Geol. Soc. Amer. Mem. Vol. 116, pp. 477-522.
- Majka, J., Rosen, Å., Janak, M., Frotzheim, N., Klonowska, I., Manecki, M., . . . Yoshida, K. (2014). *Microdiamond discovered in the Seve Nappe (Scandinavian Caledonides) and its exhumation by the "vacuum-cleaner" mechanism*. *Geology*, 42, pp 1107-1110.
- McDonough, W. F., Sund, S., Ringwood, A. E., Jagoutz, E., & Hofmann, A. W. (1991). *K, Rb and Cs in the earth and moon and the evolution of the earth's mantle*. *Geochimica Et Cosmochimica Acta*, Ross Taylor Symposium volume.
- Morton, J. L., Zierenberg, R. A., & Reiss, C. A. (1994). *Geologic, Hydrothermal, and Biologic Studies at Escanaba Trough, Gorda Ridge, Offshore Northern California*. U.S. Geological Survey Bulletin, 2022, pp 359.
- Mäki, T., Imaña, M., Kousa, J., & Luukas, J. (2015). The Vihanti-Pyhäsalmi VMS Belt. In W. Maier, R. Lahtinen, & H. O'Brien (Eds.), *Mineral Deposits of Finland*. Elsevier Inc. pp. 792.
- Nilsen, O., & Wolff, F. (1989). Berggunnsgeologisk kart Røros og Sveg, Norges Geologiske Undersøkelser. M. 1:250 000.
- Nilsson, L.-P., & Roberts, D. (2014). *A trail of ophiolitic debris and its detritus along the Trøndelag-Jämtland border: correlations and palaeogeographical implications*. *NGU Bulletin*, 453, pp 29-41.
- Nilsson, L.-P., Sturt, B. A., & Ramsay, D. M. (1997). *Ophiolitic ultramafites in the Folldal-Røros tract, and their Cr-(PGE) mineralisation*. *NGU Bulletin*, 433, pp 10-11.
- Ohmoto, H. (1996). *Formation of volcanogenic massive sulfide deposits: The Kuroko perspective*. *Ore Geology Reviews*, 10, pp 135-177.
- Passchier, C. W., & Trouw, R. A. J. (2005). *Microtectonics* (Springer Berlin Heidelberg).
- Pearce, J. A. (1975). *Basalt geochemistry used to investigate past tectonic environments on Cyprus*. *Tectonophysics*, 25, pp 41-67.
- Pearce, J. A. (1976). *Statistical analysis of major element patterns in basalt*. *Journal of Petrology*, 17, pp 15-43.
- Pearce, J. A., & Cann, J. R. (1973). *Tectonic Setting of Basic Volcanic-Rocks Determined Using Trace-Element Analyses*. *Earth and Planetary Science Letters*, 19, pp 290-300.
- Pearce, T. H., Gorman, B. E., & Birkett, T. C. (1975). *The TiO<sub>2</sub>-K<sub>2</sub>O-P<sub>2</sub>O<sub>5</sub> diagram: A method of discrimination between oceanic and non-oceanic basalts*. *Earth and Planetary Science Letters*, 24, pp 419-246.
- Pettijohn, F. J., Potter, P. E., & Siever, R. (1972). *Sand and sandstones*. New York: Springer-Verlag.
- Piercey, S. J. (2015). *A semipermeable interface model for the genesis of subseafloor replacement-type volcanogenic massive sulfide (VMS) deposits*. *Economic Geology*, 110, pp 1655-1660.
- Qian, G. J., Xia, F., Brugger, J., Skinner, W. M., Bei, J. F., Chen, G. R., & Pring, A. (2011). *Replacement of pyrrhotite by pyrite and marcasite under hydrothermal conditions up to 220 degrees C: An experimental study of reaction textures and mechanisms*. *American Mineralogist*, 96, pp 1878-1893.
- Ramberg, I. B., Nøttvedt, A., & Bryhni, I. (2007). *Landet blir til: Norges geologi* (2. oppl. ed.). Trondheim: Norsk geologisk forening.
- Ramdohr, P. (1980). *The ore minerals and their intergrowths* (2nd ed.). Oxford: Pergamon Press.

- Ramsay, D. M., & Siedlecka, A. (2001). Berggrunnskart ALVDAL 1619 II, Norges Geolgiske Undersøkelser. 1:50 000.
- Rickard, D. T., Willden, M. Y., Marinder, N. E., & Donnelly, T. H. (1979). *Studies on the Genesis of the Laisvall Sandstone Lead-Zinc Deposit, Sweden*. *Economic Geology*, 74, pp 1255-1285.
- Riiber, C. C. (1923). *Rapporter over kis- og kobber-gruber og skjerp i Foldal, Dovre og Alvdal herreder*. NGU. Bergarkivets rapport nr. 3194.
- Robb, L. (2005). *Introduction to ore-forming processes*. (Blackell Publishing.
- Roberts, D. (2003). *The Scandinavian Caledonides: event chronology, palaeogeographic settings and likely, modern analogues*. *Tectonophysics*, 365, pp 283-299.
- Roberts, D., & Gee, D. G. (1985). An introduction to the structure of the Scandinavian Caledonides. In D. G. Gee & B. A. Sturt (Eds.), *The Caledonide Orogen – Scandinavia and related areas*. John Wiley & Sons Ltd. . pp. 55-68.
- Rollinson, H. R. (1993). *Using geochemical data: evaluation, presentation, interpretation*. Harlow: Longman Group UK Limited.
- Root, D., & Corfu, F. (2012). *U–Pb geochronology of two discrete Ordovician high-pressure metamorphic events in the Seve Nappe Complex, Scandinavian Caledonides*. *Contributions to Mineralogy and Petrology*, 163, pp 769-788.
- Röshoff, K. (1978). *Structures of the Tännäs augen gneiss nappe: and its relation to under- and overlying units in the central Scandinavian caledonides*. *Sveriges geologiska undersökning/Årsbok*, C739, pp 1-35.
- Saccani, E. (2015). *A new method of discriminating different types of post-Archean ophiolitic basalts and their tectonic significance using Th-Nb and Ce-Dy-Yb systematics*. *Geoscience Frontiers*, 6, pp 481-501.
- Solomon, M. (1976). "Volcanic" massive sulfide deposits and their host rocks - a review and an explanation. In K. A. Wolf (Ed.), *Handbook of Strata-Bound and Stratiform Ore Deposits: II Regional Studies and Specific Deposits*. Elsevier, Amsterdam, Oxford. pp. 21-50.
- Steimoeggen, E. (1966). *Alvdal: ei bygdebok. 1: Bygda gjennom tidene*. Alvdal: Alvdal kommune.
- Stephens, M. B., Gustavson, M., Ramberg, B. I., & Zachrisson, E. (1985). The Caledonides of central-north Scandinavia – a tectonostratigraphic overview. In D. G. Gee & B. A. Sturt (Eds.), *The Caledonide Orogen – Scandinavia and related areas*. John Wiley & Sons Ltd. pp. 136-162.
- Streitlien, I. A. (1978). *Tynset bygdebok, bind 3*. [Tynset]: [Tynset bygdeboknemnd].
- Sundblad, K. (1980). *A tentative "volcanogenic" formation model for the sediment-hosted Ankarvattnet Zn-Cu-Pb massive sulphide deposit, central Swedish Caledonides*. *NGU Bulletin*, 57, pp 211-227.
- Sundblad, K. (1981). *Chemical Evidence for, and implications of, a Primary FeS Phase in the Ankarvattnet Zn-Cu-Pb Massive Sulphide Deposit, Central Swedish Caledonides*. *Mineralium Deposita*, 16, pp 129-146.
- Sundblad, K. (1991). *The Runoasvage massive sulphide deposit in the Norrbotten Caledonides, Sweden*. *Geol. Fören. Stockholm Förhandlingar*, 113, pp 65-67.
- Sundblad, K., Andersen, T., Beckholmen, M., & Nilsen, O. (2006). *Ordovician Escanaba type VMS deposits in the Scandinavian Caledonides*. Abstract volume, the 27th Nordic Geological Winter Meeting Oulu, Finland. pp 156.

- Sundblad, K., Beckholmen, M., Nilsen, O., & Andersen, T. (2010). *Tectono-stratigraphic position and depositional environment of the Røros sulphide ores, Norwegian Caledonides*. Abstract volume, 29<sup>th</sup> Nordic Geological Winter Meeting, Oslo, Norway.
- Sundblad, K., & Gee, D. G. (1984). *Occurrence of a uraniferous - vanadiniferous graphitic phyllite in the Köli nappes of the Stekenjokk area, central Swedish Caledonides*. Geologiska Föreningens i Stockholm Förhandlingar, 106, pp 269-274.
- Sundblad, K., & Stephens, M. B. (1983). *Lead isotope systematics of the stratabound sulphide deposits in the higher nappe complexes of the Swedish Caledonides*. Economic Geology, 78, pp 1090-1107.
- Svenningsen, O. M. (2001). *Onset of seafloor spreading in the Iapetus Ocean at 608 Ma: precise age of the Sarek Dyke Swarm, northern Swedish Caledonides*. Precambrian Research, 110, pp 241-254.
- Tarr, W. A. (1927). *Alternating deposition of pyrite, marcasite and possibly melnikovite*. The American Mineralogist, 12, pp 417-421.
- Thorkildsen, B. (1913). *St. Knuts Grubefelt, Lilleelvdal*. NO. Ba. 6440 Norges Geologiske Undersøkelse. Fagrapport, Bergarkivet NO. Ba. 6440. pp. 3.
- Travis, R. B. (1970). *Classification of Metamorphic Rocks*. Retrieved 07.05, 2016. Quarterly of the Colorado School of Mines, vol. 50, no. 1
- Vokes, F. M. (1969). *A Review of Metamorphism of Sulphide Deposits*. Earth-Science Reviews, 5, pp 99-143.
- Wellings, S. A., & Sturt, B. A. (1998). *Tectonic setting of the Tronfjell Massif: further evidence for pre-Scandian orogenesis in the Trondheim Nappe Complex, Central Norway*. NGU Bulletin, 434, pp 109-115.
- White, W. M. (2013). *Geochemistry*. Somerset, GB: Wiley-Blackwell.
- Wood, D. A., Joron, J. L., Treuil, M., Norry, M., & Tarney, J. (1979). *Elemental and Sr isotope variations in basic lavas from Iceland and the surrounding ocean floor*. Contributions to Mineralogy and Petrology, 70, pp 319-339.
- Zachrisson, E. (1984). *Lateral Metal Zonation and Stringer Zone Development, Reflecting Fissure-Controlled Exhalations at the Stekenjokk-Levi Strata-Bound Sulfide Deposit, Central Scandinavian Caledonides*. Economic Geology, 79, pp 1643-1659.

<http://www.ut.no/kart/>



# Appendices

## A. Abbreviated mineral names (from Kretz, 1983).

Table 1. Mineral Symbols

Acm	acmite	Elb	elbaite	Ntr	natrolite
Act	actinolite	En	enstatite (ortho)	Ne	nepheline
Agt	aegirine-augite	Ep	epidote	Nrb	norbergite
Ak	akermanite	Fst	fassite	Nsn	nosean
Ab	albite	Fa	fayalite	Ol	olivine
Aln	allanite	Fac	ferroactinolite	Omp	omphacite
Alm	almandine	Fed	ferroedenite	Oam	orthoamphibole
Anl	analcite	Fs	ferrosilite (ortho)	Or	orthoclase
Ant	anatase	Fts	ferrotschermakite	Opx	orthopyroxene
And	andalusite	Fl	fluorite	Pg	paragonite
Adr	andradite	Fo	forsterite	Prg	pargasite
Anh	anhydrite	Gn	galena	Pct	pectolite
Ank	ankerite	Grt	garnet	Pn	pentlandite
Ann	annite	Ged	gedrite	Per	periclase
An	anorthite	Gh	gehlenite	Prv	perovskite
Atg	antigorite	Gbs	gibbsite	Phl	phlogopite
Ath	anthophyllite	Glt	glauconite	Pgt	pigeonite
Ap	apatite	Gln	glaucophane	Pl	plagioclase
Apo	apophyllite	Gt	goethite	Prh	prehnite
Arg	aragonite	Gr	graphite	Pen	protoenstatite
Arf	arfvedsonite	Grs	grossularite	Pmp	pumpellyite
Apy	arsenopyrite	Gru	grunerite	Py	pyrite
Aug	augite	Gp	gypsum	Prp	pyrope
Ax	axinite	Hl	halite	Prl	pyrophyllite
Brt	barite	Hs	hastingsite	Po	pyrrhotite
Brl	beryl	Hyn	haüyne	Qtz	quartz
Bt	biotite	Hd	hedenbergite	Rbk	riebeckite
Bhm	boehmite	Hem	hematite	Rds	rhodochrosite
Bn	bornite	Hc	hercynite	Rdn	rhodonite
Brk	brookite	Hul	heulandite	Rt	rutile
Brc	brucite	Hbl	hornblende	Sa	sanidine
Bst	bustamite	Hu	humite	Spr	sapphirine
Cam	Ca clin amphibole	Ill	illite	Scp	scapolite
Cpx	Ca clinopyroxene	Ilm	ilmenite	Srl	schorl
Cal	calcite	Jd	jadeite	Srp	serpentine
Ccn	cancrinite	Jh	johannsenite	Sd	siderite
Crn	carnegieite	Krs	kaersutite	Sil	sillimanite
Cst	cassiterite	Kls	kalsilite	Sdl	sodalite
Cls	celestite	Kln	kaolinite	Sps	spessartine
Cbz	chabazite	Ktp	kataphorite	Sp	sphalerite
Cc	chalcocite	Kfs	K feldspar	Spn	sphene
Ccp	chalcopyrite	Krn	kornepupine	Spl	spinel
Chl	chlorite	Ky	kyanite	Spd	spodumene
Cld	chloritoid	Lmt	laumontite	St	staurolite
Chn	chondrodite	Lws	lawsonite	Stb	stilbite
Chr	chromite	Lpd	lepidolite	Stp	stilpnomelane
Ccl	chrysocolla	Lct	leucite	Str	strontianite
Ctl	chrysotile	Lm	limonite	Tlc	talc
Gen	clinoenstatite	Lz	lizardite	Tmp	thompsonite
Cfs	clinoferrosilite	Lo	loellingite	Ttn	titanite
Chu	clinohumite	Mgh	maghemite	Toz	topaz
Czo	clinozoisite	Mkt	magnesiokataphorite	Tur	tourmaline
Crđ	cordierite	Mrb	magnesioriebeckite	Tr	tremolite
Crn	corundum	Mgs	magnesite	Trd	tridymite
Cv	covellite	Mag	magnetite	Tro	trollite
Crs	cristoballite	Mrg	margarite	Ts	tschermakite
Cum	cumingtonite	Mel	melilite	Usp	ulvöspinel
Dsp	diaspore	Mc	microcline	Vrm	vermiculite
Dg	diginite	Mo	molybdenite	Ves	vesuvianite
Di	diopside	Mnz	monazite	Wth	witherite
Dol	dolomite	Mtc	monticellite	Wo	wollastonite
Drv	dravite	Mnt	montmorillonite	Wus	wüstite
Eck	eckermannite	Mul	mullite	Zrn	zircon
Ed	edenite	Ms	muscovite	Zo	zoisite



## B. Overview of samples

<b>Sample</b>	<b>Locality</b>	<b>Lithology</b>	<b>Mineralogy</b>	<b>Sample type</b>
<b>ML1501</b>	Klettgruva	Greenschist	Pyrite, sphalerite, quartz, (chlorite)	Ore
<b>ML1502</b>	Klettgruva	Greenschist	Pyrite, chalcopyrite, sphalerite, quartz, chlorite	Ore
<b>ML1503</b>	Vesletronden	Greenschist	Pyrite, chalcopyrite, sphalerite, quartz, (white mica/chlorite)	Ore/Altered rock
<b>ML1504</b>	Vesletronden	Greenschist	Pyrite, chalcopyrite, sphalerite, quartz, (white mica/chlorite)	Ore
<b>ML1507</b>	Vesletronden	Greenschist	Pyrite, chalcopyrite, sphalerite, quartz, (white mica/chlorite)	Ore
<b>ML1509</b>	Vesletronden	Greenschist	Pyrite, chalcopyrite, sphalerite, quartz, (chlorite)	Ore
<b>ML1515</b>	Gamle Tronsli	Mica schist	White mica, quartz, plagioclase, calcite	Host rock
<b>ML1516</b>	Brånå	Mica schist	Pyrrhotite, sphalerite, chalcopyrite, quartz, plagioclase, white mica, chlorite, calcite	Ore
<b>ML1517</b>	Brånå	Mica schist	Pyrrhotite, sphalerite, chalcopyrite, quartz, plagioclase, white mica, chlorite	Ore/Altered rock
<b>ML1524</b>	St. Thomas	Mica schist	Pyrrhotite, sphalerite, chalcopyrite, galena, quartz, white mica, chlorite	Ore
<b>ML1526</b>	St. Thomas	Mica schist	Pyrrhotite, sphalerite, chalcopyrite, pyrite, quartz, white mica, chlorite, calcite	Ore

<b>ML1527</b>	St. Olav	Mica schist	Pyrrhotite, pyrite, sphalerite, chalcopyrite, galena, quartz, white mica, chlorite, calcite	Ore
<b>ML1530</b>	Nedre Tjæremyr	Mica schist	Pyrrhotite, pyrite, sphalerite, chalcopyrite, quartz, white mica, chlorite	Ore
<b>ML1533</b>	Tronsvangen	Greenschist	Chlorite, plagioclase, white mica, (quartz)	Host rock
<b>ML1535</b>	Vesletronden	Greenschist	Chlorite, plagioclase, white mica, (quartz)	Host rock
<b>ML1537</b>	Vesletronden	Greenschist	Quartz, plagioclase, white mica, chlorite, pyrite	Altered rock
<b>ML1538</b>	South of Sørkletten	Greenschist	Chlorite, plagioclase, white mica, amphibole, (quartz)	Host rock
<b>ML1539</b>	St. Knut	Mica schist	Pyrrhotite, sphalerite, chalcopyrite, quartz, white mica, chlorite	Ore
<b>ML1542</b>	St. Knut	Mica schist	Pyrrhotite, sphalerite, chalcopyrite, quartz, white mica	Altered rock
<b>ML1544</b>	St. Knut west	Mica schist	White mica, chlorite, quartz, pyrrhotite, chalcopyrite, sphalerite,	Altered rock
<b>ML1546</b>	Gamle Tronsli	Mica schist	Pyrrhotite, sphalerite, chalcopyrite, quartz, white mica	Ore
<b>ML1547</b>	Gamle Tronsli	Mica schist	Pyrrhotite, sphalerite, chalcopyrite, (pyrite), quartz, white mica, chlorite	Ore
<b>ML1549</b>	Tjæremyr	Mica schist	White mica, quartz, plagioclase	Host rock
<b>ML1551</b>	Øvre Tjæremyr	Mica schist	Pyrrhotite, sphalerite, chalcopyrite, quartz, white mica, chlorite, calcite	Ore/altered rock

<b>ML1552</b>	Øvre Tjæremyr	Mica schist	Pyrrhotite, pyrite, sphalerite, chalcopyrite, quartz, white mica, chlorite, calcite	Ore
<b>ML1554</b>	Øvre Tjæremyr	Mica schist	White mica, chlorite, quartz, calcite, amphibole	Altered rock
<b>ML1555</b>	East of Tjæremyr	Mica schist	White mica, quartz, chlorite, calcite, (plagioclase)	Host rock
<b>ML1556</b>	Grøtådalen	Greenschist	Chlorite, plagioclase, calcite, amphibole	Host rock/alteration rock
<b>ML1559</b>	Grøtådalen	Greenschist	Pyrrhotite, chalcopyrite, sphalerite, quartz	Ore
<b>ML1560</b>	Grøtådalen	Greenschist	Pyrrhotite, pyrite, chalcopyrite, sphalerite, quartz, chlorite, amphibole	Ore
<b>ML1568</b>	Såttå	Mica schist	Pyrrhotite, pyrite, sphalerite, chalcopyrite	Ore
<b>ML1569</b>	Nordkletten	Greenschist	Chlorite, plagioclase, (quartz, amphibole)	Host rock
<b>ML1570</b>	Store Baugsberget	Mica schist	Pyrrhotite, sphalerite, chalcopyrite, quartz, chlorite, white mica	Ore
<b>ML1571</b>	Store Baugsberget	Mica schist	Pyrrhotite, pyrite, sphalerite, chalcopyrite	Ore
<b>ML1572</b>	Store Baugsberget	Mica schist	Pyrrhotite, sphalerite, chalcopyrite, pyrite	Ore
<b>ML1573</b>	Lille Baugsberget	Mica schist	Pyrrhotite, pyrite, sphalerite, chalcopyrite, quartz, calcite	Ore
<b>ML1574</b>	Lille Baugsberget	Mica schist	Pyrrhotite, pyrite, sphalerite, chalcopyrite, quartz, white mica	Ore



C. Scanned thin sections

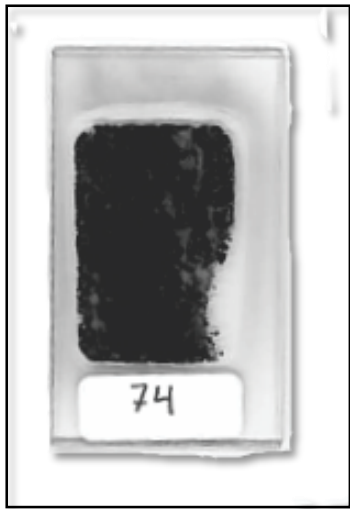














## D. Geochemical data

### D.1 Certificate of analysis, Actlabs

Quality Analysis ...



Innovative Technologies

Date Submitted: 07-Dec-15  
Invoice No.: A15-10688  
Invoice Date: 27-Jan-16  
Your Reference: PO# 81350031

University of Tromso, Norway  
N-9037 Tromso  
Norway

ATTN: Ann Pettersen

## CERTIFICATE OF ANALYSIS

34 Rock samples were submitted for analysis.

The following analytical package was requested:

REPORT A15-10688

Code 4LITHO (11+) Major Elements Fusion ICP(WRA)/Trace Elements Fusion ICP/MS(WRA4B2)

Code UT-3 INAA(INAAGEO)/Total digestion ICP(Total)/Total Digestion ICP/MS

This report may be reproduced without our consent. If only selected portions of the report are reproduced, permission must be obtained. If no instructions were given at time of sample submittal regarding excess material, it will be discarded within 90 days of this report. Our liability is limited solely to the analytical cost of these analyses. Test results are representative only of material submitted for analysis.

#### Notes:

Unaltered silicates and resistate minerals may not be dissolved. Values which exceed upper limit should be assayed.

We recommend using option 4B1 for accurate levels of the base metals Cu, Pb, Zn, Ni and Ag. Option 4B-INAA for As, Sb, high W > 100ppm, Cr > 1000ppm and Sn > 50ppm by Code 5D. Values for these elements provided by Fusion ICP/MS, are order of magnitude only and are provided for general information.

Mineralized samples should have the Quant option selected or request assays for values which exceed the range of option 4B1. Total includes all elements in % oxide to the left of total.

INAA report footnote: High Cu/Pb & Zn present in some samples may be causing suppression of INAA data.

CERTIFIED BY:

Emmanuel Esemé, Ph.D.  
Quality Control

ACTIVATION LABORATORIES LTD.  
41 Bittern Street, Ancaster, Ontario, Canada, L9G 4V5  
TELEPHONE +905 648-9611 or +1.888.228.5227 FAX +1.905.648.9613  
E-MAIL [Ancaster@actlabs.com](mailto:Ancaster@actlabs.com) ACTLABS GROUP WEBSITE [www.actlabs.com](http://www.actlabs.com)



***D.2 Major element diagram (%) of host rocks***

<b>Sample</b>	<b>SiO<sub>2</sub></b>	<b>Al<sub>2</sub>O<sub>3</sub></b>	<b>Fe<sub>2</sub>O<sub>3</sub>(T)</b>	<b>MnO</b>	<b>MgO</b>	<b>CaO</b>	<b>Na<sub>2</sub>O</b>	<b>K<sub>2</sub>O</b>	<b>TiO<sub>2</sub></b>	<b>P<sub>2</sub>O<sub>5</sub></b>	<b>LOI</b>	<b>Total</b>
<b>ML1503</b>	46,06	0,83	33,21	0,026	0,79	0,2	0,1	0,02	0,039	< 0,01	17,4	98,66
<b>ML1515</b>	65,12	11,22	4,3	0,067	2,46	5,79	3,54	0,98	0,618	0,12	5,07	99,29
<b>ML1533</b>	48,46	15,67	10,19	0,16	8,53	12,37	2,05	0,18	1,104	0,07	1,52	100,3
<b>ML1535</b>	48,86	14,43	12,03	0,202	7,45	11,42	2,68	0,05	1,593	0,13	0,7	99,53
<b>ML1537</b>	53,92	14,32	8,09	0,284	6,87	7,04	4,97	0,04	1,631	0,06	2,19	99,41
<b>ML1538</b>	48,38	14,91	13,12	0,206	6,88	11,01	2,8	0,14	2,179	0,18	0,95	100,8
<b>ML1542</b>	57,71	4,76	23,73	0,028	0,48	0,2	0,34	1,32	0,266	< 0,01	5,31	94,15
<b>ML1544</b>	28,41	10,91	35,91	0,177	6,41	0,2	0,06	0,8	0,567	0,02	10,31	93,79
<b>ML1549</b>	64,78	14,05	5,85	0,088	3,09	4,19	2,24	1,74	0,833	0,16	3,65	100,7
<b>ML1555</b>	61,65	13,58	6,04	0,114	3,47	6,07	2,36	0,94	0,774	0,16	4,91	100,1
<b>ML1556</b>	49,35	14,37	11,97	0,199	6,19	9,72	4,83	0,04	1,799	0,14	1,89	100,5
<b>ML1569</b>	48,94	14,92	11,57	0,193	7,17	12,41	2,04	0,07	1,329	0,06	0,99	99,7

**D.3 Rare-earth element diagram (ppm) (only for greenschist samples)**

Sample	La	Ce	Pr	Nd	Sm	Eu	Gd	Tb	Dy	Ho	Er	Tm	Yb	Lu
ML1503	0,3	0,7	0,08	0,3	< 0.1	< 0.05	< 0.1	< 0.1	0,2	< 0.1	0,1	< 0.05	0,2	< 0.04
ML1533	1,9	6,1	1,16	6,7	2,6	1,09	4	0,7	4,8	1	2,8	0,44	2,7	0,41
ML1535	3,6	11,2	1,96	10,7	4,1	1,57	5,5	1	6,6	1,4	3,7	0,58	3,7	0,56
ML1537	2,9	9	1,61	8,9	3,4	1,36	4,9	0,9	6	1,3	3,5	0,54	3,5	0,54
ML1538	4,4	14,7	2,62	14,4	5,3	1,77	7,3	1,3	8,9	1,8	5,2	0,8	5,2	0,79
ML1556	3,6	11,6	2,04	11,4	4,2	1,27	5,8	1	6,9	1,4	4	0,6	3,9	0,59
ML1569	2	7	1,32	7,9	3,1	1,31	4,5	0,8	5,4	1,1	3,2	0,49	3	0,45

**D.4 Trace element diagram (ppm) (only for greenschist samples)**

Sample	Rb	Ba	Th	U	K	Ta	Nb	La	Ce	Sr	Nd	P	Hf	Zr
ML1503	<2	<3	0,1	0,2	166	<0,1	<1	0,3	0,7	4	0,3	22	0,2	12
ML1533	7	29	<0,1	<0,1	1494	0,3	0,5	1,9	6,1	102	6,7	308	1,8	58
ML1535	<2	15	0,3	<0,1	415	0,3	2	3,6	11,2	112	10,7	572	2,7	95
ML1537	<2	28	0,2	0,3	332	0,3	2	2,9	9	161	8,9	264	2,7	96
ML1538	<2	15	0,2	<0,1	1162	0,3	2	4,4	14,7	155	14,4	792	4,1	148
ML1556	<2	22	0,4	0,2	332	0,4	2	3,6	11,6	106	11,4	616	3,1	109
ML1569	<2	19	<0,1	<0,1	581	0,3	<1	2	7	113	7,9	264	2	68

Sample	Sm	Ti	Tb	Y
ML1503	0,7	234	< 0.1	<2
ML1533	2,6	6624	0,7	23
ML1535	4,1	9558	1	32
ML1537	3,4	9789	0,9	29
ML1538	5,3	13074	1,3	45
ML1556	4,2	10794	1	34
ML1569	3,1	7974	0,8	27

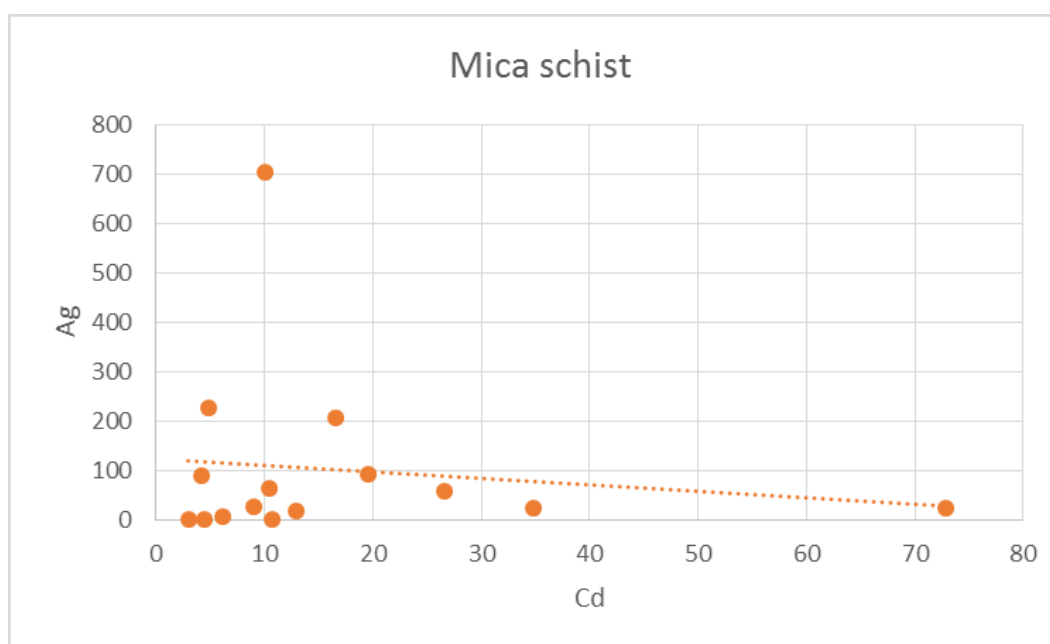
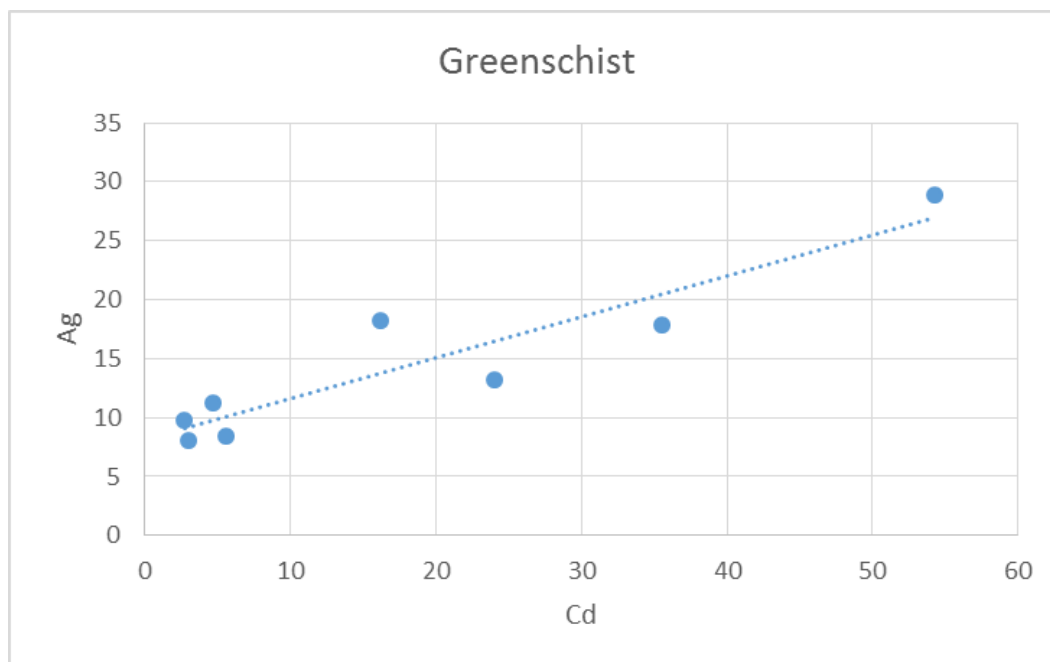
**D.5 Metal contents in ore samples**

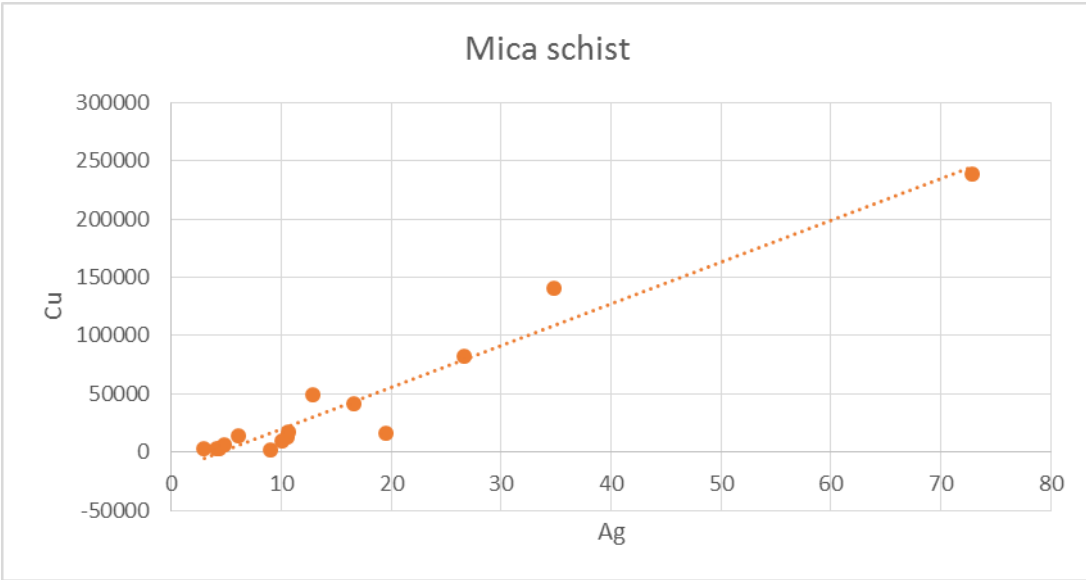
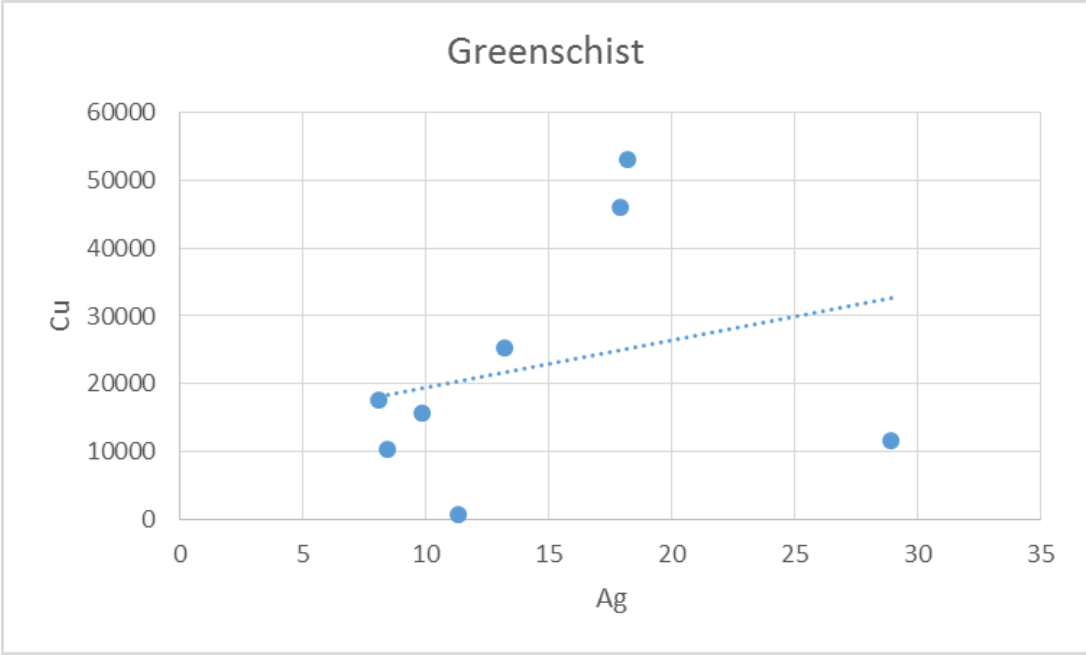
<b>Sample</b>	<b>Au (ppb)</b>	<b>Ag (ppm)</b>	<b>Cu (%)</b>	<b>Cd (ppm)</b>	<b>Mo (ppm)</b>	<b>Pb (ppm)</b>	<b>Ni (ppm)</b>	<b>Zn (%)</b>	<b>S (%)</b>	<b>Al (%)</b>	<b>As (ppm)</b>	<b>Fe (%)</b>	<b>Hg (ppb)</b>	<b>In (ppm)</b>
<b>ML1501</b>	41	11,3	0,07	4,7	41	25,1	12	0,18	35,5	0,71	27,8	28,2	< 10	< 0.1
<b>ML1502</b>	47	28,9	1,16	54,3	15	471	21,5	1,89	45	0,27	43,7	38,1	10	1,5
<b>ML1503</b>	52	8,45	1,04	5,6	45	94,4	20,9	0,17	26,8	0,42	160	21,9	< 10	0,4
<b>ML1504</b>	106	9,83	1,57	2,7	46	61	18,1	0,07	31,5	0,17	135	26,1	< 10	0,7
<b>ML1507</b>	134	8,07	1,75	3	83	87,6	10,4	0,08	35,3	1,1	206	31,3	< 10	0,7
<b>ML1509</b>	173	13,2	2,52	24	88	28,9	30	0,71	23	1,13	97	20,5	550	1,1
<b>ML1516</b>	19	4,12	0,30	88,6	6	51,4	76,7	2,19	9,92	5,25	5,4	16,4	< 10	3,7
<b>ML1517</b>	107	16,6	4,21	206	6	170	147	5,58	28,7	1,19	8,5	34,6	70	9,1
<b>ML1524</b>	30	9,02	0,20	26,5	35	1640	126	1,02	19,7	1,5	5,8	39,6	< 10	6,9
<b>ML1526</b>	< 2	2,98	0,34	0,3	23	19,1	166	0,06	14,6	3,32	4	33,1	< 10	0,2
<b>ML1527</b>	59	10,5	1,28	64,4	625	2820	74,8	2,05	27,8	0,16	8,4	38,9	10	3,9
<b>ML1530</b>	73	19,5	1,60	91,7	239	2880	65,4	3,91	19	2,45	6,9	28,7	160	8
<b>ML1537</b>	< 2	1,88	0,00	0,2	3	29,7	38,3	0,03	1,14	7,48	8,9	5,37	< 10	< 0.1
<b>ML1539</b>	654	26,6	8,21	59,8	3	9,4	100	0,96	13,7	3,8	6,4	19,9	< 10	6
<b>ML1542</b>	48	4,59	0,56	138	1	6,4	142	2,38	8,28	2,5	7,8	14,8	60	4,5
<b>ML1544</b>	340	26,6	5,06	31	68	11,8	134	0,31	11,4	5,86	6,8	22	10	7,2
<b>ML1546</b>	38	10,7	1,71	2,5	23	48,1	99,3	0,03	17,1	4,23	7,2	26,7	< 10	0,5
<b>ML1547</b>	457	72,8	23,90	25,3	35	782	16,6	0,23	29	1,46	7,7	24,3	60	2,2
<b>ML1552</b>	< 2	4,39	0,27	0,1	24	8,2	147	0,03	12,9	5,12	7,2	19,6	< 10	0,2
<b>ML1559</b>	74	17,9	4,60	35,5	5	1,8	16,4	0,13	7,69	0,18	8,9	11,4	< 10	1
<b>ML1560</b>	128	18,2	5,32	16,2	4	2,3	16,1	0,06	14,8	4,06	9,8	18,8	< 10	1,6
<b>ML1568</b>	205	34,8	14,10	23,7	4	262	77,8	0,90	26,8	2,16	10,9	27,2	50	1,8
<b>ML1571</b>	259	10,1	0,99	704	25	153	3,4	22,40	44,9	0,04	1250	27,1	7380	40,1
<b>ML1572</b>	63	4,84	0,69	226	50	116	38,5	5,73	35,1	0,12	545	40,3	3390	16,7
<b>ML1573</b>	362	6,13	1,42	8,3	27	293	24,8	0,39	38,9	0,53	1740	42,1	350	5,4
<b>ML1574</b>	1590	12,9	4,96	17,2	13	48,2	13,1	0,59	39,5	0,46	2750	34,6	870	4,4

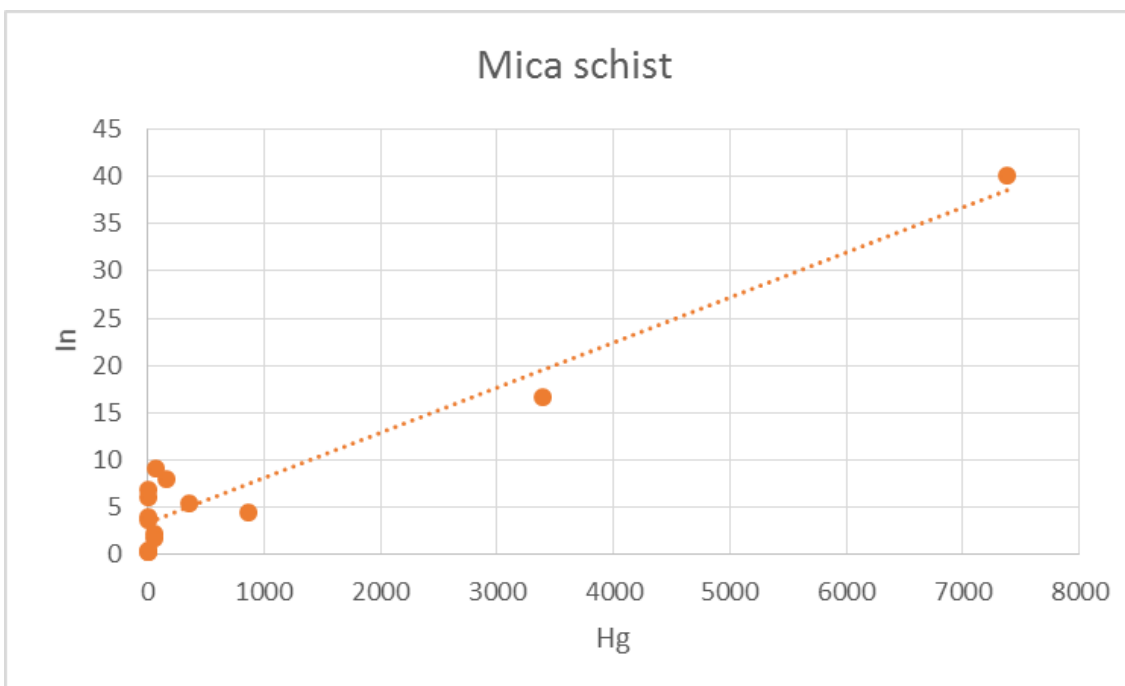
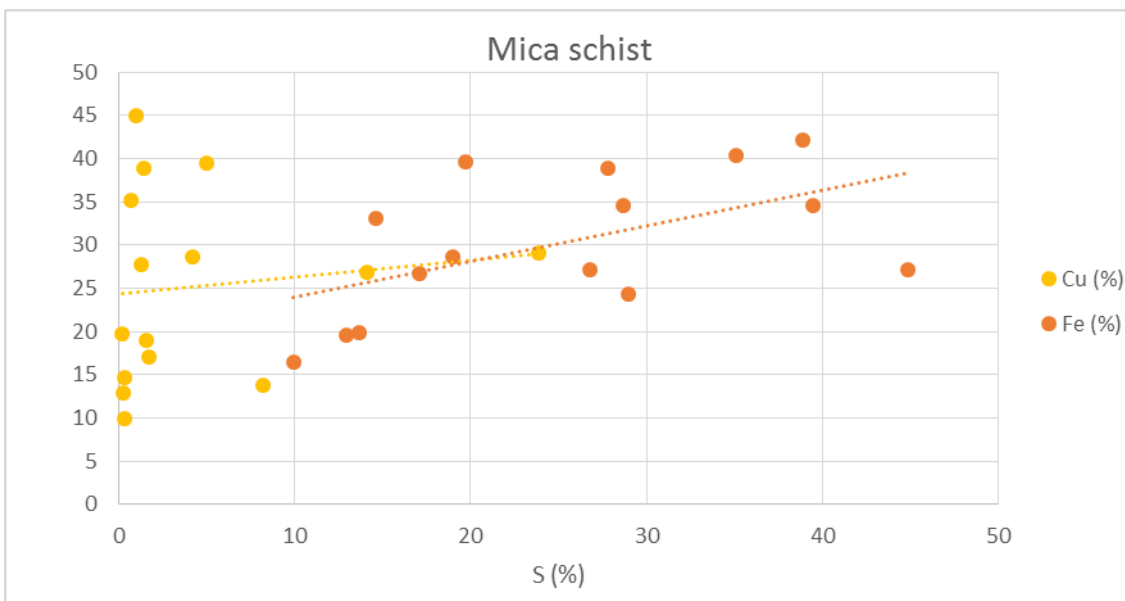
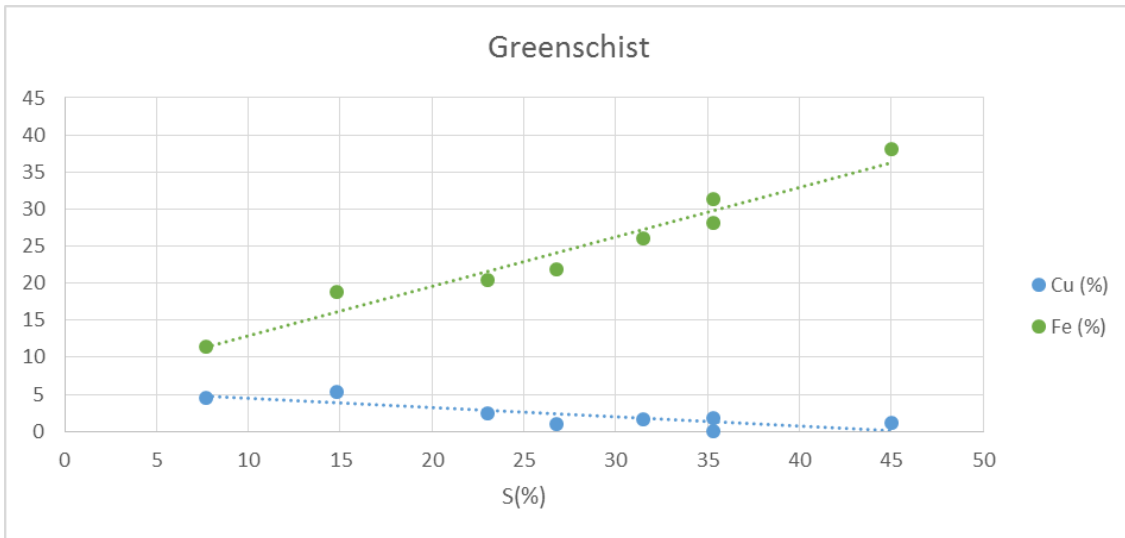


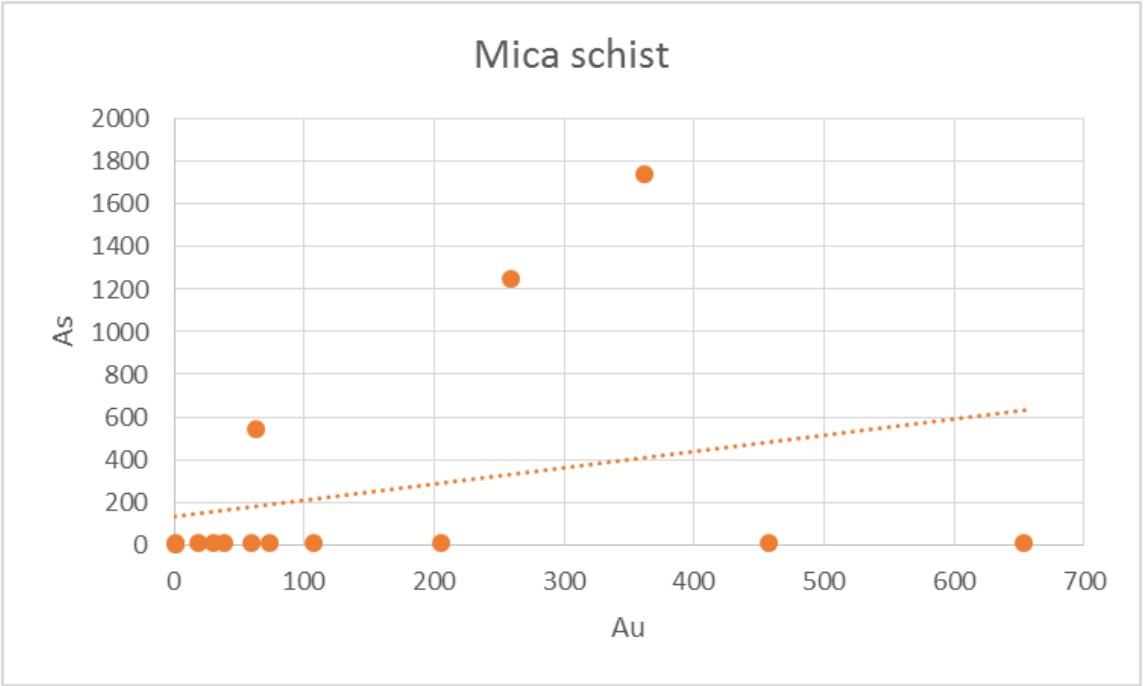
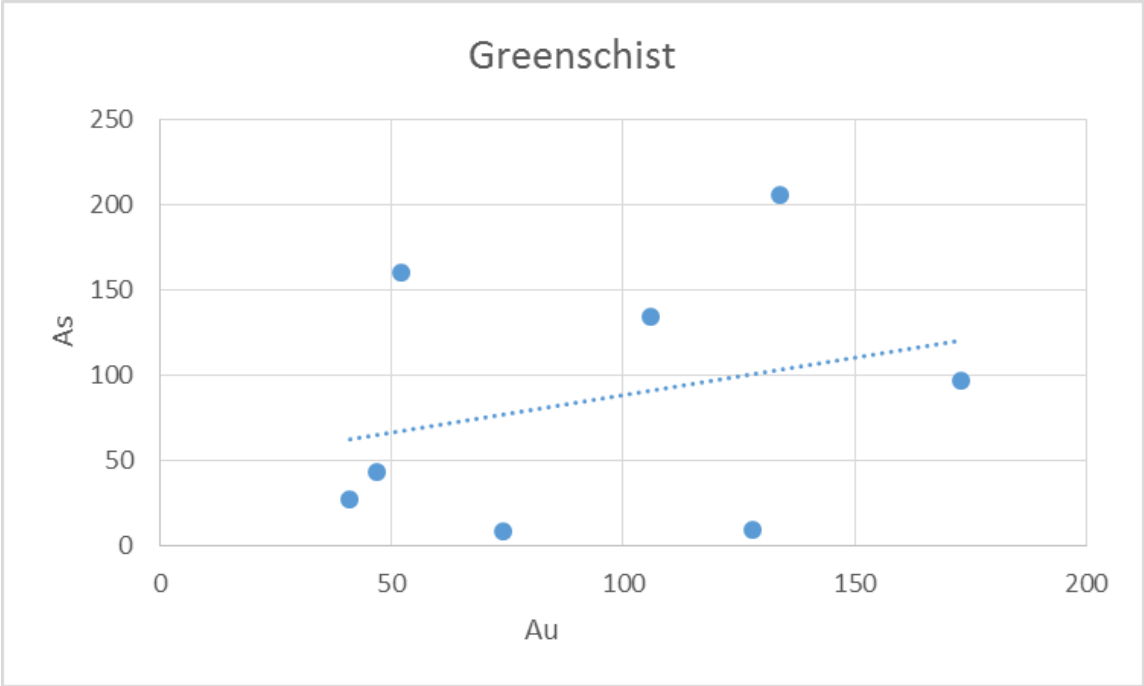
## E. Ore element correlation

### E.1 Correlation plots









## E.2 Ore element correlation tables

**Greenschist-hosted ores:** red values indicate positive correlation (>0.70) and green values indicate negative correlation (<-0.70).

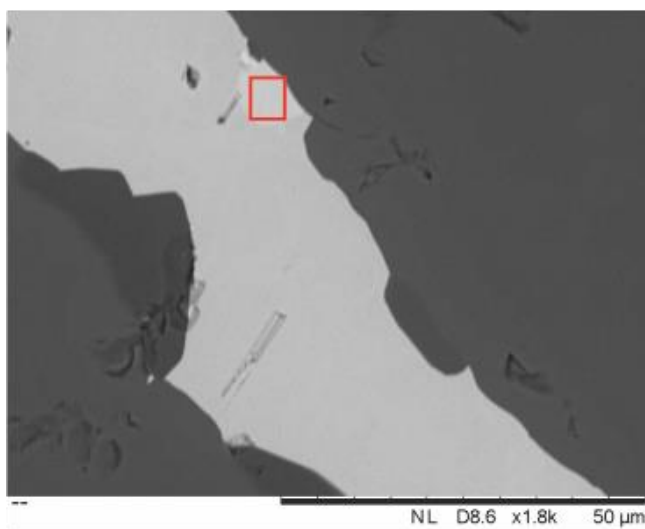
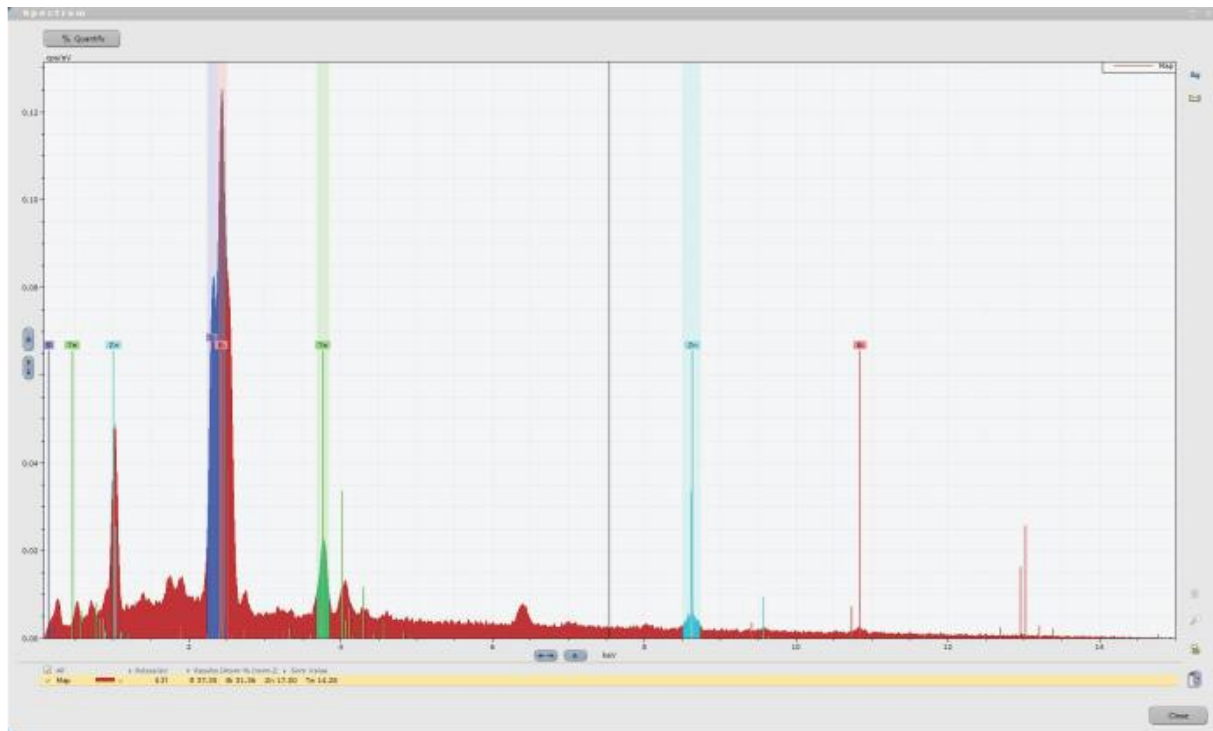
	Au	Ag	Cu	Cd	Mo	Pb	Ni	Zn	S	Al	As	Bi	Ca	Fe	Hg	In	K	Mg	Mn
Au	1																		
Ag	-0,26	1,00																	
Cu	0,44	0,27	1,00																
Cd	-0,19	0,93	0,25	1,00															
Mo	0,54	-0,64	-0,45	-0,47	1,00														
Pb	-0,40	0,69	-0,38	0,66	-0,19	1,00													
Ni	0,31	0,24	0,04	0,41	0,21	0,20	1,00												
Zn	-0,22	0,79	-0,26	0,81	-0,12	0,91	0,48	1,00											
S	-0,30	0,09	-0,84	0,01	0,31	0,70	-0,09	0,54	1,00										
Al	0,45	0,09	0,62	-0,14	-0,21	-0,31	-0,11	-0,25	-0,37	1,00									
As	0,28	-0,66	-0,44	-0,55	0,75	-0,01	-0,03	-0,22	0,37	-0,28	1,00								
Bi	0,30	-0,61	-0,42	-0,50	0,74	0,03	-0,01	-0,17	0,38	-0,29	1,00	1,00							
Ca	0,05	0,28	0,36	-0,04	-0,43	-0,09	-0,32	-0,07	-0,09	0,86	-0,52	-0,53	1,00						
Fe	-0,25	0,22	-0,70	0,10	0,23	0,76	-0,14	0,59	0,98	-0,23	0,30	0,33	0,04	1,00					
Hg	0,66	-0,07	0,06	0,13	0,59	-0,17	0,78	0,20	-0,14	0,04	0,06	0,06	-0,22	-0,19	1,00				
In	0,36	0,74	0,67	0,68	-0,39	0,36	0,36	0,48	-0,22	0,49	-0,38	-0,32	0,35	-0,05	0,17	1,00			
K	-0,19	-0,06	0,33	-0,20	-0,38	-0,35	-0,88	-0,49	-0,27	0,35	-0,30	-0,32	0,48	-0,18	-0,61	-0,12	1,00		
Mg	0,67	-0,04	0,61	-0,18	0,04	-0,35	0,06	-0,25	-0,38	0,95	-0,06	-0,07	0,68	-0,26	0,25	0,50	0,16	1,00	
Mn	0,52	0,07	0,71	-0,13	-0,20	-0,39	-0,12	-0,31	-0,47	0,99	-0,29	-0,30	0,81	-0,33	0,07	0,51	0,39	0,95	1,00

**Mica schist-hosted ores:** red values indicate positive correlation (>0.70) and green values indicate negative correlation (<-0.70).

	Au	Ag	Cu	Cd	Mo	Pb	Ni	Zn	S	Al	As	Bi	Ca	Fe	Hg	In	K	Mg	Mn
Au	1,00																		
Ag	0,23	1,00																	
Cu	0,31	0,97	1,00																
Cd	-0,08	-0,13	-0,18	1,00															
Mo	-0,19	-0,07	-0,17	-0,05	1,00														
Pb	-0,23	0,09	-0,08	-0,10	0,81	1,00													
Ni	-0,50	-0,30	-0,30	-0,38	-0,06	-0,05	1,00												
Zn	-0,08	-0,15	-0,21	0,99	-0,02	-0,05	-0,38	1,00											
S	0,43	0,08	0,12	0,53	0,03	-0,05	-0,73	0,53	1,00										
Al	-0,30	-0,10	-0,09	-0,41	-0,30	-0,27	0,57	-0,41	-0,89	1,00									
As	0,77	-0,20	-0,12	0,20	-0,18	-0,26	-0,63	0,21	0,73	-0,51	1,00								
Bi	-0,12	0,02	-0,14	0,27	0,38	0,73	-0,35	0,32	0,30	-0,51	0,06	1,00							
Ca	-0,16	-0,14	-0,20	-0,11	0,98	0,72	0,01	-0,09	-0,02	-0,23	-0,16	0,21	1,00						
Fe	0,04	-0,28	-0,28	-0,01	0,30	0,30	-0,12	0,00	0,55	-0,77	0,36	0,44	0,27	1,00					
Hg	0,04	-0,17	-0,19	0,93	-0,11	-0,19	-0,52	0,93	0,63	-0,47	0,38	0,29	-0,18	0,08	1,00				
In	-0,01	-0,16	-0,21	0,97	-0,06	-0,06	-0,46	0,97	0,60	-0,50	0,30	0,41	-0,14	0,10	0,96	1,00			
K	-0,15	0,13	0,12	-0,37	-0,23	-0,17	0,39	-0,37	-0,67	0,76	-0,48	-0,33	-0,22	-0,62	-0,40	-0,42	1,00		
Mg	-0,25	-0,09	-0,10	-0,47	-0,26	-0,22	0,60	-0,46	-0,88	0,97	-0,48	-0,45	-0,22	-0,70	-0,52	-0,55	0,80	1,00	
Mn	-0,24	-0,13	-0,22	-0,29	0,81	0,63	0,31	-0,26	-0,45	0,23	-0,42	0,05	0,84	-0,10	-0,42	-0,34	0,29	0,28	1,00

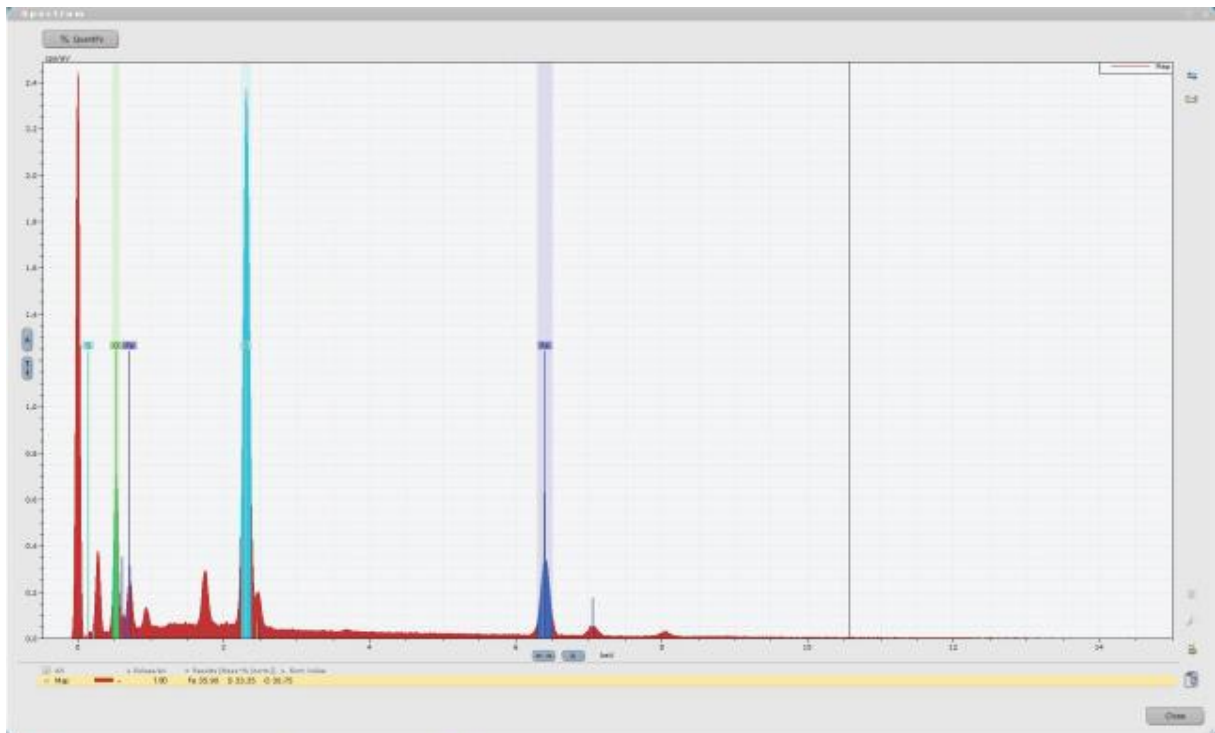
## F. SEM/EDS analysis

### F.1 Bi-Te bearing phases in galena, ML1526

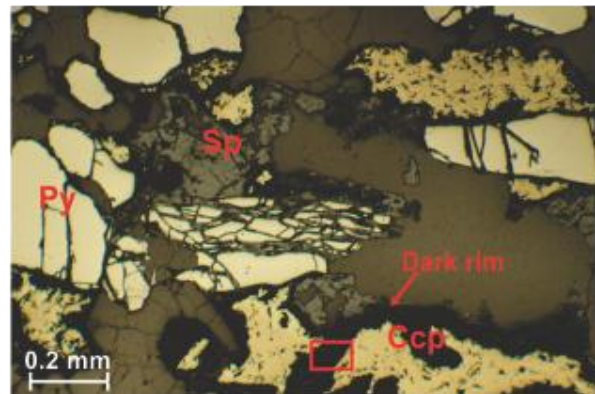
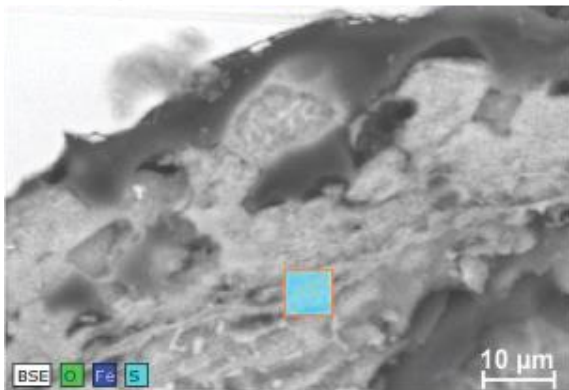


- Bismuth
- Zink
- Tellerium
- Sulphur

## F.2 Altered chalcopyrite, ML1503

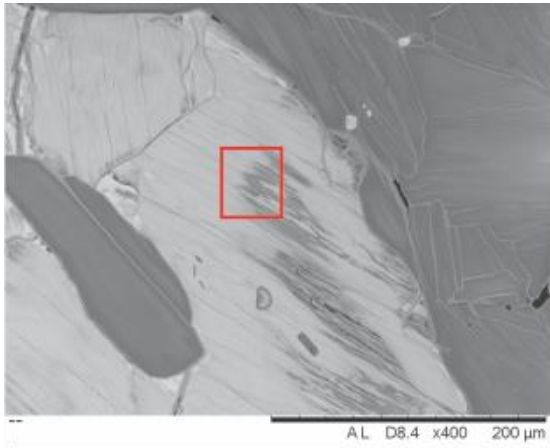


**Sulphur** **Iron** **Oxygen**





**F.3 Altered pyrrhotite, ML1544**



-  Iron
-  Sulphur
-  Oxygen

